



12-2016

Development of an Analytical Model for Beams with Two Dimples in Opposing Directions

Mofareh H. Ghazwani

Western Michigan University, eng-mof@saudieng.org

Follow this and additional works at: http://scholarworks.wmich.edu/masters_theses



Part of the [Aerospace Engineering Commons](#), and the [Mechanical Engineering Commons](#)

Recommended Citation

Ghazwani, Mofareh H., "Development of an Analytical Model for Beams with Two Dimples in Opposing Directions" (2016). *Master's Theses*. 761.

http://scholarworks.wmich.edu/masters_theses/761

This Masters Thesis-Open Access is brought to you for free and open access by the Graduate College at ScholarWorks at WMU. It has been accepted for inclusion in Master's Theses by an authorized administrator of ScholarWorks at WMU. For more information, please contact maira.bundza@wmich.edu.



DEVELOPMENT OF AN ANALYTICAL MODEL FOR BEAMS WITH TWO
DIMPLES IN OPPOSING DIRECTIONS

by

Mofareh H. Ghazwani

A thesis submitted to the Graduate College
in partial fulfillment of the requirements
for the degree of Master of Science in Engineering
Mechanical and Aerospace Engineering
Western Michigan University
December 2016

Thesis Committee:

Koorosh Naghshineh, Ph.D., Chair
Rick Meyer, Ph.D.
Kyle R. Myers, Ph.D.

DEVELOPMENT OF AN ANALYTICAL MODEL FOR BEAMS WITH TWO DIMPLES IN OPPOSING DIRECTIONS

Mofareh H. Ghazwani, M.S.E.

Western Michigan University, 2016

Structures such as beams and steel plates can produce potentially high levels of unwanted vibrations and noises in the environment. A method of improving the vibration and acoustic characteristics of beams based on introducing dimples on its surfaces will be presented in this study. This method focuses on creating two dimples in the same and opposite direction on beam's surface where the effect of dimples on the change in beam's natural frequencies is the problems of interest.

A boundary value model (BVM) is developed for a beam with two dimples and subjected to various boundary conditions using Hamilton's Variational Principle. Differential equations that describe the equations of motion of each segment are derived. Beam natural frequencies and mode shapes are obtained using a numerical solution of the differential equations. Four examples will be presented in this research. Two cases will be presented, first case is by creating two dimples in the same direction on beam's surface and the other case is by creating another beam model with two dimples in the opposite direction. A finite element method (FEM) is used to model the dimpled beam and verify the natural frequencies of the BVM. Both methods are also validated experimentally. The experimental results show a good agreement with the BVM and FEM results.

The change in the natural frequencies of the beam with two dimples in the same direction exhibits a different trend than positioning two dimples in the opposite direction. Various boundary conditions are studied, and the effect of dimple locations and angles are investigated. Earlier studies demonstrated that the natural frequencies of each model represent a greater sensitivity to changes in dimple angle for dimples placed at high modal strain energy regions of a uniform beam. This study confirms the same behavior for both cases (beams with dimples in the same and opposite directions). Finally, conclusions have been drawn from both the analytical and experimental results for the two cases.

© 2016 Mofareh H. Ghazwani

ACKNOWLEDGMENTS

First and foremost, I would like to express how thankful I am to my advisor Dr.Koorosh Naghshineh, for his inspiration, tolerance, excellent guidance, unweaving confidence and support throughout this project. He has provided countless helpful suggestions and has pushed me to be my best. I am grateful to my committee member Dr. Rick Meyer for his assistance, confidence, and support on this project. Also, I express my gratitude to Dr. Kyle Myers, whose research started much of this work. I would like to thank him for his sound guidance and input, and for his time and effort. I would like to thank my wife, Aisha and my daughter Joanna, for their loving support and have provided me with strength and conviction to conclude this project. I wish to express my heartfelt gratitude for the government of Saudi Arabia in financing my studies and provided me with a generous scholarship. I am also very much obliged to Glenn Hall, WMU Lab technician, who helped me a lot in the manufacturing process of dimpled beam model. Thanks for my friends, Alla Attar, Aaron Dean, Blair LaCross, Hadi Madkhali, Hassan Fagehi, Hassan Ghazwani, Ibrahim Alnaghmouh and Varad Pendse, for their unconditional support. Finally, I would like to thank my wonderful parents Hassan and Salama for supporting me all throughout my educational studies. Their belief in my capacity to follow my dreams has guided me to achieve my goals education and it has made me who I am today. They are dearly missed.

Mofareh H. Ghazwani

TABLE OF CONTENTS

ACKNOWLEDGMENTS	ii
LIST OF TABLES	viii
LIST OF FIGURES	xii
NOMENCLATURE.....	xvii
1 INTRODUCTION AND OBJECTIVES.....	1
1.1 Overview.....	1
1.2 Dimpled Beams.....	1
1.3 Research Motivation	2
1.4 Thesis Objectives	3
1.5 Thesis Organization	4
2 PERTINENT LITERATURE.....	5
2.1 Overview of Hamilton’s Principle.....	5
2.2 Vibrations of Curved Structures	6
2.3 Literature on Dimpled Beams	6
3 ANALYTICAL MODEL OF VIBRATING BEAMS.....	9

3.1	The Boundary Value Model.....	9
3.1.1	Dimpled Beam Model.....	10
3.1.2	Formulation of the Lagrangian	11
3.1.3	Equations of Motion	14
3.1.4	Boundary Conditions at $x = 0$ and $\theta = \alpha$	15
3.1.5	Continuity Conditions at $x = l$	17
3.2	Analytical Model Development (Dimpled Beam Model)	22
3.2.1	Equations of Motion	23
3.2.2	Boundary Conditions at $x_1 = 0$ and $x_3 = l_3$	24
3.2.3	Continuity Conditions at $x_1 = l_1$ and $x_2 = 0$	25
3.2.4	Continuity Conditions at $x_2 = l_2$ and $x_3 = 0$	25
3.3	Solutions to the Equations of Motion	27
3.3.1	Straight Segments	27
3.3.2	Dimpled Segments.....	30
3.4	Formulation of the Coefficient Matrix.....	32
3.5	Sample Results of Natural Frequency and Mode Shape.....	38
3.5.1	Cantilever Beam	39
3.5.2	Fixed-Fixed Beam	43
4	FINITE ELEMENT MODEL.....	52
4.1	Dimpled Beam Modeling.....	52

4.2	Cantilever Beam Model	54
4.2.1	Geometrical and Material Properties	56
4.2.2	Uniform Cantilevered Beam Model	57
4.2.3	Calculation of Natural Frequencies for the Cantilever Dimpled Beam	57
4.2.4	Convergence Study	60
4.3	Fixed-Fixed Beam Model	60
4.3.1	Geometrical and Material Properties	61
4.3.2	Uniform Fixed-Fixed Beam Model	61
4.3.3	Calculation of Natural Frequencies for the Fixed-Fixed Dimpled Beam	61
4.3.4	Convergence Study	64
4.4	BVM Results vs. FE Results.....	64
4.4.1	Cantilevered Beam.....	65
4.4.2	Fixed-Fixed Beam	66
5	EXPERIMENTAL VALIDATION.....	68
5.1	Manufacturing Process of Dimpled Beam.....	68
5.2	Equipment and Specifications.....	70
5.3	Experiment Setup and Measurement Procedure	72
5.4	Experimental Results	79

5.4.1	Cantilever Beam	79
5.4.2	Fixed-Fixed Beam	81
5.5	Comparison of BVM, FEM, and Experimental Results	84
5.5.1	Cantilever Beam	84
5.5.2	Fixed-Fixed Beam	86
6	INVESTIGATION OF EFFICIENCY OF THE ANALYTICAL MODEL	88
6.1	Boundary Condition.....	88
6.1.1	Example 1: Pin-Pin Beam Model	88
6.1.2	Example 2: Pin-Pin Roller Beam Model	90
6.2	Effect of Dimple Location	91
6.2.1	Example 1: Pin-Pin Beam.....	91
6.2.2	Example 2: Fixed- Fixed Beam Model.....	106
6.3	Effect of Dimple Angle.....	112
6.3.1	Example 1: Pin-Pin Beam Model	112
6.3.2	Example 2: Fixed-Fixed Beam Model.....	120
7	CONCLUSION AND FUTURE WORK	125
7.1	Conclusion	125
7.2	Future Work.....	126
	REFERENCES.....	128

APPENDICES

A. MATLAB CODE (UNIFORM CANTILEVER BEAM)	130
B. PLOTTING MODE SHAPES OF DIMPLED BEAM	132
C. FINITE ELEMENT CODE (DIMPLED BEAM).....	135
D. FINITE ELEMENT CODE (UNIFORM BEAM).....	142

LSIT OF TABLES

3.1	Parameters for cantilever dimpled beam ($N = 2$).....	39
3.2	Values of transverse frequency parameter for the uniform cantilever beam .	40
3.3	Natural frequencies for the cantilever beam without dimples (uniform beam)	41
3.4	Comparison between natural frequencies of a uniform cantilever beam against one with two dimples in the same or opposite directions.....	42
3.5	Parameters for fixed-fixed dimpled beam ($N = 2$)	44
3.6	Values of parameters $\beta_n L$ for the uniform fixed-fixed beam	45
3.7	Comparison between natural frequencies of a uniform fixed-fixed beam against one with two dimples in the same or opposite directions	46
3.8	Comparison between the first three modes of the uniform fixed-fixed beam against one with two dimples in the same or opposite directions in terms of shifting the nodal points (zero crossings)	48
4.1	Parameters for cantilever dimpled beam ($N = 2$).....	56
4.2	A comparison between natural frequencies for a cantilever beam with two dimples for the two cases with and without dimples	58
4.3	Convergence of the natural frequencies for the cantilever dimpled beam, (dimples are in the opposite direction), with a different number of elements	60

4.4	Parameters for the fixed-fixed dimpled beam ($N = 2$).....	62
4.5	A comparison between natural frequencies for a fixed-fixed beam with two dimples for the two models.....	63
4.6	Convergence of the natural frequencies of the fixed-fixed dimpled beam, (dimples are in the opposite direction), with a different number of elements	64
4.7	First five natural frequencies for the cantilevered beam with two dimples in the same direction (BVM vs. FEM).....	65
4.8	First five natural frequencies for the cantilevered beam with two dimples in the opposite direction (BVM vs. FEM)	66
4.9	First five natural frequencies for the fixed-fixed beam with two dimples in the same direction (BVM vs. FEM).....	67
4.10	First five natural frequencies for the fixed-fixed beam with two dimples in the opposite direction (BVM vs. FEM)	67
5.1	Experiment equipment.....	71
5.2	Parameters for the cantilever dimpled beam ($N = 2$).....	76
5.3	Parameters for the fixed-fixed beam ($N = 2$).....	78
5.4	Comparison between natural frequencies for a cantilever beam with ($N = 2$) with and without dimples	79
5.5	Comparison between natural frequencies for a fixed-fixed beam ($N = 2$) with and without dimples.....	83

5.6	First five natural frequencies of the cantilever beam with two dimples in the same direction, Experiment vs. BVM vs. Finite Element.....	84
5.7	First five natural frequencies of the cantilever beam with two dimples in the opposite direction.....	85
5.8	First five natural frequencies of the fixed-fixed beam with two dimples in the same direction	86
5.9	First five natural frequencies of the fixed-fixed beam with two dimples in the opposite direction.....	87
6.1	First five natural frequencies for the pin-pin beam with two dimples in the same direction	89
6.2	First five natural frequencies for the pin-pin beam with two dimples in the opposing direction.....	89
6.3	First five natural frequencies for the pin-pin roller beam with two dimples in the same direction	90
6.4	First five natural frequencies for the pin-pin roller beam with two dimples in the opposing direction.....	90
6.5	Parameters for dimpled beams.....	91
6.6	Change in the fundamental frequency of pin-pin beam with two dimples in the same direction with respect to dimple location.....	93
6.7	Change in the second frequency of pin-pin beam with two dimples in the same direction with respect to dimple location.....	100

6.8	Change in the fundamental frequency of pin-pin beam with two dimples in the opposing direction with respect to change in dimple location.....	102
6.9	Change in the fundamental frequency of fixed-fixed beam with two dimples in the same direction with respect to dimple location.....	107
6.10	Change in the fundamental frequency of fixed-fixed beam with two dimples in the opposing direction with respect to dimple location	108
6.11	Modal strain energy parameters (fixed-fixed beam).....	110

LIST OF FIGURES

1.1	A beam with two straight segments and one arch segment	1
1.2	A dimpled beam with two dimples (convex and concave)	2
3.1	Schematic of a three-segment model: two straight segments and one dimple	10
3.2	Isometric view of a three-segment model	11
3.3	Isometric view of the two-segment model, straight segment and dimple (convex)	17
3.4	Isometric view of the two-segment model, straight segment and dimple (concave).....	18
3.5	Schematic of a two-segment model: one straight segment and one dimple (second model).....	20
3.6	Schematic of a beam with two dimples	22
3.7	Schematic of a beam with two straight segments and one dimple segment ..	33
3.8	A range of frequencies vs. determinant magnitude	38
3.9	A beam with two dimples in the same (a) and opposing (b) directions.....	39
3.10	First three mode shapes of the uniform fixed-fixed beam	45

3.11	First three mode shapes (fixed-fixed, a beam with two dimples in the same direction).....	47
3.12	First three mode shapes (fixed-fixed, a beam with two dimples in the opposing direction)	48
4.1	Schematic representation of a dimpled cantilever beam.....	53
4.2	ANSYS Beam3 (2D elastic beam) element.....	54
4.3	3D structure of a cantilever beam with two dimples in the same (a) and opposite directions (b).....	55
4.4	Cantilever beam without dimples (uniform beam)	57
4.5	Cantilever beam with two dimples in the same (a) and opposite (b) directions	58
4.6:	Two V-notch formed on a cantilever beam	59
5.1	The die and the punch which are used in the manufacturing of the dimpled beams [1].....	68
5.2	The beam is clamped well into the die, (a) and (b).....	69
5.3	Manufacturing process of dimpled beam in four steps, (a), (b), (c), and (d).	70
5.4	Experiment arrangement and instruments	72
5.5	Three possible places where the dimpled beam is excited using the impact hammer, (a) indicates point (1), (b) indicates point (2), and (c) indicates point (3).....	73

5.6	A four-channel (NI -9234) data acquisition card	74
5.7	Three beam models, a beam without dimples, a beam with dimples in the same direction, and a beam with dimples in opposite direction	75
5.8	Cantilever beam vibration excitation without (a) and with dimples (b)	75
5.9	Fixed-fixed beam model, (a) with two dimples in the same direction (a) and (b) two dimples in the opposing direction	77
5.10	The FRF of the cantilever beam before and after dimpling for two the cases	80
5.11	The FRF of the fixed-fixed beam before and after dimpling for two the cases	82
6.1	Pin-pin beam with two dimples in the same (a) and opposite (b) direction ..	92
6.2	Pin-pin beam with the highest change in the fundamental frequency	94
6.3	Pin-pin beam with the lowest change in the fundamental frequency	95
6.4	First three mode shapes of a uniform pin-pin beam	96
6.5	Modal strain energy, modes 1-3 (uniform pin-pin beam)	96
6.6	Change in the second frequency of pin-pin beam with two dimples in same direction	97
6.7	Pin-pin beam with the highest frequency for second mode	98
6.8	Pin-pin beam with two dimples in the same direction for the second mode)	99

6.9	Pin-pin beam with the lowest change in frequency for the second mode.....	100
6.10	Change in the fundamental frequency vs. dimple location (pin-pin beam).....	104
6.11	Change in the second frequency vs. dimple location (pin-pin beam).....	105
6.12	Fixed-fixed beam with the highest change in fundamental frequency (the beam with two dimples in the same direction)	109
6.13	Modal strain energy, modes 1-3 (uniform fixed-fixed beam).....	110
6.14	Change in the fundamental frequency vs. dimple locations (fixed-fixed beam)	111
6.15	Change in fundamental frequency vs. dimple location, five different dimple angles for the pin-pin beam with two dimples in the same direction	113
6.16	Change in fundamental frequency vs. dimple locations, five different dimple angles for the pin-pin beam with two dimples in the opposing direction	114
6.17	Change in fundamental frequency vs. dimple angles, three different dimple locations (pin-pin beam with two dimples in the same direction)	115
6.18	Change in fundamental frequency vs. dimple angles, three different dimple locations (pin-pin beam with two dimples in the opposing direction).....	116
6.19	Change in second frequency vs. dimple locations, five different dimple angles for pin-pin beam with two dimples in the opposing direction.....	117

6.20	Change in second frequency vs. dimple angles, four different dimple locations (pin-pin beam with two dimples in the same direction).....	118
6.21	Change in second frequency vs. dimple angles, four different dimple locations (pin-pin beam with two dimples in the opposing direction).....	119
6.22	Change in fundamental frequency vs. dimple location, five different dimple angles fixed-fixed beam (the beam with two dimples in the same direction)	120
6.23	Change in fundamental frequency vs. dimple location, five different dimple angles fixed-fixed beam (the beam with two dimples in the opposing direction)	121
6.24	Change in fundamental frequency vs. dimple angle, four different dimple locations (fixed-fixed beam with two dimples in the same direction).....	122
6.25	Change in fundamental frequency vs. dimple angle, four different dimple locations (fixed-fixed beam with two dimples in the opposing direction)	123
6.26	Change in second frequency vs. dimple location, five different dimple angles fixed-fixed beam (the beam with two dimples in the opposing direction)	124

NOMENCLATURE

Acronyms

BVM	Boundary Value Model
FEM	Finite Element Method
FEA	Finite Element Analysis
FRF	Frequency Response Function
MSE	Modal Strain Energy (per length)

General

$[\mathcal{A}]$	coefficient matrix
b	beam width
D_i	modal strain energy constant,
E	elastic modulus
f	natural frequency (dimpled beam) [Hz]
f^*	natural frequency (uniform beam) [Hz]
i	segment index number
j	imaginary unit, $j = \sqrt{-1}$
k	summation index
L	total beam length
$\delta\mathcal{L}$	Lagrangian functional
N	number of dimples
T	total kinetic energy functional
t	time
V	total strain energy functional

$\{X\}$	vector of modal coefficients
δ	first order variation
ρ	beam density
σ	modal strain energy per length
$\{\emptyset\}$	mass-normalized mode shape vector

Straight Segment Parameters

A_{ik}	transverse modal coefficient
C_{ik}	longitudinal modal coefficient
h	segment thickness
I	area moment of inertia, $bh^3/12$ in this study
l	segment length
q	roots of transverse characteristic equation
r	roots of longitudinal characteristic equation
S	cross-sectional area, bh in this study
T	kinetic energy functional
U	longitudinal coordinate (space only)
u	longitudinal coordinate (space and time)
v	strain energy functional
x	axial position, local coordinate
Y	transverse coordinate (space only)
y	transverse coordinate (space and time)
β	transverse frequency parameter
γ	longitudinal frequency parameter

Dimple Parameters (bar denotes equivalent dimple quantities)

B_{ik}	modal coefficient
D_{ik}	modal coefficient

\bar{h}	segment thickness
\bar{I}	area moment of inertia, $b\bar{h}^3/12$ in this study
\bar{l}	chord length
\mathcal{M}	bending moment
\mathcal{P}	tangential force
p_i	extensional vibration parameter
Q	radial shear force
R	radius
\bar{S}	cross-sectional area
s	roots of tangential and radial characteristic equation
\bar{T}	kinetic energy functional
V	tangential coordinate (space only)
\bar{v}	strain energy functional
W	radial coordinate (space only)
w	radial coordinate (space and time)
x_c	location of dimple center
α	dimple angle
ζ_i	frequency parameters
ζ_i	angular position, local coordinate
λ_{ik}	multiplicative constant for modal coefficient
v	tangential coordinate (space and time)
ψ	bending slope

CHAPTER 1

INTRODUCTION AND OBJECTIVES

1.1 Overview

Most of mechanical and civil engineering use beams heavily in structural design and commercial construction applications. Since beams are often subjected to dynamic excitations or moving loads and masses, reducing the vibration of these structures is a topic of interest and has been investigated by many researchers in engineering. Shifting the natural frequencies of a structure away from the frequency range of the excitation force is a significant method to improve the dynamics of the structure. Many methods can be used to reduce the vibration of structures. One of the newly emerging techniques is that of introducing dimples onto structure's surfaces. One or more dimples can be created on structure's surface to not only shifting the natural frequencies but also changing the mode shapes of the structure.

1.2 Dimpled Beams

Figure 1.1 represents an illustration of a single dimple connected to two straight segments on each side.

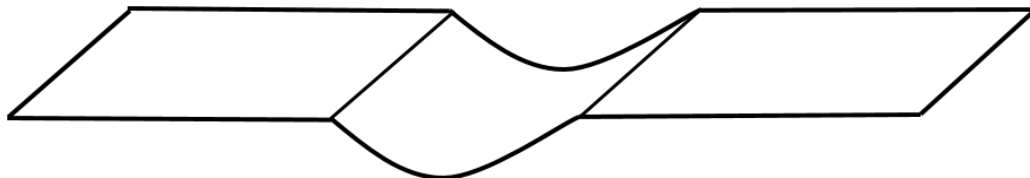


Figure 1.1: A beam with two straight segments and one arch segment.

When more than one dimple is present, it is assumed that each dimple is connected to a straight segment on each side [1]. The focus of this thesis is on the study of a beam with one and two

dimples. It is noted that in previous publications by others the word “dimple” may be referred to an “arch” or a “ring segment.” Leissa [2], defines the dimple as an open circular cylindrical shell which means that the radius of the dimple is assumed to be constant. Furthermore, throughout this study, terminologies “convex” and “concave” are used to define two types of dimples where the top view is considered the reference view (e.g., looking at the dimpled beam from the top view). The convex and concave referenced in this study refer to the type shown in Fig. 1.2. Using the terminology of Merriam-Webster [3], a “convex” is defined as curved or rounded outward like the exterior of a sphere or circle whereas “concave” is curved or rounded like the inside of the bowl which is curving inward.

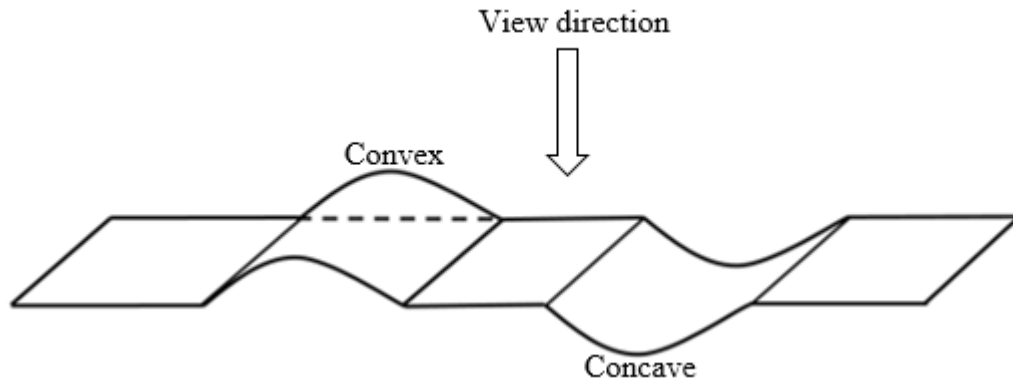


Figure 1.2: A dimpled beam with two dimples (convex and concave).

1.3 Research Motivation

The original motivation of this thesis was to extend the work of Myers [1] to investigate the change in natural frequencies of beams by creating two dimples in opposite direction on the beam’s surface. Since Myers’ work focused primarily on beams with dimples in one direction, in this thesis we will investigate the effect of creating two dimples in opposite direction (one concave and one convex) on shifting beam natural frequencies. This could conceivably be extended to the case of N dimples consisting of a mix of concave and convex direction. Another key point is to understand the “curvature effect” that is used to explain significant trends in natural frequencies of using two dimples in the same directions and using two dimples in the opposite directions and then comparing the natural frequencies for the two cases.

An important part regarding the modal strain energy arose during the study of the dynamics of dimpled beams with two dimples in the same and opposite direction. Al-shabatat [4] and Myers [1] suggested that the regions of high and low strain energy of a uniform beam (a beam without dimples) could use to design optimal dimpled beams where the dimples placed in these areas would exhibit a maximization, minimization, or no change in the natural frequencies for different dimple angles. The significant of using the modal strain energy could be utilized as a measurement to investigate the optimum dimples placement. Therefore, in this thesis, this concept will be used to understand the behavior of natural frequencies when two dimples in the same direction or opposite direction are placed in the areas of high or low modal strain energy of a uniform beam. The earlier studies focused on the fundamental frequency of beams with more than one dimple in the same direction. In this thesis, we will focus on the first five natural frequencies to investigate the change in the natural frequencies between the beam with two dimples in the same direction and the beam with two dimples in the opposite direction. The reason for focusing on the first five natural frequencies is that some boundaries may not exhibit a change in natural frequencies between the two cases mentioned previously. So, with investigating the higher modes, we can investigate the difference between the two cases mentioned above.

1.4 Thesis Objectives

The aim of this study is to study the change in natural frequencies of beams by creating two dimples in the opposite direction on the beam's surface. A stamping technique is used to create dimples in order to change the vibration characteristics of beam structures. The main objective of this method is to shift the natural frequencies away from the frequency of the excitation force by creating two dimples in the opposite direction on beam's surface. Also, this thesis will investigate the percentage change in the natural frequency by creating two dimples in the same and opposite direction on beam's surface. An analytical model of a beam with two dimples in the same and opposite direction is developed to predict the beam natural frequencies and mode shapes, also considering different boundary conditions. This can be obtained by using Hamilton's Variational Principle to develop an analytical model (i.e., a boundary value model, BVM) with two dimples. The notations used in this study are borrowed heavily from Dr. Myers who developed most of the equations presented here for his PhD dissertation [1]. Modeling and analysis of dimpled beams

are performed using *MATLAB*[®] and *ANSYS*[®]. Furthermore, the beam dimpling approach is validated experimentally, and all methods are compared in terms of the natural frequency results.

1.5 Thesis Organization

Chapter 2 presents a literature study relevant to this thesis. Chapter 3 contains a derivation of a boundary value model for a beam with two dimples. In Chapter 4 the results of the natural frequencies of the analytical model (BVM) will be checked using Finite Element Method (FEM). This will be followed by validating the results of natural frequencies for uniform and dimpled beams, which is obtained using BVM and FEM, experimentally. Next in Chapter 6, additional investigation on the analytical model will be studied. Finally, Chapter 7 contains a conclusions and the author's view of future work.

CHAPTER 2

PERTINENT LITERATURE

2.1 Overview of Hamilton's Principle

The importance of using a boundary value model is to describe a system governed by the equation of motion with various boundary conditions. Hamilton's Principle depends on formulating the kinetic and strain energy of the system. It is utilized to formulate a boundary value model of a dimpled beam. The reader can find some good references on Hamilton's Principle such as Meirovitch [5] and Rao [6] in which several examples are given on the transverse and longitudinal vibration of beams [5]. Rao [6] presents some excellent basic definitions such as a variational operator in Hamilton's Principle and gives some examples of using it. Moreover, Han et al. [7] examined four approximate models for a beam vibrating transversely: the Euler-Bernoulli, Rayleigh, shear, and Timoshenko models. Hamilton's Variational Principle was used to develop the equation of motion, boundary conditions and then inserting them into the Lagrangian. Then, the frequency equations are obtained and solved for the four boundary boundaries. Myers [1] also used Hamilton's Principle to develop an analytical model for a dimpled beam with any number of dimples. The dimpled beam is made of two types of segments: a straight and dimpled segment where the equations of motion for each segment is derived by Myers [1]. In one example, a fixed-fixed beam model is presented [8]. Then, Hamilton's principle is used to derive the equations of motion. A coefficient matrix for a beam with one dimple is formulated. The natural frequency and mode shapes are then found numerically.

2.2 Vibrations of Curved Structures

Many investigators have studied the vibrations of curved beams, Petyt and Fleischer [9] have investigated various boundary conditions in the free vibration of a curved beam. Chidamparam and Leissa [10] have presented many studies on vibrations of curved beams, arches, and rings where about 407 studies were collected. Lee and Hsiao [11] have analyzed the free vibration of curved non-uniform beams where they examined the effect of the center angles, taper ratio, and arch length on the beam natural frequencies. Henrych [12] also presented a study on development of mechanics and dynamics of arches and frames. Rao [13] also have published a study on the effect of transverse shear and rotary inertia on the coupled twist bending vibrations of circular rings. Also, the extensional and inextensional vibration of complete and incomplete rings were studied by Lang [14]. An equilibrium approach was used to develop the equations of motion of complete circular rings. In addition, a method was developed for uncoupling the equation of motion where his study considered free and forced vibration. Myers [1, p. 36] borrowed most of Lang's notation when he presented the process of obtaining the general solutions of equations of motion for dimple segments.

2.3 Literature on Dimpled Beams

Recently dimples and beads play a crucial role to improve the vibroacoustic of structures (beams, plates, shells). In one recent study of changing the natural frequencies of beams using the dimpling technique, Cheng et al [15] studied the shifting of the natural frequencies of beams to prescribed values. They used a series of cylindrical dimples on the beam's surface. They divided the dimpled beam into two kinds of structural segments: a curved beam which was modeled as a dimple and a straight beam. This study was based on finding combinations of dimple angles and locations to "tune" all natural frequencies to designated values using an impedance matching technique. The mass of the beam is assumed to be constant before and after creating dimples so the dimple segment is thinner than the straight segment. They presented an example of a simply supported beam and showed that its fundamental natural frequency decreased for all combinations of dimple angles and locations. They attributed this drop in the fundamental frequency to the

dimple thinning. Their stipulation was that the thinning of the dimple area resulted in a reduction in overall beam bending stiffness.

Cheng et al. [16] also presented a study that showed one could minimize the sound radiation from a vibrating beam. In their study, they used a finite element model of dimpled beams to calculate its natural frequencies and mode shapes. Their study showed a minimization in radiation efficiency of the dimpled beam compared to the beams without dimples.

Alshabat published two studies [17], [18] on vibration and acoustic properties of dimpled beams and plates where the finite elements method (FEM) was used to calculate the beam and plate vibration characteristics. The dimpling technique was used to alter the local stiffness of the beam with considering constant mass. ANSYS (finite element software package) was used to build the dimpled beam models and then to calculate the natural frequencies and mode shapes of the dimpled beams. An optimization technique based on genetic algorithm (GA) was used to design optimum dimpled beams. The results of the simulation were also compared to the experimental results where they showed a good agreement. The study suggested some manufacturing limitations must be taken into consideration such as “material capacity to deform plastically without cracking” [4]. Various boundary conditions were studied, for the case of simply supported and free-free beams, the fundamental natural frequencies decreased by creating dimples on its surface while the fundamental frequencies of fixed-fixed beams might be increased.

Myers et al. also published two studies [1], [8] on vibroacoustic properties and optimization of vibrating dimpled beams. Boundary Value model (BVM) was used for calculation of all vibration properties. It also was used to calculate the natural frequencies and mode shapes of dimpled beams in free transverse and longitudinal vibrations. A model was developed to describe the vibrations in the transverse and longitudinal displacement for the straight segment and also the tangential and radial displacement for the dimple (arch) segment. Natural frequencies and mode shapes were computed analytically for beams with any number of dimples (in the same direction) for various boundary conditions. He validated the accuracy of BVM by different ways. The dimpled beam was approximated as a uniform beam by letting the dimple angle about zero, and the results showed good in agreement to exact values. Moreover, Myers modeled an arch by considering a beam with one dimple where the straight segment length considered very small. The results were good comparing to arch studies.

It is evident from the literature that the studies conducted to date all treat the dimples in the same directions. Thus, there is a need to investigate the effect of creating dimples in the opposing directions on a beam surface with different boundary conditions. The natural frequencies and mode shapes obtained will then be compared to a straight beam (i.e., no dimples and beams with the dimples in the same direction. Modifications to the Boundary Values Model equations of the dimple segment is needed to account for a concave dimple as shown in the next chapter.

CHAPTER 3

ANALYTICAL MODEL OF VIBRATING BEAMS

In this study, the equations of motion, boundary conditions, and continuity conditions for a beam with a single straight segment connected to a dimple segment is derived using Hamilton's Variational Principle. In Section 3.2, a dimpled beam model with two dimples in opposing direction is developed. In Section 3.3, the general solutions to the equations of motion are given. Then, the formulation of the coefficient matrix of a beam with one dimple (concave) is presented in Section 3.4. This formulation relies heavily on Myers' research [1]. Finally, in Section 3.5, sample results of natural frequency and mode shape are given for two beam models with and without dimples.

3.1 The Boundary Value Model

The objective of this study is to investigate the change in natural frequencies of beams by creating dimples on beam's surface. An analytical model (i.e., a boundary value model, BVM) with any number of dimples in the same direction was developed by Myers [1]. The work presented here focuses on developing an analytical model with two dimples in opposite direction. The natural frequencies of a dimpled beam in transverse and longitudinal vibration will be computed. The model will describe the vibrations of the transverse and longitudinal displacement in the straight segments and the tangential and radial displacement in the dimples. In general, shear force and rotary inertia have an effect on the natural frequencies, but these effects are considered negligible and are neglected in this study. The notation used in this section is borrowed heavily from Dr. Myers who developed most of the equations presented here for his PhD's dissertation [1]. He derived equations of motion, boundary conditions, and continuity conditions for any combination of straight segments and N dimples.

This study derives the equations of motion, boundary conditions, and continuity conditions for a beam with two dimples in opposite direction. The equations of motion, boundary conditions are still the same for the beams with dimples in the opposite direction as the beams with dimples in the same direction, except for the continuity conditions. In Section 3.1.1, the two-segment model of Myers [1] will be shown, and in the following Sections 3.1.3 and 3.1.4, the derivation of equations of motion and boundary conditions originally presented by Myers [1] will be presented. Continuity conditions will be derived for two models in Sections 3.1.5.1 and 3.1.5.2. These are a straight segment connected to one dimple (convex) and respectively a straight segment connected to one dimple (concave). As we mentioned before, continuity conditions will be different for the case of using a straight segment connected to a dimple (convex) than the case of using a straight segment connected to a dimple (concave).

3.1.1 Dimpled Beam Model

Myers [1] derived the equations of the model which consists two segments, a straight segment connected to dimple segment. Figure 3.1 shows a schematic of a dimpled beam consisting of three segments where the lengths l_1 and l_2 is connected to an arched segment (dimple) with chord length \bar{l}_1 . Also, $u_1, u_2, y_1, y_2, v_1, v_2, w_1$, and w_2 define the eigenfunctions in the straight and dimple segments, respectively.

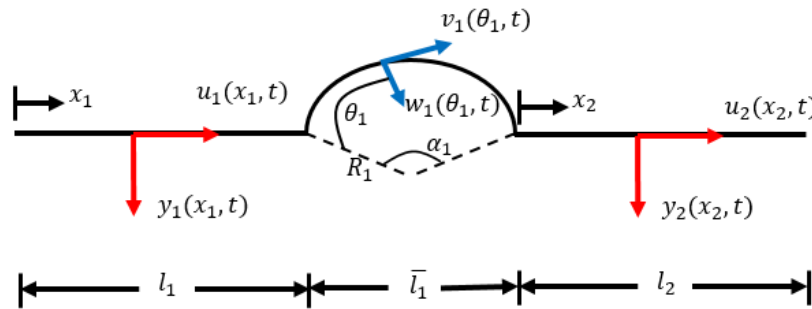


Figure 3.1: Schematic of a three-segment model: two straight segments and one dimple.

The dimple is defined by two parameters: a constant radius R and dimple angle α . It is assumed that the straight segment thickness h and the dimple segment thickness \bar{h} are uniform as shown in Fig. 3.2. Also, the beam width b is constant [1].

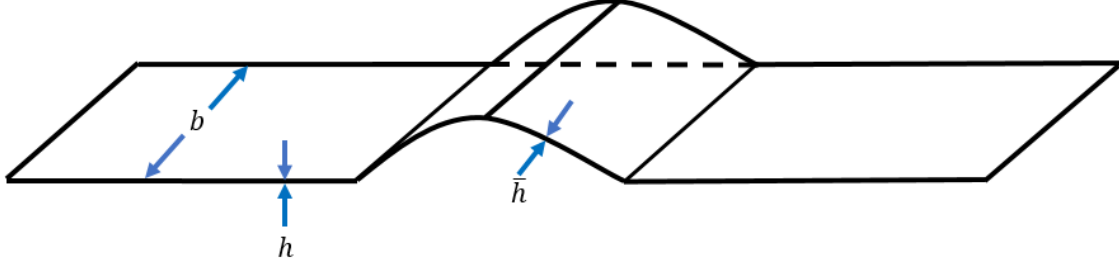


Figure 3.2: Isometric view of a three-segment model.

$$\begin{aligned} u(x, t), y(x, t) \quad 0 \leq x \leq l, \\ v(\theta, t), w(\theta, t) \quad 0 \leq \theta \leq \alpha, \end{aligned} \quad (3.1)$$

Equation (3.1) [1] represents the Eigen-functions in the straight segment (longitudinal and transverse) and the dimple (tangential and radial) which is defined over a local coordinate system. The coordinate systems as shown in Fig. 3.1 illustrates the positive directions.

The thickness of the dimple is defined such that the mass of the beam does not change. As such the relationship between the thickness of the straight segment and the dimple is defined as

$$\bar{h} = \frac{2 \sin(\alpha/2)}{\alpha} h, \quad (3.2)$$

where h and \bar{h} represent the original thickness of the beam and of the dimpled beam. Throughout this study, the dimple thickness is assumed to be uniform to simplify the mathematical model. In manufacturing process, dimple thickness (\bar{h}) is not uniform (the dimple is thicker at its center) .

3.1.2 Formulation of the Lagrangian

Hamilton's Principle is used to derive the equations of motion of the model [5, p. 44]

$$\delta \int_{t_1}^{t_2} (\mathcal{T} - \mathcal{V}) dt = 0, \quad (3.3)$$

where \mathcal{T} and \mathcal{V} are kinetic and strain energy functional, respectively. The total kinetic energy for the model shown in Fig 3.1, is equal to the kinetic energy of a straight segment [6, p. 652] and kinetic energy of the dimple [19], which is given by [1]

$$\mathcal{T}(t) = T(t) + \bar{T}(t), \quad (3.4a)$$

where

$$T(t) = \frac{1}{2} \rho S \int_0^l \left(\frac{\partial y}{\partial t} \right)^2 + \left(\frac{\partial u}{\partial t} \right)^2 dx, \quad (3.4b)$$

$$\bar{T}(t) = \frac{1}{2} \rho \bar{S} R \int_0^\alpha \left(\frac{\partial v}{\partial t} \right)^2 + \left(\frac{\partial w}{\partial t} \right)^2 d\theta. \quad (3.4c)$$

Also, the total strain energy is the sum of the strain energy from the straight segment [6, p. 652] and dimple [19], [1],

$$\mathcal{V}(t) = v(t) + \bar{v}(t), \quad (3.5a)$$

where

$$v(t) = \frac{1}{2} EI \int_0^l \left(\frac{\partial^2 y}{\partial x^2} \right)^2 dx + \frac{1}{2} ES \int_0^l \left(\frac{\partial u}{\partial x} \right)^2 dx, \quad (3.5b)$$

$$\bar{v}(t) = \frac{1}{2} \frac{E\bar{I}}{R^3} \int_0^\alpha \left(\frac{\partial v}{\partial \theta} + \left(\frac{\partial^2 w}{\partial \theta^2} \right) \right)^2 d\theta + \frac{1}{2} \frac{E\bar{S}}{R} \int_0^\alpha \left(\frac{\partial v}{\partial \theta} - w \right)^2 d\theta. \quad (3.5c)$$

Now, inserting equations (3.4)-(3.5) into equation (3.3) to formulate the Lagrangian for the two-segment model [1]. Then, applying the first order variation δ to each term and commutative property can be used yields [6, p. 89], [1],

$$\begin{aligned}
& \int_{t_1}^{t_2} \left\{ \rho S \int_0^l \frac{\partial y}{\partial t} \frac{\partial}{\partial t} (\delta y) + \frac{\partial u}{\partial t} \frac{\partial}{\partial t} (\delta u) dx + \rho \bar{S} R \int_0^\alpha \frac{\partial v}{\partial t} \frac{\partial}{\partial t} (\delta v) \right. \\
& \quad + \frac{\partial w}{\partial t} \frac{\partial}{\partial t} (\delta w) d\theta - EI \int_0^l \frac{\partial^2 y}{\partial x^2} \frac{\partial}{\partial x^2} (\delta y) dx \\
& \quad - ES \int_0^l \frac{\partial u}{\partial x} \frac{\partial}{\partial x} (\delta u) dx \\
& \quad - \frac{E\bar{I}}{R^3} \int_0^\alpha \left(\frac{\partial v}{\partial \theta} + \frac{\partial^2 w}{\partial \theta^2} \right) \left(\frac{\partial}{\partial \theta} (\delta v) + \frac{\partial^2}{\partial \theta^2} (\delta w) \right) d\theta \\
& \quad \left. - \frac{E\bar{S}}{R} \int_0^\alpha \left(\frac{\partial v}{\partial \theta} - w \right) \left(\frac{\partial}{\partial \theta} (\delta v) - \delta w \right) d\theta \right\} dt = 0. \tag{3.6}
\end{aligned}$$

By integrating each variation by parts where we have to integrate each variation a number of times which equal the operator acting on. Equation (3.6) can be integrated and similar variations grouped yields

$$\int_{t_1}^{t_2} \delta \mathcal{L} dt = 0, \tag{3.7}$$

where $\delta \mathcal{L}$ is the Lagrangian functional which is given by [1]

$$\begin{aligned}
\delta \mathcal{L} = & \int_0^l \left[-\rho S \frac{\partial^2 y}{\partial t^2} - EI \frac{\partial^4 y}{\partial x^4} \right] \delta y dx \\
& + \int_0^l \left[-\rho S \frac{\partial^2 u}{\partial t^2} + ES \frac{\partial^2 u}{\partial x^2} \right] \delta u dx \\
& \int_0^\alpha \left[-\rho \bar{S} R \frac{\partial^2 v}{\partial t^2} + \frac{E\bar{I}}{R^3} \left(\frac{\partial^2 v}{\partial \theta^2} + \frac{\partial^3 w}{\partial \theta^3} \right) + \dots \right]
\end{aligned}$$

$$\begin{aligned}
& -\frac{E\bar{S}}{R}\left(\frac{\partial w}{\partial\theta} + \frac{\partial^2 v}{\partial\theta^2}\right)\delta v d\theta \\
& + \int_0^\alpha \left[-\rho\bar{S}R\frac{\partial^2 w}{\partial t^2} - \frac{E\bar{I}}{R^3}\left(\frac{\partial^3 v}{\partial\theta^3} + \frac{\partial^4 w}{\partial\theta^4}\right) + \dots \right. \\
& \quad \left. + \frac{E\bar{S}}{R}\left(\frac{\partial v}{\partial\theta} - w\right) \right] \delta w d\theta \\
& + \left[-EI\frac{\partial^2 y}{\partial x^2}\frac{\partial}{\partial x}(\delta y) + EI\frac{\partial^3 y}{\partial x^3}(\delta y) - ES\frac{\partial u}{\partial x}\delta u \right] \Bigg|_{x=0}^{x=l} \\
& + \left[-\frac{E\bar{S}}{R}\left(\frac{\partial v}{\partial\theta} - w\right)\delta v + \frac{E\bar{I}}{R^3}\left(\frac{\partial^2 v}{\partial\theta^2} + \frac{\partial^3 w}{\partial\theta^3}\right)\delta w + \dots \right. \\
& \quad \left. - \frac{E\bar{I}}{R^2}\left(\frac{\partial v}{\partial\theta} + \frac{\partial^2 w}{\partial\theta^2}\right)\frac{1}{R}\left(\delta v + \frac{\partial}{\partial\theta}(\delta w)\right) \right] \Bigg|_{\theta=0}^{\theta=\alpha}.
\end{aligned} \tag{3.7a}$$

Now, we can obtain the equations of motion, boundary conditions and continuity conditions from Eq. (3.7a)

3.1.3 Equations of Motion

Inspections of Eq. (3.7a), it is shown that the expressions in brackets inside each of the four integrals are all zero. Thus, the equations of motion of the two-segment beam are given by

$$\rho S \frac{\partial^2 y}{\partial t^2} + EI \frac{\partial^4 y}{\partial x^4} = 0, \tag{3.8}$$

$$\rho S \frac{\partial^2 u}{\partial t^2} - ES \frac{\partial^2 u}{\partial x^2} = 0, \tag{3.9}$$

$$\rho\bar{S}R\frac{\partial^2 v}{\partial t^2} - \frac{E\bar{I}}{R^3}\left(\frac{\partial^2 v}{\partial\theta^2} + \frac{\partial^3 w}{\partial\theta^3}\right) - \frac{E\bar{S}}{R}\left(\frac{\partial^2 v}{\partial\theta^2} - \frac{\partial w}{\partial\theta}\right) = 0, \tag{3.10}$$

$$\rho\bar{S}R\frac{\partial^2 w}{\partial t^2} + \frac{E\bar{I}}{R^3}\left(\frac{\partial^3 v}{\partial\theta^3} + \frac{\partial^4 w}{\partial\theta^4}\right) - \frac{E\bar{S}}{R}\left(\frac{\partial v}{\partial\theta} - w\right) = 0. \tag{3.11}$$

Equation (3.8) defines the free transverse vibrations of the straight segment [6, pp. 236, 325]. It is obvious that shear deformation and rotary inertia are negligible in this equation. Equation (3.9) defines the longitudinal vibrations of the straight segment [6, pp. 236, 325]. Equations (3.10) and (3.11) governs the free tangential and radial vibrations of the dimple. Both Eqs. (3.10) and (3.11) are coupled differential equations, which means the variable (v) and (w) appear in each equation. The uncoupled equations can be obtained by algebraic manipulation of the differential operators acting on (v) and (w) [14]. Therefore, the uncoupled equations are given by [1]

$$\begin{aligned} \frac{\partial^6 v}{\partial \theta^6} + 2 \frac{\partial^4 v}{\partial \theta^4} - \frac{\rho R^2}{E} \frac{\partial^6 v}{\partial t^2 \partial \theta^4} + \frac{\partial^2 v}{\partial \theta^2} + \frac{\rho R^2}{E} \frac{\partial^4 v}{\partial t^2 \partial \theta^2} \\ + \frac{\rho \bar{S} R^4}{E \bar{I}} \frac{\partial^4 v}{\partial t^2 \partial \theta^2} - \frac{\rho \bar{S} R^4}{E \bar{I}} \frac{\partial^2 v}{\partial t^2} - \frac{\rho^2 \bar{S} R^6}{E^2 \bar{I}} \frac{\partial^4 v}{\partial t^4} = 0, \end{aligned} \quad (3.12)$$

$$\begin{aligned} \frac{\partial^6 w}{\partial \theta^6} + 2 \frac{\partial^4 w}{\partial \theta^4} - \frac{\rho R^2}{E} \frac{\partial^6 w}{\partial t^2 \partial \theta^4} + \frac{\partial^2 w}{\partial \theta^2} + \frac{\rho R^2}{E} \frac{\partial^4 w}{\partial t^2 \partial \theta^2} \\ + \frac{\rho \bar{S} R^4}{E \bar{I}} \frac{\partial^4 w}{\partial t^2 \partial \theta^2} - \frac{\rho \bar{S} R^4}{E \bar{I}} \frac{\partial^2 w}{\partial t^2} - \frac{\rho^2 \bar{S} R^6}{E^2 \bar{I}} \frac{\partial^4 w}{\partial t^4} = 0, \end{aligned} \quad (3.13)$$

3.1.4 Boundary Conditions at $x = 0$ and $\theta = \alpha$

By inspections of equation (3.7), the boundary conditions of the two-segment beam model can be demonstrated. So, the boundary conditions can be obtained at $x = 0$ (the left edge of the straight segment [1])

$$\left[EI \frac{\partial^2 y}{\partial x^2} \frac{\partial}{\partial x} (\delta y) - EI \frac{\partial^3 y}{\partial x^3} \delta y + ES \frac{\partial u}{\partial x} \delta u \right] \Bigg|_{x=0} = 0. \quad (3.14)$$

Because of the fact that the first order variations of the eigenfunctions are arbitrary over their domains and independent of each other, all of the three terms should be zero [1]. As a result, two boundary conditions are needed for transverse motion and one boundary condition is needed for longitudinal motion [1]

$$\left[EI \frac{\partial^2 y}{\partial x^2} \frac{\partial}{\partial x} (\delta y) \right] \Big|_{x=0} = 0, \quad (3.15a)$$

$$\left[EI \frac{\partial^3 y}{\partial x^3} \delta y \right] \Big|_{x=0} = 0, \quad (3.15b)$$

$$\left[ES \frac{\partial u}{\partial x} \delta u \right] \Big|_{x=0} = 0, \quad (3.15c)$$

where it is obvious that from Eq. (3.15), at $x = 0$, either $EI (\partial^2 y / \partial x^2)$ (the bending moment), or $(\partial y / \partial x)$ (the bending slope) is zero. Also, $EI (\partial^3 y / \partial x^3)$ (the shear force) or transverse deflection is zero. In addition, $ES (\partial u / \partial x)$ (axial force) or the longitudinal deflection is zero. From Eq. (3.7), three boundary conditions on the dimple at $\theta = \alpha$ are computed by setting the last bracket term equal to zero [1]. Similarly, each of the three terms is equal to zero because the variations are arbitrary over their domains and independent of each other [1]. As a result, three equations are defined under these conditions [1]:

$$\mathcal{M} \delta \psi |^{\theta=\alpha} = 0, \quad (3.16a)$$

where: \mathcal{M} = bending moment and $\delta \psi$ = bending slope.

$$Q \delta w |^{\theta=\alpha} = 0, \quad (3.16b)$$

where: Q = radial shear and δw = radial deflection.

$$\mathcal{P}\delta v|_{\theta=\alpha} = 0, \quad (3.16c)$$

where: \mathcal{P} = tangential force and δv = tangential deflection.

In addition:

$$\psi = \frac{1}{R} \left(v + \frac{\partial w}{\partial \theta} \right), \quad (3.17)$$

$$\mathcal{M} = \frac{E\bar{I}}{R^2} \left(\frac{\partial v}{\partial \theta} + \frac{\partial^2 w}{\partial \theta^2} \right), \quad (3.18)$$

$$\mathcal{Q} = \frac{E\bar{I}}{R^3} \left(\frac{\partial^2 v}{\partial \theta^2} + \frac{\partial^3 w}{\partial \theta^3} \right), \quad (3.19)$$

$$\mathcal{P} = \frac{E\bar{S}}{R} \left(\frac{\partial v}{\partial \theta} - w \right). \quad (3.20)$$

3.1.5 Continuity Conditions at $x = l$

In this section, continuity conditions at $x = l$ are obtained for two models. First, a model of a beam with combination of straight segment and dimple (convex) segment (see Fig. 3.3) is derived.

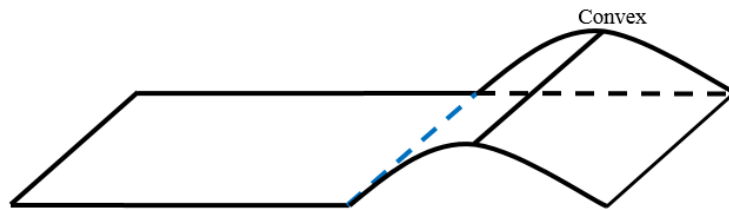


Figure 3.3: Isometric view of the two-segment model, straight segment and dimple (convex). The dashed line represents the location where the straight segment and dimple meet.

Next, a model of a beam with a combination of straight segment and dimple (concave) segment as shown in Fig. 3.4 is derived.

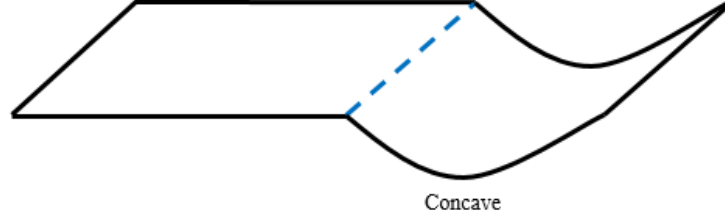


Figure 3.4: Isometric view of the two-segment model, straight segment and dimple (concave), the dashed line represents the location where the straight segment and dimple meet.

3.1.5.1 Continuity Conditions at $x = l$ (Convex dimple)

Figure 3.1 illustrates that the straight segment at $x = l$ is joined to the dimple at $\theta = 0$ where six continuity conditions are needed at this location. So, the solutions to the Eqs. (3.8), (3.9), (3.12), and (3.13) must satisfy these conditions of continuity. To find the conditions of continuity, we have to set sum of the bracketed portion in Eq. (3.7) terms evaluated at $x = l$ and $\theta = 0$ [1], such that

$$\begin{aligned}
 & \left[-EI \frac{\partial^2 y}{\partial x^2} \frac{\partial}{\partial x} (\delta y) + EI \frac{\partial^3 y}{\partial x^3} \delta y - ES \frac{\partial u}{\partial x} \delta u \right] \Bigg|_{x=l} \\
 & + \left[\frac{EI}{R^2} \left(\frac{\partial v}{\partial \theta} + \frac{\partial^2 w}{\partial \theta^2} \right) \delta \psi - \frac{EI}{R^3} \left(\frac{\partial^2 v}{\partial \theta^2} + \frac{\partial^3 w}{\partial \theta^3} \right) \delta w \right. \\
 & \left. + \frac{ES}{R} \left(\frac{\partial v}{\partial \theta} - w \right) \delta v \right] \Bigg|_{\theta=0} = 0.
 \end{aligned} \tag{3.21}$$

Equation (3.21) contains six different variations ($\delta u, \delta y, \delta y', \delta v, \delta w, \delta w'$), where prime means the slope. Three different variations can be eliminated using three geometrical conditions of continuity (i.e. horizontal and vertical deflection, slope). Figure 3.1 illustrates how the straight and dimple segments are connected both horizontally and vertically at all times. The geometrical conditions are inserted into Lagrangian functional to obtain three natural conditions (moment, axial and shear force). Thus, the following relation [1] is obtained

$$\begin{Bmatrix} u(l, t) \\ y(l, t) \end{Bmatrix} = \begin{bmatrix} \cos(\alpha/2) & \sin(\alpha/2) \\ -\sin(\alpha/2) & \cos(\alpha/2) \end{bmatrix} \begin{Bmatrix} v(0, t) \\ w(0, t) \end{Bmatrix}. \quad (3.22)$$

The above equation demonstrates a clockwise rotation of $(\alpha/2)$ degrees in horizontal and vertical directions. Moreover, the bending is continuous [1] , so

$$y'(l, t) \equiv \frac{\partial y(l, t)}{\partial x} = \frac{1}{R} (v(0, t) + w'(0, t)), \quad (3.23)$$

governs the slope. By substituting of expressions $y(l, t)$, $y'(l, t)$ and $w(0, t)$ into equation (3.21) and grouping similar remaining variations in $\delta u(l, t)$, $\delta v(0, t)$, $\delta w'(0, t)$, three equilibrium conditions are computed. The following equation [1] represents equilibrium of moment force at $x = l$ and $\theta = 0$,

$$EI \frac{\partial^2 y(l, t)}{\partial x^2} = \frac{E\bar{I}}{R^2} (v'(0, t) + w''(0, t)). \quad (3.24)$$

Also, Eq. (3.25) represents equilibrium of axial force at $x = l$ and $\theta = 0$, where the radial shear force in the dimple is transformed by a rotation matrix into force components in the horizontal and vertical directions [1].

$$\begin{aligned} ES \frac{\partial u(l, t)}{\partial x} &= \frac{E\bar{S}}{R} (v'(0, t) - w(0, t)) \cos\left(\frac{\alpha}{2}\right) \\ &\quad - \frac{E\bar{I}}{R^3} (v''(0, t) + w'''(0, t)) \sin\left(\frac{\alpha}{2}\right). \end{aligned} \quad (3.25)$$

In addition, the following equation defines equilibrium of shear force at $x = l$ and $\theta = 0$, where the tangential shear force in the dimple is transformed by a rotation matrix into force components in the horizontal and vertical directions [1].

$$EI \frac{\partial^3 y(l, t)}{\partial x^3} = \frac{E\bar{S}}{R} (v'(0, t) - w(0, t)) \sin\left(\frac{\alpha}{2}\right) + \frac{E\bar{I}}{R^3} (v''(0, t) + w'''(0, t)) \cos\left(\frac{\alpha}{2}\right), \quad (3.26)$$

where primes indicate derivatives with respect to θ . For instance, $v' = (\partial v / \partial \theta)$, $v'' = (\partial^2 v / \partial \theta^2)$ and $v''' = (\partial^3 v / \partial \theta^3)$.

3.1.5.2 Continuity Conditions at $x = l$ (Concave dimple)

Similarly, we need the continuity conditions where the straight segment meets the dimple segment at $x = l$ and $\theta = 0$ as shown in Fig. (3.5).

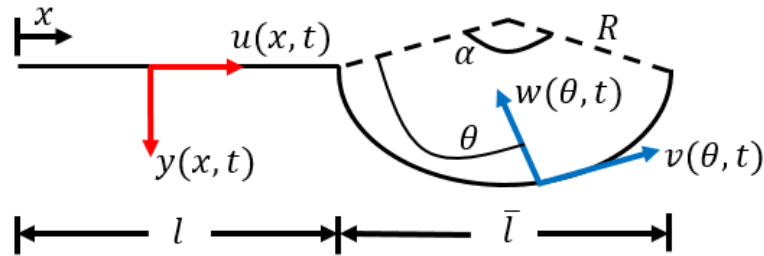


Figure 3.5: Schematic of a two-segment model: one straight segment and one dimple (second model).

We need six continuity conditions at this location. To find the conditions of continuity, we have to set sum of the bracketed portion in Eq. (3.7) terms evaluated at $x = l$ and $\theta = 0$, such that

$$\left[-EI \frac{\partial^2 y}{\partial x^2} \frac{\partial}{\partial x} + EI \frac{\partial^3 y}{\partial x^3} \delta y - ES \frac{\partial u}{\partial x} \delta u \right] \Big|_{x=l} + [\mathcal{M} \delta \psi - \mathcal{Q} \delta w + \mathcal{P} \delta v] \Big|_{\theta=0} = 0. \quad (3.27)$$

Equation (3.27) contains six different variations ($\delta u, \delta y, \delta y', \delta v, \delta w, \delta w'$), where prime means the slope. Figure 3.5 illustrates how the straight segment and dimple are connected both horizontally and vertically at all times. Thus, the following relation is obtained

$$\begin{Bmatrix} u(l, t) \\ y(l, t) \end{Bmatrix} = \begin{bmatrix} \cos(\alpha/2) & \sin(\alpha/2) \\ \sin(\alpha/2) & -\cos(\alpha/2) \end{bmatrix} \begin{Bmatrix} v(0, t) \\ w(0, t) \end{Bmatrix}. \quad (3.28)$$

As shown in Fig. 3.5 the relative orientations of the eigenfunctions are essential for writing the equations of continuity where the two segments meet. As a check, note that when the dimple becomes flat ($\alpha/2$ goes to zero), the radial and transverse components align in opposite direction, as do the tangential and longitudinal components. This means, the matrix reduces to $\begin{bmatrix} 1 & 0 \\ 0 & -1 \end{bmatrix}$ because the transverse displacement (y) and radial displacement (w) are in opposite direction. Moreover, the slope due to the bending is continuous because the connection is assumed to be rigid. Thus, the slope due to the bending can be obtained using the following equation,

$$y'(l, t) \equiv \frac{\partial y(l, t)}{\partial x} = -\psi(0, t). \quad (3.29)$$

The physical meaning of this equation is apparent. For instance, if the radial displacement (w) at a point just to the right of another point is larger, $w_2(\alpha + d\alpha) > w_1(\alpha)$, the dimple will deflect up. So, the slopes are opposite, and that's why we need a negative in the front of Eq. (3.29). Furthermore, it follows from the slope that the dimple moment (3.24) needs a negative in front of it. The following three equilibrium conditions are obtained as the same criterion mentioned in Section 3.1.5.1:

$$EI \frac{\partial^2 y(l, t)}{\partial x^2} = -\mathcal{M}(0, t), \quad (3.30)$$

$$ES \frac{\partial u(l, t)}{\partial x} = \mathcal{P}(0, t) \cos\left(\frac{\alpha}{2}\right) - \mathcal{Q}(0, t) \sin\left(\frac{\alpha}{2}\right), \quad (3.31)$$

$$EI \frac{\partial^3 y(l, t)}{\partial x^3} = -\mathcal{P}(0, t) \sin\left(\frac{\alpha}{2}\right) - \mathcal{Q}(0, t) \cos\left(\frac{\alpha}{2}\right). \quad (3.32)$$

In summary, the two-segment model needs to be described by four equations of motions (two for each segment) which are given by Eqs. (3.8-3.11). Six boundary conditions are required where Eq. (3.15) is given for the straight segment, and Eq. (3.16) is given for the dimple. The total numbers of continuity conditions that exist at $x = l$ and $\theta = 0$ are six. The continuity conditions for the convex dimple are given in Eqs. (3.22)-(3.26) [1]. The continuity conditions for the concave dimple are given in Eqs. (3.28)-(3.32). Therefore, twelve un-determined coefficients can be obtained in general solution for the two segment model.

3.2 Analytical Model Development (Dimpled Beam Model)

The purpose of this section is to generalize the equation developed in section 3.1 to describe a beam with two dimples. This study considers a beam with two dimples ($N=2$) in the opposing direction as shown in Fig. 3.6.

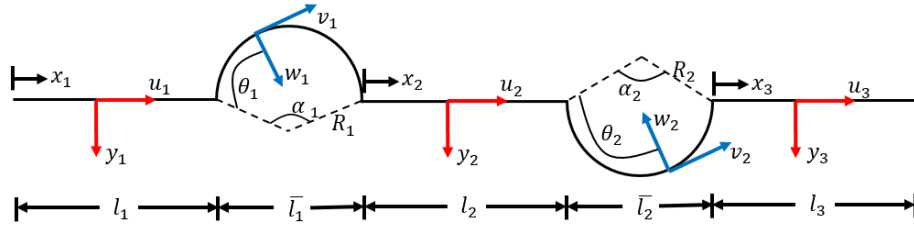


Figure 3.6: Schematic of a beam with two dimples.

The model can be defined by the longitudinal displacements (u_1) , (u_2) and (u_3) and by transverse displacements (y_1) , (y_2) and (y_3) where this model can be defined locally over $0 \leq x_1 \leq l_1$, $0 \leq x_2 \leq l_2$ and $0 \leq x_3 \leq l_3$ for the three straight segment. Similarly, the tangential and radial displacement v_1 , v_2 , w_1 and w_2 are defined locally over $0 \leq \theta_1 \leq \alpha_1$ and $0 \leq \theta_2 \leq \alpha_2$, respectively for the two dimple. Formulation of the Lagrangian for this model is follows the same procedure that was given in Section 3.1. The total kinetic and strain energy for the model shown in Fig. 3.6, is equal to ten integrals. Five integrals for straight segments and dimple segments given

by the form of Eqs. (3.4b)-(3.4c) are needed to describe the kinetic energy. Similarly, to compute the strain energy of the straight segments and dimple segments, five integrals given by the form of Eqs. (3.5b)-(3.5c) are required. Then, Equation of motions, boundary conditions, and continuity conditions can be obtained by using the Lagrangian ($\mathcal{T} - \mathcal{V}$) where additional terms will be added. The following sections are heavily borrowed from Myers [1] where this study also derived the same equations for the model of a beam with two dimples in opposite direction. Unlike the equations of motion and boundary conditions, conditions for continuity are different when creating dimple (concave) on it comparing to the continuity conditions in the case of beam with a dimple (convex).

3.2.1 Equations of Motion

The equations of motions that govern the straight segments where $i = 1, 2, \dots, N + 1$, with N dimples in general are given by

$$\rho S \frac{\partial^2 y_i}{\partial t^2} + EI \frac{\partial^4 y_i}{\partial x_i^4} = 0, \quad (3.33)$$

$$\rho S \frac{\partial^2 u_i}{\partial t^2} - ES \frac{\partial^2 u_i}{\partial x_i^2} = 0. \quad (3.34)$$

In this thesis, we consider a beam with two dimples ($N = 2$). In other words, Eqs.(3.33)-(3.34) will be repeated for $i = 1, 2, 3$ to describe the equations of motion for all three straight segments. Furthermore, the uncoupled equations of motion that govern the i^{th} dimple where $i = 1, 2, \dots, N$ (in this thesis: $N = 2$) are given by

$$\begin{aligned} & \frac{\partial^6 v_i}{\partial \theta_i^6} + 2 \frac{\partial^4 v_i}{\partial \theta_i^4} - \frac{\rho R_i^2}{E} \frac{\partial^6 v_i}{\partial t^2 \partial \theta_i^4} + \frac{\partial^2 v_i}{\partial \theta_i^2} + \frac{\rho R_i^2}{E} \frac{\partial^4 v_i}{\partial t^2 \partial \theta_i^2} \\ & + \frac{\rho \bar{S}_i R_i^4}{E \bar{I}_i} \frac{\partial^4 v_i}{\partial t^2 \partial \theta_i^2} - \frac{\rho \bar{S}_i R_i^4}{E \bar{I}_i} \frac{\partial^2 v_i}{\partial t^2} - \frac{\rho^2 \bar{S}_i R_i^6}{E^2 \bar{I}} \frac{\partial^4 v_i}{\partial t^4} = 0, \end{aligned} \quad (3.35)$$

$$\begin{aligned}
& \frac{\partial^6 w_i}{\partial \theta_i^6} + 2 \frac{\partial^4 w_i}{\partial \theta_i^4} - \frac{\rho R_i^2}{E} \frac{\partial^6 w_i}{\partial t^2 \partial \theta_i^4} + \frac{\partial^2 w_i}{\partial \theta_i^2} + \frac{\rho R_i^2}{E} \frac{\partial^4 w_i}{\partial t^2 \partial \theta_i^2} \\
& + \frac{\rho \bar{S} R_i^4}{E \bar{I}_i} \frac{\partial^4 w_i}{\partial t^2 \partial \theta_i^2} - \frac{\rho \bar{S}_i R_i^4}{E \bar{I}_i} \frac{\partial^2 w_i}{\partial t^2} - \frac{\rho^2 \bar{S}_i R_i^6}{E^2 \bar{I}} \frac{\partial^4 w_i}{\partial t^4} = 0.
\end{aligned} \tag{3.36}$$

Myers throughout his study [1] assumed that the straight segments have the same thickness unlike the thickness of the dimple segments is not the same because each dimple has different geometry (see Eq. (3.2)).

3.2.2 Boundary Conditions at $x_1 = 0$ and $x_3 = l_3$

This study considers that the dimples are located between two straight segments. Thus, six boundary conditions are required, three at $x_1 = 0$ and three at $x_3 = l_3$. These are previously derived for the straight segment in Section 3.1.4,

$$\left[EI \frac{\partial^2 y_1}{\partial x^2} \frac{\partial}{\partial x} (\delta y_1) = EI \frac{\partial^3 y_1}{\partial x^3} \delta y_1 = ES \frac{\partial u_1}{\partial x} \delta u_1 \right] \Bigg|_{x=0} = 0, \tag{3.37}$$

$$\left[EI \frac{\partial^2 y_3}{\partial x^2} \frac{\partial}{\partial x} (\delta y_3) = EI \frac{\partial^3 y_3}{\partial x^3} (\delta y_3) = ES \frac{\partial u_3}{\partial x} \delta u_3 \right] \Bigg|_{x=l_3} = 0, \tag{3.38}$$

Different boundary conditions are considered in this study and listed below for convenience.

- 1- Fixed: $u = y = y' = 0$.
- 2- Free: $u' = y'' = y''' = 0$.
- 3- Pin support: $u = y = y'' = 0$.
- 4- Pin support on roller (horizontal motion): $u' = y = y'' = 0$.

The primes indicate derivatives with respect to x , and each function should be evaluated at either boundary, $x_1 = 0$ or $x_3 = l_3$.

3.2.3 Continuity Conditions at $x_1 = l_1$ and $x_2 = 0$

The reader is referred to Section 3.1.5.1. for the derivation of the continuity conditions for the beam with one straight segment connected to dimple (convex). Equations (3.22)-(3.26) describes the continuity conditions where the right end of a straight segment meets the left end of the first dimple (convex). Also, there is another set of six conditions exist on the right end of this dimple with $-\alpha/2$. In the next section, the continuity conditions for the second dimple (concave, Fig. 3.6) will be derived in details.

3.2.4 Continuity Conditions at $x_2 = l_2$ and $x_3 = 0$

The continuity conditions on the right end of a straight segment when it meets the left end of the dimple segment are presented here. The beam with one straight segment connected to dimple (concave), which was presented in Section 3.1.5.2 is considered in this section. It is assumed that the dimples are located between two straight segments. These conditions can be applied to the model of a beam with two dimples at $x_2 = l_2$ and $\theta_2 = 0$. Therefore, the following conditions for continuity are given by

$$\begin{Bmatrix} u_2(l_2, t) \\ y_2(l_2, t) \end{Bmatrix} = \begin{bmatrix} \cos(\alpha_2/2) & \sin(\alpha_2/2) \\ \sin(\alpha_2/2) & -\cos(\alpha_2/2) \end{bmatrix} \begin{Bmatrix} v_2(0, t) \\ w_2(0, t) \end{Bmatrix}, \quad (3.39a)$$

$$\frac{\partial y_2(l_2, t)}{\partial x} = -\psi_2(0, t), \quad (3.39b)$$

$$EI \frac{\partial^2 y_2(l_2, t)}{\partial x^2} = -\mathcal{M}_2(0, t), \quad (3.39c)$$

$$ES \frac{\partial u_2(l_2, t)}{\partial x} = \mathcal{P}_2(0, t) \cos\left(\frac{\alpha_2}{2}\right) - \mathcal{Q}_2(0, t) \sin\left(\frac{\alpha_2}{2}\right), \quad (3.39d)$$

$$EI \frac{\partial^3 y_2(l_2, t)}{\partial x^3} = -\mathcal{P}_2(0, t) \sin\left(\frac{\alpha_2}{2}\right) - \mathcal{Q}_2(0, t) \cos\left(\frac{\alpha_2}{2}\right), \quad (3.39e)$$

where bending slope (ψ_2), bending moment (\mathcal{M}_2), radial shear (\mathcal{Q}_2), and tangential force (\mathcal{P}_2) are given below for convenience.

$$\psi_2 = \frac{1}{R_2} \left(v_2 + \frac{\partial w_2}{\partial \theta} \right), \quad (3.40)$$

$$\mathcal{M}_2 = \frac{E\bar{I}_2}{R_2^2} \left(\frac{\partial v_2}{\partial \theta} + \frac{\partial^2 w_2}{\partial \theta^2} \right), \quad (3.41)$$

$$\mathcal{Q}_2 = \frac{E\bar{I}_2}{R_2^3} \left(\frac{\partial^2 v_2}{\partial \theta^2} + \frac{\partial^3 w_2}{\partial \theta^3} \right), \quad (3.42)$$

$$\mathcal{P}_2 = \frac{E\bar{S}_2}{R_2} \left(\frac{\partial v_2}{\partial \theta} - w_2 \right). \quad (3.43)$$

At the right side of the dimple, another set of six continuity conditions describes the connection to the straight segment. Similarly, these conditions are derived in a similar manner as the previous set of continuity conditions by considering the differential Lagrangian at $\theta_2 = \alpha_2$ and $x_3 = 0$. Replacing $(\alpha_2/2)$ in Eq. (3.39a), (3.39d) and (3.39e) with $(-\alpha_2/2)$. With this substitution, the continuity conditions are given by

$$\begin{Bmatrix} u_3(0, t) \\ y_3(0, t) \end{Bmatrix} = \begin{bmatrix} \cos(\alpha_2/2) & -\sin(\alpha_2/2) \\ -\sin(\alpha_2/2) & -\cos(\alpha_2/2) \end{bmatrix} \begin{Bmatrix} v_2(\alpha_2, t) \\ w_2(\alpha_2, t) \end{Bmatrix}, \quad (3.44a)$$

$$\frac{\partial y_3(0, t)}{\partial x} = -\psi_2(\alpha_2, t), \quad (3.44b)$$

$$EI \frac{\partial^2 y_3(0, t)}{\partial x^2} = -\mathcal{M}_2(\alpha_2, t), \quad (3.44c)$$

$$ES \frac{\partial u_3(0, t)}{\partial x} = \mathcal{P}_2(\alpha_2, t) \cos\left(\frac{\alpha_2}{2}\right) + \mathcal{Q}_2(\alpha_2, t) \sin\left(\frac{\alpha_2}{2}\right), \quad (3.44d)$$

$$EI \frac{\partial^3 y_3(0, t)}{\partial x^3} = \mathcal{P}_2(\alpha_2, t) \sin\left(\frac{\alpha_2}{2}\right) - \mathcal{Q}_2(\alpha_2, t) \cos\left(\frac{\alpha_2}{2}\right). \quad (3.44e)$$

In the summary, we need $4N + 2$ equations of motion to describe a beam with N dimples, so ten equations of motion are needed to describe our model ($N = 2$). Moreover, there are six boundary conditions and $12N$ continuity conditions (six on each side of the dimple), meaning that there are $12N + 6$ model coefficients need to be determined. As a results, since the model beam used in this thesis consists three straight segments which are connected to two dimples (Fig. 3.6), 30 unknown coefficients are needed to be determined.

3.3 Solutions to the Equations of Motion

In this section, the solutions to the equations of motion are presented. In Section 3.3.1, the general solutions to Eqs. (3.33)-(3.34) governing the transverse and longitudinal motion of the straight segment are given, Then, Section 3.3.2 presents the general solution to Eqs.(3.35)-(3.36) governing the tangential and radial motion of dimples.

3.3.1 Straight Segments

Since Eq. (3.33) involves a second-order derivative with respect to time and a fourth order derivative with respect to x , two initial conditions and four boundary conditions are needed for finding a unique solution for $y_i(x, t)$. Equation (3.33) is separable, and the vibration is harmonic in time with frequency ω . Therefore, a solution of the form

$$y_i(x, t) = Y_i(x)e^{j\omega t}, \quad (3.45)$$

is valid for i^{th} segment. Insertion of Eq. (3.45) into Eq. (3.33) yields

$$\frac{d^4 Y_i}{dx^4} - \beta^4 Y_i = 0. \quad (3.46)$$

The equation is satisfied if

$$\beta = \left(\frac{\rho S}{EI} \omega^2 \right)^{1/4}, \quad (3.47)$$

where β is the transverse frequency parameter, which is the same for all straight segments. For the solution of Eq. (3.46), we assume

$$Y_i(x) = Ae^{qx}, \quad (3.48)$$

where A and q are constants, and derive the auxiliary equation as

$$q^4 - \beta^4 = 0. \quad (3.49)$$

The roots of this equation are

$$\begin{aligned} q_1 = +\beta & \quad , \quad q_2 = -\beta, \\ q_3 = +j\beta & \quad , \quad q_4 = -j\beta. \end{aligned}$$

Hence, the solution of Eq. (3.46) becomes

$$Y_i(x) = A'_{i1}e^{\beta x} + A'_{i2}e^{-\beta x} + A'_{i3}e^{i\beta x} + A'_{i4}e^{-i\beta x}. \quad (3.50)$$

Equation (3.50) can also be expressed as

$$Y_i(x) = A'_{i1} \cos \beta x + A'_{i2} \sin \beta x + A'_{i3} \cosh \beta x + A'_{i4} \sinh \beta x . \quad (3.51)$$

Also, Eq. (3.50) can also be written in the exponential form as

$$Y_i(x) = \sum_{k=1}^4 A_{ik} e^{q_k x} . \quad (3.52)$$

This form is more convenient for formulating the coefficients in a matrix form and will be presented in Section (3.4). The modal coefficients A_{ik} will be determined from the boundary and continuity conditions.

The solution of Eq. (3.34) is derived in a similar manner. After a separation of variables, an ordinary an ordinary differential equation is obtained,

$$\frac{d^2 U_i}{dx^2} + \gamma^2 U_i = 0 , \quad (3.53)$$

where the longitudinal frequency parameter γ is defined as

$$\gamma = \left(\frac{\rho}{E} \omega^2 \right)^{1/2} . \quad (3.54)$$

The longitudinal frequency parameter γ is the same for the two segments, and the general solution is given by

$$U_i = \sum_{k=1}^2 C_{ik} e^{r_k x}, \quad (3.55)$$

where C_{ik} is modal coefficients and roots $r_1 = j\gamma$ and $r_2 = -j\gamma$.

3.3.2 Dimpled Segments

The notation used in this section is borrowed heavily from Myers [1] where the reader is referred to Lang [14] for an excellent background on the underlying theory. The general solutions of Eqs. (3.35)-(3.36) are of the form

$$v_i(\theta, t) = V_i(\theta) e^{j\omega t}, \quad (3.56)$$

and

$$w_i(\theta, t) = W_i(\theta) e^{j\omega t}. \quad (3.57)$$

Since Eqs. (3.35) - (3.36) are not separable; a harmonic solution can be assumed. Inserting Eq. (3.56) into Eq. (3.35) yields

$$\frac{d^6 V_i}{d\theta^6} (2 + p_i \zeta_i) \frac{d^4 V_i}{d\theta^4} + (1 - p_i \zeta_i - \zeta_i) \frac{d^2 V_i}{d\theta^2} + (\zeta_i - p_i \zeta_i^2) V_i = 0. \quad (3.58)$$

Similarly, inserting Eq. (3.57) into Eq. (3.36) yields

$$\frac{d^6 W_i}{d\theta^6} (2 + p_i \zeta_i) \frac{d^4 W_i}{d\theta^4} + (1 - p_i \zeta_i - \zeta_i) \frac{d^2 W_i}{d\theta^2} + (\zeta_i - p_i \zeta_i^2) W_i = 0, \quad (3.59)$$

where the frequency parameter for the i^{th} dimple is defined as

$$\zeta_i = \frac{\rho \bar{S}_i R_i^4}{E \bar{I}_i} \omega^2 . \quad (3.60)$$

In general, the parameters are different because each dimple has a different geometry. Also, a parameter associated with the extensional vibration of the dimple is defined as

$$p_i = \frac{\bar{I}_i}{\bar{S} R_i^2} , \quad (3.61)$$

where this parameter is required to satisfy force equilibrium [1]. The general solutions of Eqs. (3.58) and (3.59) are of the form

$$V_i(\theta) = B e^{s\theta} , \quad (3.62)$$

$$W_i(\theta) = D e^{s\theta} . \quad (3.63)$$

The tangential coordinate is considered, insertion of Eq. (3.62) into Eq. (3.58) yields

$$s^6 + (2 + p_i \zeta_i) s^4 + (1 - p_i \zeta_i - \zeta_i) s^2 + (\zeta_i - p_i \zeta_i^2) = 0 . \quad (3.64)$$

Equation (3.64) describes the characteristic equation for the dimple, so six roots are computed per dimple, s_{i1}, \dots, s_{i6} . Those roots are used to formulate the general solutions to Eqs. (3.58)-(3.59) given by

$$V_i(\theta) = \sum_{k=1}^6 B_{ik} e^{s_{ik}\theta} , \quad (3.65)$$

$$W_i(\theta) = \sum_{k=1}^6 D_{ik} e^{s_{ik}\theta} . \quad (3.66)$$

In general, since the constants B_{ik} and D_{ik} can be related by a multiplicative constant λ_{ik} [1], for instance, $D_{ik} = \lambda_{ik} B_{ik}$, as a result

$$W_i(\theta) = \sum_{k=1}^6 \lambda_{ik} B_{ik} e^{s_{ik}\theta} . \quad (3.67)$$

Equations (3.65) and (3.67) represent the mode shape for the i^{th} dimple written in exponential form where the multiplicative constant λ_{ik} is given by

$$\lambda_{ik} = \frac{p_i \zeta_i + (p_i + 1) s_{ik}^2}{s_{ik} - p_i s_{ik}^3} , \quad (3.68)$$

This relation illustrates that total of six unknown modal coefficients are required not twelve because six boundary conditions are needed for an arch (three at each side). The reader is referred to reference [1, p. 39] for an excellent background on underlying details.

3.4 Formulation of the Coefficient Matrix

For the sake of brevity, although this thesis presents a model with two dimples, this section presents a formulation of the coefficient matrix for a beam with a single dimple (concave). The general solutions developed in Section 3.3 with boundary and continuity conditions are given in Section (3.2.2)-(3.2.3) are needed to formulate the coefficients matrix. As a result, a system of $12N + 6$ homogenous algebraic equations given by:

$$[\mathcal{A}(\omega)]\{\mathcal{X}\} = \{0\} , \quad (3.69)$$

where $[\mathcal{A}(\omega)]$ is the coefficient matrix which depends on natural frequency ω , and $\{x\}$ defined as column vector of modal coefficients given by $\{A_{ik}, B_{ik}, C_{ik}\}^T$. In this thesis, the coefficient matrix is derived for a fixed-fixed beam with a single dimple ($N = 1$). This means, two straight segments connected to one dimple (concave) segment will be considered (Fig. 3.7).

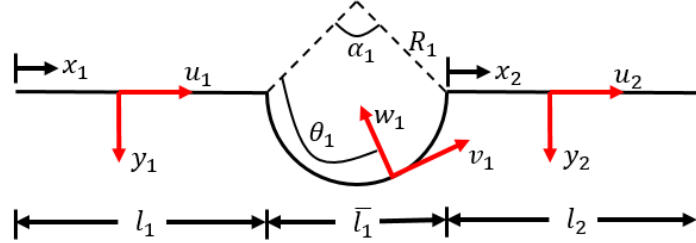


Figure 3.7: Schematic of a beam with two straight segments and one dimple segment.

In this case, there are 18 conditions to satisfy. Three boundary conditions are needed on each side of the model (the total is six), and six continuity conditions are required at left and right side of the dimple (the total is 12). Equations (3.70)-(3.73) represent the general solutions for each coordinate

$$y_i(x, t) = e^{j\omega t} \sum_{k=1}^4 A_{ik} e^{q_k x}, \quad (3.70)$$

$$u_i(x, t) = e^{j\omega t} \sum_{k=1}^2 C_{ik} e^{r_k x}, \quad (3.71)$$

$$v_i(\theta, t) = e^{j\omega t} \sum_{k=1}^6 B_{ik} e^{S_{ik} \theta}, \quad (3.72)$$

$$w_i(\theta, t) = e^{j\omega t} \sum_{k=1}^6 \lambda_{ik} B_{ik} e^{S_{ik} \theta}. \quad (3.73)$$

The roots $q_k = \pm\beta, \pm j\beta$ and $r_k = \pm j\gamma$. The frequency parameter for the straight segments, β, γ , are obtained using Eqs. (3.47) and (3.54). The dimple roots S_{ik} are found using Eq. (3.64), where the parameters ζ_i and extensional parameters p_i for each dimple are computed using Eqs. (3.60) and (3.61). The modal parameter λ_{ik} is found using Eq. (3.68).

To start the process of formulating the coefficients matrix. The boundary conditions for fixed-fixed beam ($u(0, l) = y(0, l) = y'(0, l) = 0$). Eqs. (3.70)-(3.73) are inserted into these boundary conditions. Then, the following six equations are obtained

$$\sum_{k=1}^2 C_{1k} = 0, \quad (3.74)$$

$$\sum_{k=1}^4 A_{1k} = 0, \quad (3.75)$$

$$\sum_{k=1}^4 q_k A_{1k} = 0, \quad (3.76)$$

$$\sum_{k=1}^2 C_{2k} e^{r_k l_2} = 0, \quad (3.77)$$

$$\sum_{k=1}^4 A_{2k} e^{q_k l_2} = 0, \quad (3.78)$$

$$\sum_{k=1}^4 q_k A_{2k} e^{q_k l_2} = 0. \quad (3.79)$$

Substituting the general solution into twelve continuity conditions yields

$$\sum_{k=1}^2 C_{1k} e^{r_k l_1} - \sum_{k=1}^6 B_{1k} \left(\cos\left(\frac{\alpha_1}{2}\right) + \lambda_{1k} \sin\left(\frac{\alpha_1}{2}\right) \right) = 0. \quad (3.80)$$

The above equation describes the continuity of horizontal deflections at $x_1 = l_1, \theta_1 = 0$, see Eq. (3.39a). Also, from Eq. (3.39a) we can describe the continuity vertical deflections at $x_1 = l_1, \theta_1 = 0$ using

$$\sum_{k=1}^4 A_{1k} e^{q_k l_1} - \sum_{k=1}^6 B_{1k} \left(\sin\left(\frac{\alpha_1}{2}\right) - \lambda_{1k} \cos\left(\frac{\alpha_1}{2}\right) \right) = 0. \quad (3.81)$$

The continuity slope (see Eq. (3.39b)) at $x_1 = l_1, \theta_1 = 0$ can be described as

$$\sum_{k=1}^4 q_k A_{1k} e^{q_k l_1} - \frac{1}{R_1} \sum_{k=1}^6 (-B_{1k} (1 + s_{1k} \lambda_{1k})) = 0, \quad (3.82)$$

moreover, the Eq. (3.83) describes the equilibrium of moment (see Eq. (3.39c))

at $x_1 = l_1, \theta_1 = 0$,

$$EI \sum_{k=1}^4 q_k^2 A_{1k} e^{q_k l_1} - \frac{EI \bar{I}_1}{R_1^2} \sum_{k=1}^6 (-B_{1k} (s_{1k} + s_{1k}^2 \lambda_{1k})) = 0. \quad (3.83)$$

Moreover, the following Eq. (3.84) describe the equilibrium of axial force (see Eq. (3.39d))

at $x_1 = l_1, \theta_1 = 0$,

$$\begin{aligned}
ES \sum_{k=1}^2 r_k C_{1k} e^{r_k l_1} - \sum_{k=1}^6 B_{1k} \left(\frac{E \bar{S}_1}{R_1} (s_{1k} - \lambda_{1k}) \cos \left(\frac{\alpha_1}{2} \right) \right. \\
\left. - \frac{E \bar{I}_1}{R_1^3} (s_{1k}^2 + s_{1k}^3) \sin \left(\frac{\alpha_1}{2} \right) \right) = 0,
\end{aligned} \tag{3.84}$$

and Eq. (3.85) describes equilibrium of shear force (see Eq. (3.39e)) at $x_1 = l_1$, $\theta_1 = 0$,

$$\begin{aligned}
EI \sum_{k=1}^4 q_k^3 A_{1k} e^{q_k l_1} - \sum_{k=1}^6 B_{1k} \left(-\frac{E \bar{S}_1}{R_1} (s_{1k} - \lambda_{1k}) \sin \left(\frac{\alpha_1}{2} \right) \right. \\
\left. - \frac{E \bar{I}_1}{R_1^3} (s_{1k}^2 + s_{1k}^3) \cos \left(\frac{\alpha_1}{2} \right) \right) = 0.
\end{aligned} \tag{3.85}$$

The continuity of horizontal deflection (Eq. (44a)) at $x_2 = 0$, $\theta_1 = \alpha_1$, vertical deflection (Eq. (3.44a)) at $x_2 = 0$, $\theta_1 = \alpha_1$, and slope (Eq. (3.44b)) at $x_2 = 0$, $\theta_1 = \alpha_1$ are described by the following equations, respectively

$$\sum_{k=1}^2 C_{2k} - \sum_{k=1}^6 B_{1k} \left(\cos \left(\frac{\alpha_1}{2} \right) - \lambda_{1k} \sin \left(\frac{\alpha_1}{2} \right) \right) e^{s_{1k} \alpha_1} = 0, \tag{3.86}$$

$$\sum_{k=1}^4 A_{2k} - \sum_{k=1}^6 B_{1k} \left(-\sin \left(\frac{\alpha_1}{2} \right) - \lambda_{1k} \cos \left(\frac{\alpha_1}{2} \right) \right) e^{s_{1k} \alpha_1} = 0, \tag{3.87}$$

$$\sum_{k=1}^4 q_k A_{2k} - \frac{1}{R_1} \sum_{k=1}^6 (-B_{1k} (1 + s_{1k} \lambda_{1k}) e^{s_{1k} \alpha_1}) = 0. \tag{3.88}$$

In addition, equilibrium of moment (Eq. (3.44c)) at $x_2 = 0$, $\theta_1 = \alpha_1$, axial force (Eq. (3.44d)) at $x_2 = 0$, $\theta_1 = \alpha_1$, and shear force (Eq. (3.44e)) at $x_2 = 0$, $\theta_1 = \alpha_1$ can be described by Eqs. (3.89)-(3.91) as following

$$EI \sum_{k=1}^4 q_k^2 A_{2k} - \frac{E\bar{I}_1}{R_1^2} \sum_{k=1}^6 (-B_{1k}(s_{1k} + s_{1k}^2 \lambda_{1k}) e^{s_{1k}\alpha_1}) = 0, \quad (3.89)$$

$$ES \sum_{k=1}^2 r_k C_{2k} - \sum_{k=1}^6 B_{1k} \left(\frac{E\bar{S}_1}{R_1} (s_{1k} - \lambda_{1k}) \cos\left(\frac{\alpha_1}{2}\right) + \frac{E\bar{I}_1}{R_1^3} (s_{1k}^2 + s_{1k}^3 \lambda_{1k}) \sin\left(\frac{\alpha_1}{2}\right) \right) e^{s_{1k}\alpha_1} = 0, \quad (3.90)$$

$$EI \sum_{k=1}^4 q_k^3 A_{2k} - \sum_{k=1}^6 B_{1k} \left(\frac{E\bar{S}_1}{R_1^2} (s_{1k} - \lambda_{1k}) \sin\left(\frac{\alpha_1}{2}\right) - \frac{E\bar{I}_1}{R_1^3} (s_{1k}^3 \lambda_{1k}) \cos\left(\frac{\alpha_1}{2}\right) e^{s_{1k}\alpha_1} \right) = 0. \quad (3.91)$$

The coefficients in front of each modal coefficient A_{1k} , A_{2k} , B_{1k} , C_{1k} , C_{2k} are assembled into 18×18 coefficients matrix $[\mathcal{A}(\omega)]$ using Eqs. (3.74)-(3.91). The coefficient matrix for a fixed-fixed beam with single dimple (concave) is assembled using *MATLAB*[®]. Moreover, *MATLAB*[®] is used to assemble a coefficient matrix for a beam with N dimples for various boundary conditions. For the analytical model of this study, a 30×30 coefficients matrix $[\mathcal{A}(\omega)]$ is formulated for a beam with two dimples in the opposing direction (see Fig. 3.6) and considered for different boundary conditions. Myers [1] also formulated the coefficient matrix for a beam with N dimples in the same direction whereas this study considers a beam with two dimples in opposite direction.

Equations (3.80)-(3.91) are repeated two times by replacing the straight segment and dimple number with the following segment number when we need to assemble the coefficient matrix for a beam with two dimples. Furthermore, the coefficients in six rows of the matrix can be modified to use the same matrix with different boundary conditions. Then, Eq. (3.69) is solved numerically to calculate the natural frequencies ω and mode shapes $\{x\}$ using an iterative procedure, and it depends on a frequency (ω) . Frequencies that produce a very small determinant

of this matrix are natural frequencies. A better way to find the natural frequency is to plot the magnitude of the determinant against range of frequencies and to see where the magnitude reaches a local minimum. An example of this method is shown in Fig. 3.8, a fundamental frequency for a beam with one dimple.

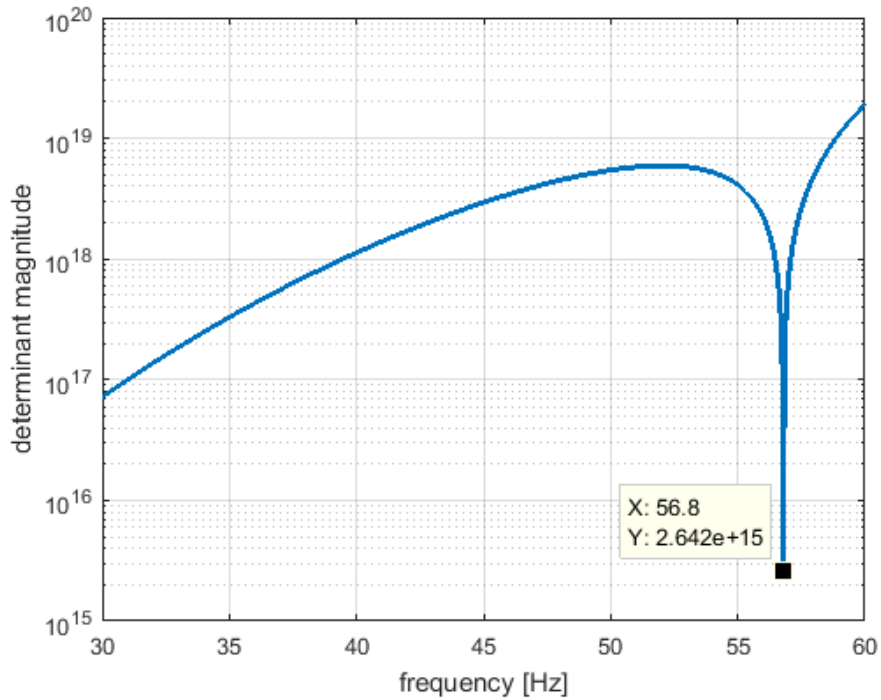


Figure 3.8: A range of frequencies vs. determinant magnitude.

In the next section, sample results of natural frequency are given where the mode shape is also plotted.

3.5 Sample Results of Natural Frequency and Mode Shape

Cantilever and fixed-fixed beams are used as examples below in order to obtain their natural frequencies and mode shapes using the BVM. The natural frequencies are computed using *MATLAB*[®], for a beam without dimples and a beam with two dimples in the same and opposing directions as shown in Figs.3.9 (a) and (b).

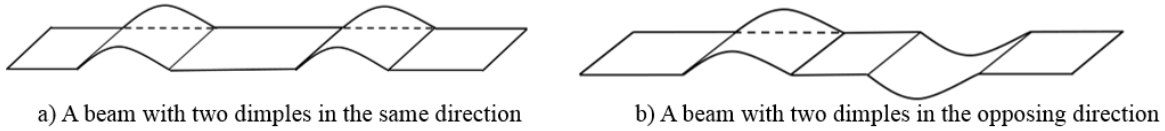


Figure 3.9: A beam with two dimples in the same (a) and opposing (b) directions.

3.5.1 Cantilever Beam

Consider a steel cantilever beam with a length of 0.2210 m, width 0.026 m, thickness 0.00118 m, dimple chord length 0.03 m, elastic of modules 200 GPa, and density 7870 kg/m³ (Table 3.1). Two cases are considered here: a cantilever beam with two dimples in the same direction (Fig.3.9a) and a cantilever beam with two dimples in the opposing directions (Fig.3.9b). Also, the mathematical analysis of cantilever beam without dimples is presented (straight beam).

Table 3.1: Parameters for cantilever dimpled beam ($N = 2$).

Parameter	Value
First segment length, l_1	0.055 m
Dimple cord segment length, \bar{l}_1	0.03 m
Second segment length, l_2	0.062 m
Dimple cord segment length, \bar{l}_2	0.03 m
Third segment length, l_3	0.044 m
Dimple angle, α_1	135°
Dimple angle, α_2	135°

3.5.1.1 Free vibration of a Uniform cantilever beam

For a uniform cantilever beam subjected to a free vibration where its mass is considered as distributed. The equation of motion is given [5] by

$$\frac{d^2}{dx^2} \left\{ EI(x) \frac{d^2 Y(x)}{dx^2} \right\} = \omega^2 m(x) Y(x), \quad (3.92)$$

where, E is young's modules, I is the area moment of inertia of beam cross section, $Y(x)$ is the displacement in y direction with respect to distance x from the fixed end, ω is the circular natural frequency, m is the mass per unit length of beam. Refereeing to Eq. 3.47 which can be written as

$$\omega = \beta^2 \sqrt{\frac{EI}{\rho S}}, \quad (3.93)$$

where the values of β^2 here for the first five modes is given in Table 3.2.

Table 3.2: Values of transverse frequency parameter for the uniform cantilever beam [6].

Mode	β^2
1	3.52
2	22.03
3	61.69
4	120.90
5	200.01

Also, the natural frequency (in Hz) can be obtained using

$$f = \omega/2\pi . \tag{3.94}$$

In general, the mode shapes for a continuous cantilever beam is given as [6]

$$f_n(x) = A_n \{(\sin \beta_n L - \sinh \beta_n L)(\sin \beta_n x - \sinh \beta_n x) + (\cos \beta_n L - \cosh \beta_n L) (\cos \beta_n x - \cosh \beta_n x)\} , \tag{3.95}$$

where the constant A is arbitrary, $n = 1,2,3, \dots, \infty$, and $\beta_n L = n\pi$.

As a result, the natural frequencies of the cantilever beam (described by Table 3.1) are calculated (see Appendix (A)) and given in Table 3.3.

Table 3.3: Natural frequencies for the cantilever beam without dimples (uniform beam).

Mode	Frequency [Hz]
1	19.7
2	123.3
3	345.3
4	676.6
5	1118.3

3.5.1.2 Natural frequencies of a Cantilever Dimpled Beam

The first five natural frequencies of a cantilever beam with two dimples in the same and opposite directions are given in Table 3.4 where the percentage change between the two cases can be obtained by

$$\% \text{ Change} = \frac{(f_{\text{same}} - f_{\text{opp}})}{f_{\text{same}}} * 100 , \quad (3.96)$$

where f_{same} is the natural frequency of a dimpled beam with two dimples in the same direction and f_{opp} the natural frequency of a dimpled beam with two dimples in the opposite direction.

Table 3.4: Comparison between natural frequencies of a uniform cantilever beam against one with two dimples in the same or opposite directions.

Frequency [Hz]	Beam without dimples (uniform beam)	Dimples are in the same direction	Dimples are in the opposite direction	% Change
f_1	19.7	17.20	17.19	0.06%
f_2	123.3	107.38	107.70	- 0.3%
f_3	345.3	254.46	227.60	10.6%
f_4	676.6	398.78	554.19	- 39.0%
f_5	1118.3	677.27	591.92	12.6%

In general, creating two dimples in the same direction or in the opposite direction on beams may increase or decreases the natural frequencies of beams. The results demonstrate that creating two dimples on a cantilever beam decreases its first five natural frequencies. The change in the

first two natural frequencies is very small. However, by creating two dimples, third natural frequency of the beam with two dimples in the same direction increased by 10.6% more than the one with two dimples in the opposing direction. The fourth natural frequency of the beam with two dimples in the same direction decreased by -39.0% lower than the beam with two dimples in the opposite direction. In contrast, the fifth natural frequency of the beam with two dimples in the same direction increased by 12.6% greater than the natural frequency of the one with two dimples in the opposite direction. More detailed investigation of the effect of introducing dimples in opposing directions is presented in Chapter 5.

3.5.2 Fixed-Fixed Beam

In this section, a fixed-fixed beam is considering as an example to predict its natural frequencies using the BVM method. A fixed-fixed beam with length of 0.2170 m and $N = 2$ ($E = 200$ GPa, $\rho = 7870$ kg/m³, $h = 0.00118$ m) is presented to investigate the effect of adding two dimples to beams in the same and opposite directions. Table 3.5 lists the beam dimensions which used in this study.

Table 3.5: Parameters for fixed-fixed dimpled beam ($N = 2$).

Parameter	Value
First segment length, l_1	0.04 m
Dimple cord segment length, \bar{l}_1	0.03 m
Second segment length, l_2	0.062 m
Dimple cord segment length, \bar{l}_2	0.03 m
Third segment length, l_3	0.055 m
Dimple angle, α_1	135°
Dimple angle, α_2	135°

3.5.2.1 Uniform Fixed-Fixed Beam

The first five natural frequencies of the fixed-fixed beam (Specified in Table 3.5) without dimples is given in Table 3.7, and its first three mode shapes are plotted in Fig. 3.10. These mode shapes clearly reflect the fixed-fixed conditions as both beam ends are constrained. The following equation governs the mode shapes of the fixed-fixed beam [20]

$$f_n(x) = A_n \{(\sinh \beta_n x - \sin \beta_n x) + \sigma_n(\cosh \beta_n x - \cos \beta_n x)\}, \quad (3.97)$$

where $\sigma_n = (\sinh \beta_n L - \sin \beta_n L) / (\cos \beta_n L - \cosh \beta_n L)$ and $\beta_n L$ values have been tabulated in Table 3.6. The constant A is chosen arbitrary ($A = 0.35$) such that the maximum amplitude is about 0.057.

Table 3.6: Values of parameters $\beta_n L$ for the uniform fixed-fixed beam [6].

Mode	β^2
1	4.73
2	7.85
3	11.00
4	14.14
5	17.26

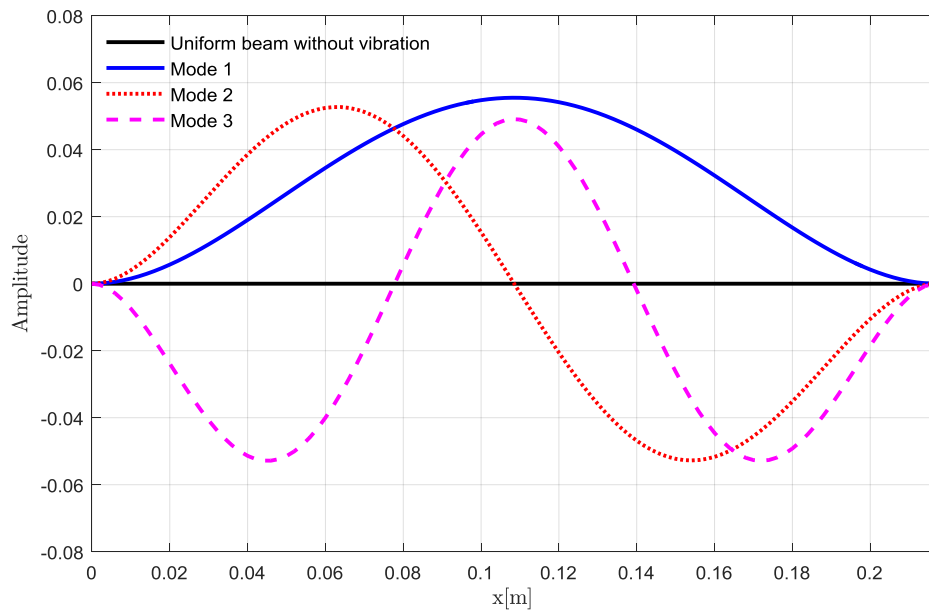


Figure 3.10: First three mode shapes of the uniform fixed-fixed beam.

3.5.2.2 Fixed-Fixed Dimpled Beam

The following table (Table 3.7) represents a comparison between the fixed-fixed beam with two dimples in the same and opposite direction. The percentage change between the two cases is calculated by Eq. 3.96.

Table 3.7: Comparison between natural frequencies of a uniform fixed-fixed beam against one with two dimples in the same or opposite directions.

Frequency [Hz]	Beam without dimples (uniform beam)	Dimples are in the same direction	Dimples are in the opposite direction	% Change
f_1	130.4	127.7	123.6	3.2%
f_2	359.5	282.8	411.4	- 45.4%
f_3	704.8	672.4-	589.6	12.3 %
f_4	1165.1	1011.0	885.5	12.3%
f_5	1740.6	1140.0	1104.4	3.1%

The results show that the natural frequencies of the fixed-fixed beam model can be modified by creating two dimples which may increase or decrease the natural frequencies of fixed-fixed beams. The natural frequencies of the two cases given above have a different trend. The change in the fundamental frequency of the two cases is small (about 3.2%). The change in the second frequency, which is - 45.4 % is the most significant of all the natural frequencies shown. The change in the third and fourth natural frequencies of the beam with two dimples in the same direction, which is about 12.3%, are higher than the natural frequencies of the beam with two dimples in the opposing direction. There is a small change in the fifth natural frequency between the beam with two dimples in the same direction and the beam with two dimples in the opposing direction.

The first three mode shapes for the two cases are shown in Figs. 3.11 and 3.12, respectively where these figures show that the nodal points (zero crossings) for second and third mode shapes have shifted drastically (see Table 3.8).

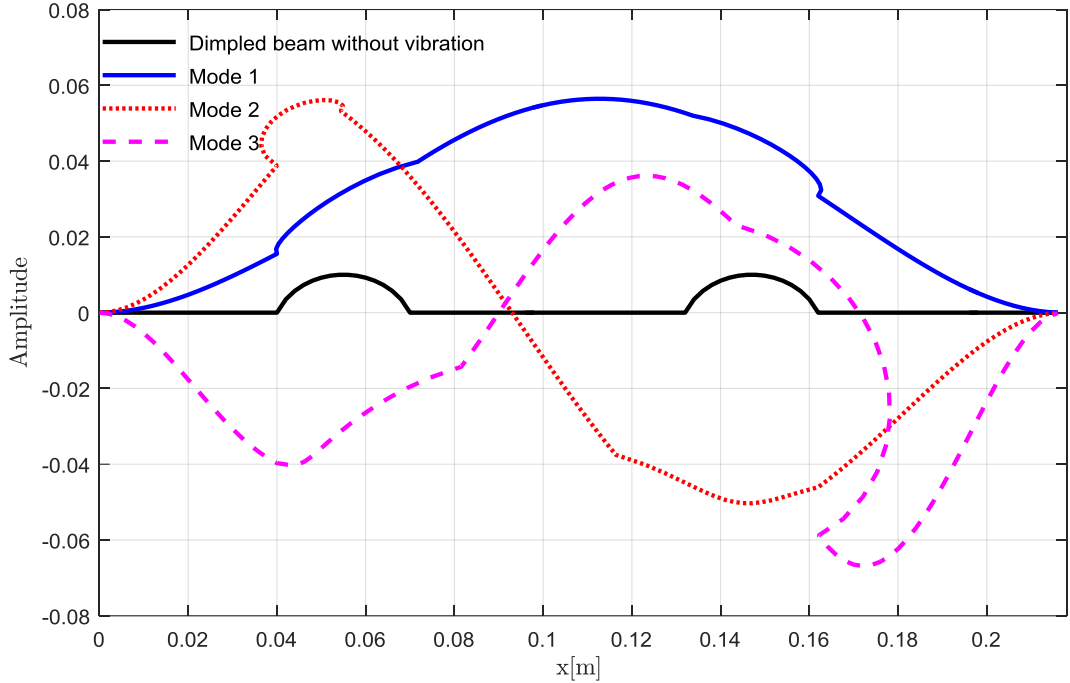


Figure 3.11: First three mode shapes (fixed-fixed, a beam with two dimples in the same direction).

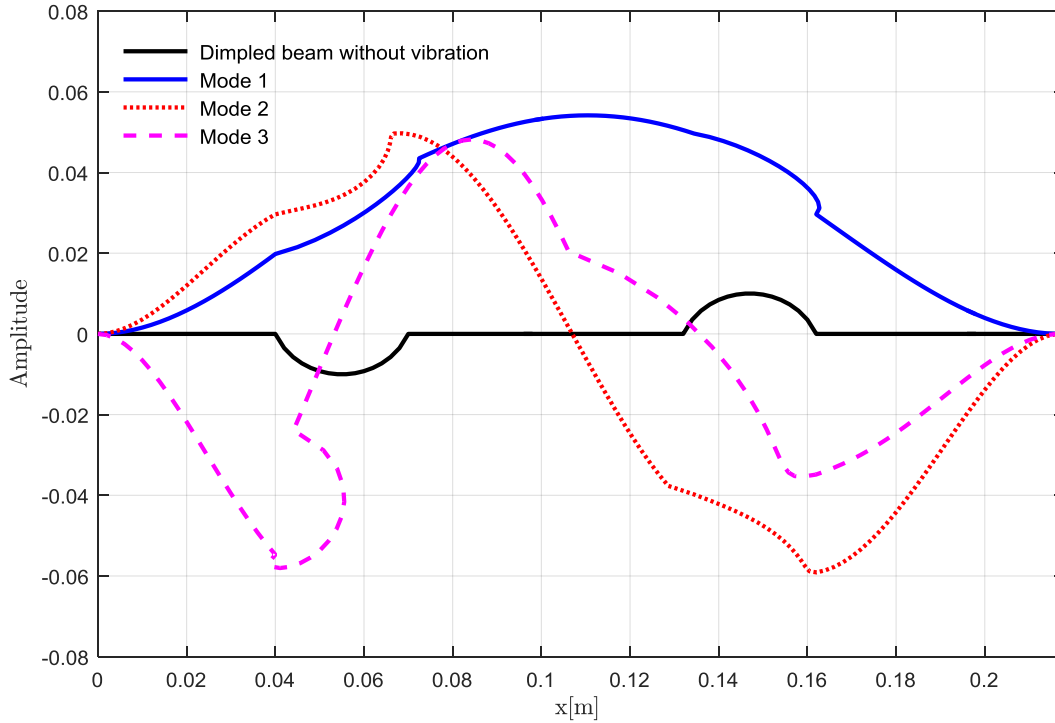


Figure 3.12: First three mode shapes (fixed-fixed, a beam with two dimples in the opposing direction).

Table 3.8: Comparison between the first three modes of the uniform fixed-fixed beam against one with two dimples in the same or opposite directions in terms of shifting the nodal points (zero crossings).

Mode	Beam without dimples (uniform beam)	Dimples are in the same direction	Dimples are in the opposite direction
1	N/A	N/A	N/A
2	0.108 m	0.0935 m	0.106 m
3	0.077 m 0.139 m	0.089 m 0.170 m	0.049 m 0.136 m

The mode shapes are plotted using *MATLAB*[®] where these mode shapes are eigenfunctions obtained from the BVM. In Fig. 3.12, there are three straight segments, so three longitudinal and

three transverse eigenfunctions are needed. For the first mode, the first two eigenfunctions are defined locally over $0 \leq x \leq 0.04$ and given by

$$U_1(x) = 6.3 * 10^{-07} * \cos(0.15x) + 0.007 * \sin(0.15x), \quad (3.98)$$

$$\begin{aligned} Y_1(x) = & -0.43 * \cos(21.30x) + 0.40 * \sin(21.30x) \\ & + 0.430 * \cosh(21.30x) + -0.40 \\ & * \sinh(21.30 * x). \end{aligned} \quad (3.99)$$

The second straight segment can be described by the following eigenfunctions

$$U_2(x) = 0.028 * \cos(0.15x) + 0.0041 * \sin(0.15x), \quad (3.100)$$

$$\begin{aligned} Y_2(x) = & 0.40 * \cos(21.30x) + 0.40 * \sin(21.30x) + 0.15 \\ & * \cosh(21.30x) - 0.10 * \sinh(21.30x), \end{aligned} \quad (3.101)$$

where it defines locally over $0 \leq x \leq 0.132$ and globally over $0.07 \leq x \leq 0.132$. The eigenfunctions of the third straight segment are given by

$$U_3(x) = -2.93 * 10^{-05} * \cos(0.15x) + 0.0034 * \sin(0.15x), \quad (3.102)$$

$$\begin{aligned} Y_3(x) = & 0.20 * \cos(21.30x) + -0.51 * \sin(21.30x) + 0.15 \\ & * \cosh(21.30x) + 0.09 * \sinh(21.30x), \end{aligned} \quad (3.103)$$

defined locally over $0 \leq x \leq 0.216$. Globally, this segment lies in the beam domain $0.162 \leq x \leq 0.216$.

For the dimple segments, we need two tangential and two radial eigenfunctions which are defined locally over $0 \leq \theta \leq -135^\circ$ and $0 \leq \theta \leq 135^\circ$. The first two tangential eigenfunctions are given by

$$V_1(\theta) = 0.30 * \cos(1.10\theta) - 0.04 * \sin(1.10\theta) + 0.01 * \cos(0.88\theta) + 0.14 * \sin(0.88\theta) - 0.1 * \cos(0.16\theta) + 0.10 * \sin(0.16\theta), \quad (3.104)$$

$$V_2(\theta) = -0.11 * \cos(1.10\theta) + 0.13 * \sin(1.10\theta) - 0.44 * \cos(0.88\theta) + 0.16 * \sin(0.88\theta) + 0.01 * \cos(0.16\theta) - 0.57 * \sin(0.16\theta), \quad (3.105)$$

where defined globally over $0.04 \leq x \leq 0.07$ and $0.132 \leq x \leq 0.162$, respectively. Also, the radial eigenfunctions within the second dimple segment are

$$W_1(\theta) = -0.05 * \cos(1.10\theta) - 0.33 * \sin(1.10\theta) + 0.12 * \cos(0.88\theta) - 0.01 * \sin(0.88\theta) + 0.01 * \cos(0.16\theta) + 0.02 * \sin(0.16\theta), \quad (3.106)$$

$$W_2(\theta) = 0.14 * \cos(1.10\theta) + 0.12 * \sin(1.10\theta) + 0.14 * \cos(0.88\theta) + 0.40 * \sin(0.88\theta) - 0.09 * \cos(0.16\theta) - 0.001 * \sin(0.16\theta). \quad (3.107)$$

These segments can be defined globally in the beam domain $0.04 \leq x \leq 0.07$ and $0.132 \leq x \leq 0.162$, respectively (this domain is important to plot the mode shape of a dimpled beam). Appendix (B) illustrates how to plot the mode shapes of a dimpled beam using multiple eigenfunctions given from the BVM. The reader is referred to reference [1, p. 148] for an excellent background on plotting the mode shape of dimpled beams.

The results presented previously (natural frequencies) are checked and verified using the finite element method (FEM) in the next chapter in Chapter 4, two examples of modeling the dimpled beams using finite element method are presented and the results are compared to those obtained from BVM. In Chapter 5, the beam dimpling approach is validated experimentally (using Impact testing).

CHAPTER 4

FINITE ELEMENT MODEL

The objective of this chapter is to show the accuracy of the analytical solution by comparing the results obtained against those of finite element method. Two examples are presented here to compare the natural frequencies obtained using these two methods. In this study, finite element modal analysis of dimpled beam is performed using *ANSYS*[®]. In particular, the ANSYS Parametric Design Language (APDL) is used to model the dimpled beams. APDL is a powerful scripting language that allows us to parametrize the model and automate common tasks. APDL enables the user to build a model in terms of parameters (i.e., model dimensions, material properties of beams, and the locations of dimples are defined as variables). This chapter starts with basic of modeling of the dimpled beam using finite element method (Section 4.1), followed by an example of cantilever dimpled beam model (Section 4.2). In Section 4.3, the fixed-fixed dimpled beam model is presented as an example. Finally, a comparison between the natural frequencies obtained using the analytical model and finite element model (FEM) is presented in Section 4.4.

4.1 Dimpled Beam Modeling

As mentioned before, the dimple is positioned between two straight segments where the dimpled beam can be modeled as shown in Fig. 4.1. Along with the chord length \bar{l} , R represents the constant radius, and α represents the angle. The distance between the dimple center and the left beam boundary is assumed to be x .

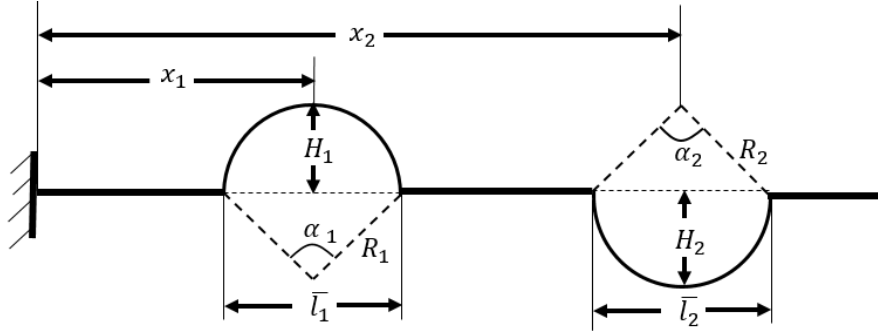


Figure 4.1: Schematic representation of a dimpled cantilever beam.

Assuming the constant mass, the mathematical relation between the dimple and straight segment thicknesses is given by Eq. (3.2). All straight segments and dimples have uniform thickness where h and \bar{h} represents the thickness of the beam and the dimple thickness, respectively. Also, the mathematical relation between the beam dimple radius R , the dimple cord length, and the dimple angle can be approximately by [4]

$$R = \frac{\bar{l}_i}{2 \sin(\alpha_i/2)} \quad , \quad (4.1)$$

the height of the dimple H is also given by [4]

$$H = R_i \left(1 - \cos\left(\frac{\alpha_i}{2}\right) \right). \quad (4.2)$$

The ANSYS Parametric Design Language (APDL) is used to model the dimpled beams where the dimple locations and geometric parameters can be defined as variables. In this finite element study, a beam element is used (ANSYS Beam3 (2D elastic beam)). The beam element is defined by two nodes. This element has three degrees of freedom at each node: two translations in the nodal x and y directions and one rotation about the nodal z -axis. Figure 4.2 shows the geometry, node locations, and the coordinate system for this beam element.

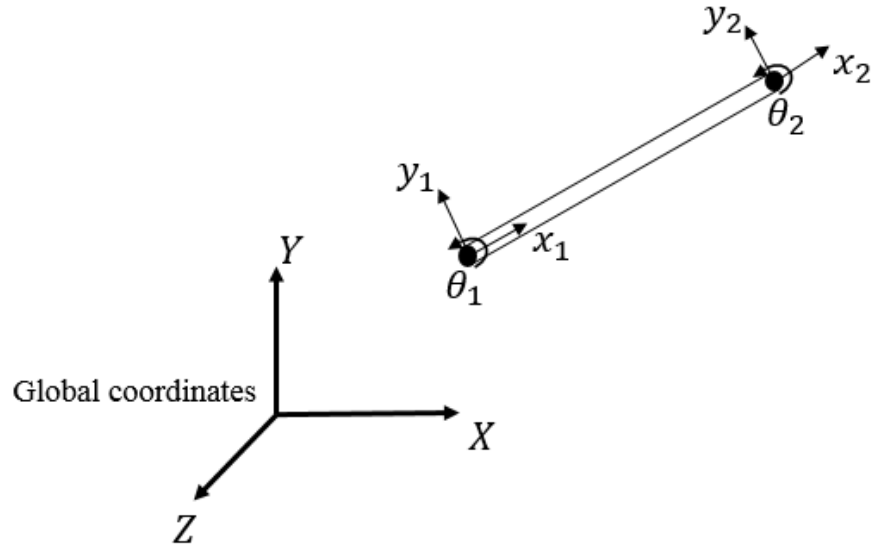
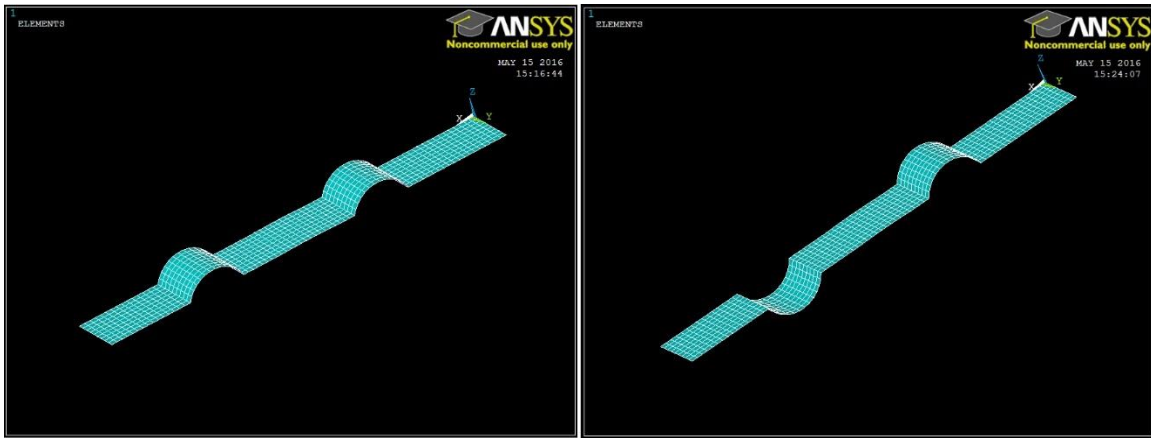


Figure 4.2: ANSYS Beam3 (2D elastic beam) element.

The APDL code which is used to build a cantilever beam with two dimples in opposing directions is given in Appendix (C). The natural frequencies are calculated using a modal analysis (ANTYPE, 2). Also, the results of the natural frequencies for two examples, cantilever, and fixed-fixed dimpled beams, are given at Sections 4.2 and 4.3 where the convergence study for the finite element mesh used to model the dimpled beam is given at the end of each section.

4.2 Cantilever Beam Model

In this section, two beam models are presented. A cantilever beam with two dimples in the same direction and a cantilever beam with two dimples in the opposite direction, respectively. Also, the modal of a uniform cantilevered beam is given as well. Figures 4.3 (a) and (b) show the 3D rendition of the cantilever beam models with two dimples in the same and opposite directions, respectively.



(a)

(b)

Figure 4.3: 3D structure of a cantilever beam with two dimples in the same (a) and opposite directions (b).

4.2.1 Geometrical and Material Properties

A dimpled cantilever beam is considered with the properties lists in Table 4.1.

Table 4.1: Parameters for cantilever dimpled beam ($N = 2$).

Parameter	Value
Beam length, L	0.2210 m
First distance between the dimple center and the beam boundary, x_1	0.07 m
Dimple cord segment length, \bar{l}_1	0.03 m
Second distance between the dimple center and the beam boundary, x_2	0.1620 m
Dimple cord segment length, \bar{l}_2	0.03 m
Width, b	0.0260 m
Thickness, h	0.00118 m
Dimple angle, α_1	135°
Dimple angle, α_2	135°
Elastic modulus, E	200 GPa
Density, ρ	7870 kg/m ³

4.2.2 Uniform Cantilevered Beam Model

Figure 4.4 illustrates a uniform beam model for the cantilever boundary condition where finite element method (see Appendix (D)) is used to build the model. The first natural frequencies of the cantilevered beam without dimples are calculated and tabulated in Table 4.2.

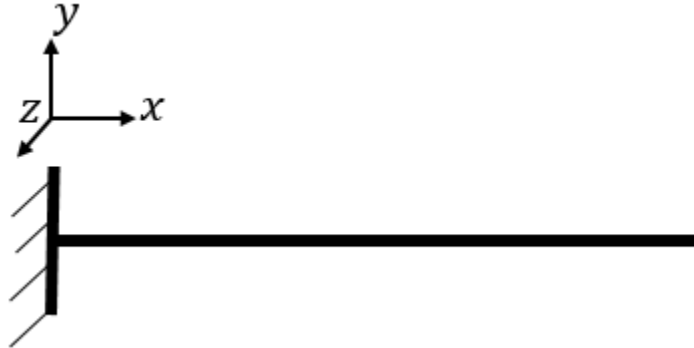
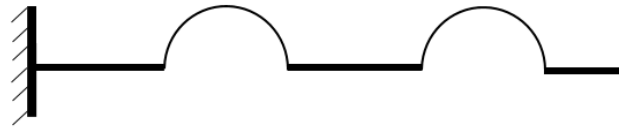


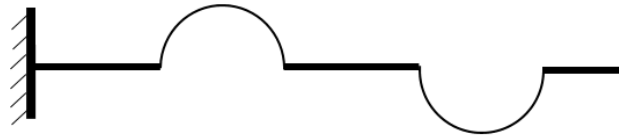
Figure 4.4: Cantilever beam without dimples (uniform beam).

4.2.3 Calculation of Natural Frequencies for the Cantilever Dimpled Beam

In the cantilever beam boundary condition, one end is constrained while the other end is free. After discretizing this beam into 81 equal elements (82 nodes), the results of the first five natural frequencies are evaluated numerically using Finite Element method. Figure 4.5 represent the cantilever beam models with two dimples in the same and opposite directions where the first five natural frequencies for these two models are computed.



(a)



(b)

Figure 4.5: Cantilever beam with two dimples in the same (a) and opposite (b) directions.

The first five natural frequencies of the dimpled cantilever beam with two dimples in the same and opposite directions are given below in Table 4.2 where the percentage change between these two cases are calculated by Eq. (3.96) and given in the far right column.

Table 4.2: A comparison between natural frequencies for a cantilever beam with two dimples for the two cases with and without dimples.

Frequency [Hz]	Beam without dimples (uniform beam)	Dimple are in the same direction	Dimple are in the opposite direction	The change in the natural frequency (%)
f_1	19.67	17.20	17.19	0.06
f_2	123.29	107.43	107.75	-0.3
f_3	345.21	254.57	228.06	10.8
f_4	676.42	400.01	554.77	-38.6
f_5	1118.1	678.16	593.59	12.4

The results show that there can be a significant difference between the natural frequencies results for the two models. The fundamental and second frequencies results for the two cases are closed to each other while the third, fourth, and fifth natural frequencies have a large change in the natural frequency. In the third mode, the natural frequency of a cantilever beam with two dimples in the same direction is about 10.8 larger than the natural frequency of a cantilever beam with two dimples in the opposite direction. In contrast, the fourth natural frequency of the cantilever beam with two dimples in the opposite direction is decreased by -38.6% less than the fourth natural frequency of the cantilever beam with dimples in the same directions. The fifth natural frequency of the beam with two dimples in the same direction is 12.4% higher than the natural frequency of the beam with two dimples in the opposing direction. As a result, the effect of creating two dimples in the same direction in shifting the natural frequencies of dimpled beams has a different trend comparing to creating two dimples in the opposite direction. Some detail and explanations for this comparison will present in Chapter 5 where the two models will validate experimentally. also, we can see that the addition of two dimples (with same or opposite direction) clearly changes the natural frequencies of the uniform beam.

With a low number of elements (i.e., 12 elements), or an unreasonably coarse mesh, ANSYS does not build the required dimpled beam. Instead, a V-notch is formed on the beam (see Fig. 4.6).

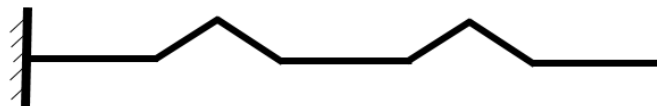


Figure 4.6: Two V-notch formed on a cantilever beam.

As a result, with coarse mesh, ANSYS does not calculate the natural frequencies of the cantilever beam with two dimples (arches) accurately. In other words, a high number of elements must be taken into consideration when the dimpled beam is modeled to get precise results of natural frequencies, and that is why about 81 elements are considered to build the model. The following section presents a convergence study of a cantilever beam with two dimples in the opposite direction with a different number of elements.

4.2.4 Convergence Study

As we increase the number of elements of the model, our mesh is refined and the results of the natural frequencies converge to the solution. Table 4.3 shows the convergence of the natural frequencies of the cantilever beam with two dimples in the opposite directions with a different number of elements.

Table 4.3: Convergence of the natural frequencies for the cantilever dimpled beam, (dimples are in the opposite direction), with a different number of elements.

	Mode Number	Number of Elements							
		5	12	81	121	1189	2376	3395	11878
f_1	1	18.431	17.510	17.195	17.188	17.184	17.207	17.099	12.045
f_2	2	115.74	109.97	107.75	107.70	107.68	107.68	107.68	104.76
f_3	3	298.86	246.40	228.06	227.70	227.50	227.50	227.50	226.65
f_4	4	647.34	578.50	554.77	554.25	553.97	553.97	553.97	553.37
f_5	5	1096.30	661.48	593.59	592.34	591.64	591.63	591.63	591.32

As we can see from the table, the results of the fundamental frequency converge to 17.195 at about 81 elements, and the natural frequency results converge about that value till the number of elements is increased about 11878 elements where the fundamental frequency starts to decrease due to numerical errors. The other natural frequencies behave in a similar manner as well. Thus, this a good check to make sure the results of the natural frequencies are adequate to use them to validate the BVM results.

4.3 Fixed-Fixed Beam Model

Two fixed-fixed dimpled beam models will be presented in this section to compare the results of the natural frequencies of the two models. The first model is that a beam model with the fixed-

fixed boundary condition, (i.e. the motion of the end of the fixed boundary is fully constrained), which has two dimples in the same direction whereas the second model is that a fixed-fixed beam model with two dimples in the opposite direction. Also, the natural frequencies of the uniform cantilevered beam model are calculated here for convenience.

4.3.1 Geometrical and Material Properties

For the numerical analysis, consider a dimpled fixed-fixed beam with the properties which tabulated in Table 4.4

4.3.2 Uniform Fixed-Fixed Beam Model

This section explores the free vibration of a fixed-fixed beam modeled with 2D elastic beam element. The first five natural frequencies of a clamped uniform beam (beam without dimples) are computed using FEM (see Table 4.5).

4.3.3 Calculation of Natural Frequencies for the Fixed-Fixed Dimpled Beam

To calculate the natural frequency of the fixed-fixed beam with two dimples in the same direction as well as, the opposite direction, APDL is used to build and model the dimpled beam. The beam is modeled using 81 elements to make sure the results of the natural frequencies are converging to the solution. A modal analysis (ANTYPE,2) is used to solve for the natural frequencies.

Table 4.4: Parameters for the fixed-fixed dimpled beam ($N = 2$).

Parameter	Value
Beam length, L	0.2170 m
First distance between the dimple center and the beam boundary, x_1	0.055 m
Dimple cord segment length, \bar{l}_1	0.03 m
Second distance between the dimple center and the beam boundary, x_2	0.147 m
Dimple cord segment length, \bar{l}_2	0.03 m
Width, b	0.0260 m
Thickness, h	0.00118 m
Dimple angle, α_1	135°
Dimple angle, α_2	135°
Elastic modulus, E	200 GPa
Density, ρ	7870 kg/m ³

The results of the natural frequencies computed by ANSYS for the two models are tabulated in Table 4.5. The change in the natural frequencies between the beam with two dimples in the same direction and the beam with two dimples in the opposite direction are calculated by Eq. (3.96) and given in the far right column.

Table 4.5: A comparison between natural frequencies for a fixed-fixed beam with two dimples for the two models.

Frequency [Hz]	Beam without dimples (uniform beam)	Dimple are in the same direction	Dimple are in the opposite direction	The change in the natural frequency (%)
f_1	129.85	127.79	123.70	3.2%
f_2	358.02	282.94	411.33	- 45.37%
f_3	702.32	672.91	590.09	12.30%
f_4	1162.8	1011.9	887.09	12.33%
f_5	1742.1	1142.8	1106.4	3.18%

The results show that the natural frequencies of the fixed-fixed beam with two dimples in the same direction can be drastically different from the results of the natural frequencies of the fixed-fixed beam with two opposing dimples. A detailed discussion of these results will be in Chapter 5 where the numerical and analytical results are validated and compared to the experimentally measured values.

4.3.4 Convergence Study

The concept of the convergence that is used here is to increase the number of elements gradually and see how the natural frequencies vary. When the natural frequencies do not change, we have reached convergence and can select our mesh. A fixed -fixed beam with two dimples in opposite directions is considered as an example. Table 4.6 illustrates the results obtained.

Table 4.6: Convergence of the natural frequencies of the fixed-fixed dimpled beam, (dimples are in the opposite direction), with a different number of elements.

	Mode Number	Number of Elements							
		5	16	42	81	468	1169	3338	5839
f_1	1	129.82	124.70	123.85	123.70	123.65	123.64	123.65	123.62
f_2	2	328.18	408.65	411.13	411.33	411.40	411.40	411.40	411.40
f_3	3	684.22	601.87	591.82	590.09	589.40	589.38	589.38	589.37
f_4	4	1150.5	921.38	891.93	887.09	885.15	885.10	885.10	885.09
f_5	5	1923.5	1151.6	1112.6	1106.40	1104.0	1103.9	1103.9	1103.9

The fundamental frequency tends to converge about 123 Hz whereas the second natural frequency tends to converge about 411 Hz. Also, the other frequencies follow the similar manner which means the numerical results of the natural frequencies are accurate with 81 elements.

4.4 BVM Results vs. FE Results

This section compares the results of the natural frequencies for two models with two boundary conditions: cantilever beam and fixed-fixed beam. The natural frequencies of a cantilevered and fixed-fixed beams with two dimples in the same direction and opposite direction are computed analytically using BVM and numerically using the finite element method. In Sections 4.4.1 and

4.4.2, a comparison between the results of the natural frequencies computing by BVM and finite element method is made for the two models.

4.4.1 Cantilevered Beam

The natural frequencies of the cantilevered beam with two dimples in the same and opposite directions are compared in Table 4.7 and Table 4.8 respectively. The percentage error between the two methods can be defined as

$$\% \text{ Difference} = \text{abs} \left(\frac{f_{BVM} - f_{FEM}}{f_{BVM}} \right) 100, \quad (4.3)$$

where f_{BVM} is the natural frequency computed using BVM and f_{FEM} is the natural frequency calculated using finite element method.

Table 4.7: First five natural frequencies for the cantilevered beam with two dimples in the same direction (BVM vs. FEM).

Frequency [Hz]	BVM	FEM	Difference (%)
f_1	17.20	17.20	0.0%
f_2	107.38	107.43	0.04%
f_3	254.46	254.57	0.04%
f_4	398.78	400.01	0.3%
f_5	677.27	678.16	0.1%

Table 4.8: First five natural frequencies for the cantilevered beam with two dimples in the opposite direction (BVM vs. FEM).

Frequency [Hz]	BVM	FEM	Difference (%)
f_1	17.19	17.19	0.00%
f_2	107.70	107.75	0.05%
f_3	227.60	228.06	0.20%
f_4	554.19	554.77	0.10%
f_5	591.92	593.59	0.28%

Although there is a small difference between the BVM and FEM, the agreement is good between them.

4.4.2 Fixed-Fixed Beam

A fixed-fixed beam with two dimples in the same and opposite directions is used as an example so the natural frequencies obtained using BVM could be compared to those obtained using FEM. These results are listed in Tables 4.9 and 4.10.

Table 4.9: First five natural frequencies for the fixed-fixed beam with two dimples in the same direction (BVM vs. FEM).

Frequency [Hz]	BVM	FEM	Difference (%)
f_1	127.7	127.8	0.08%
f_2	282.8	282.9	0.04%
f_3	672.4	672.9	0.07%
f_4	1011.0	1011.9	0.09%
f_5	1140.0	1142.8	0.25%

Table 4.10: First five natural frequencies for the fixed-fixed beam with two dimples in the opposite direction (BVM vs. FEM).

Frequency [Hz]	BVM	FEM	Difference (%)
f_1	123.6	123.7	0.08%
f_2	411.4	411.3	0.02%
f_3	589.6	590.1	0.08%
f_4	885.5	887.1	0.18%
f_5	1104.4	1106.4	0.18%

These results show a good match between the natural frequencies computed by BVM and the natural frequencies obtained by FEM. The following chapter (Chapter 5) will present an experimental validation of these results for two examples: cantilevered and fixed-fixed beams.

CHAPTER 5

EXPERIMENTAL VALIDATION

In this chapter, cantilever, and fixed-fixed beams are used as examples to compare their natural frequencies to those found using the BVM and the finite elements methods. All measurements were conducted at Western Michigan University's Noise and Vibration Laboratory.

5.1 Manufacturing Process of Dimpled Beam

The manufacturing of dimpled beam is done in the Western Michigan University's machine shop. After taking the required beam and the dimple dimensions, dimple is created in the beams by stamping technique. In particular, the stretching process is used. The die and the punch that are used in the stamping process were manufactured by Alshabatat [4] and are shown in Fig. 5.1.

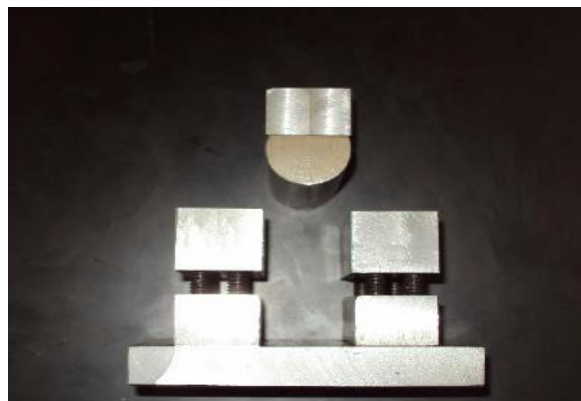


Figure 5.1: The die and the punch which are used in the manufacturing of the dimpled beams [4].

The following steps illustrate the dimple forming:

Step 1) In Figs. 5.2 (a) and (b) the beam is clamped into the die with suitable clamping force to ensure that the clamped metal is not drawn during the pressing process.



(a)

(b)

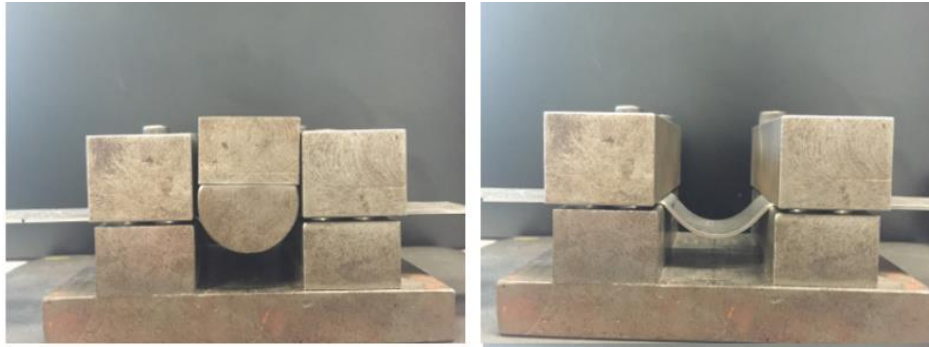
Figure 5.2: The beam is clamped well into the die, (a) and (b).

Step 2) Using a punch, the dimple shape is pressed on the beam. Figures 5.3 (a), (b), (c) and (d) show the steps of the pressing process where the punch is used to press the die onto the beam to create dimples on the beam's surface.



(a)

(b)



(c)

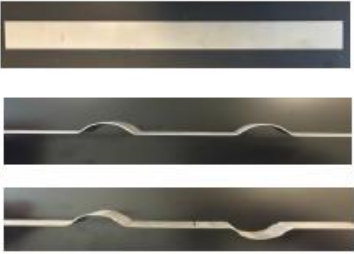


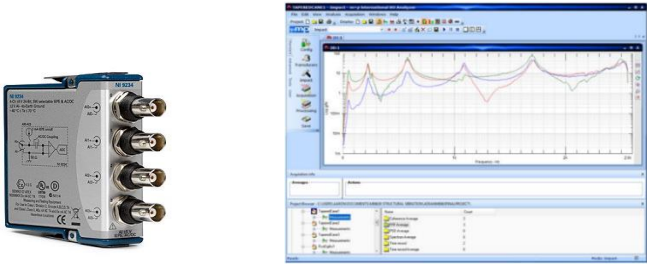
(d)

Figure 5.3: Manufacturing process of dimpled beam in four steps, (a), (b), (c), and (d).

5.2 Equipment and Specifications

The equipment that used for this experiment is prepared as shown in the following Table 5.1.

Table 5.1: Experiment equipment.

Equipment	Function
<p>Three beam models.</p> 	<p>The material of the experiment model is steel where the uniform and dimpled beams have the same material properties.</p>
<p>Impact hammer model (PCB piezotronic/model 208C02), with rubber tip.</p> 	<p>To generate the impulse force, that is used as the excitation to the beam.</p>
<p>A single axis accelerometer (PCB piezotronic/ model 352C22) and Petro wax.</p> 	<ul style="list-style-type: none"> ➤ A single axis accelerometer is used to measure the acceleration. ➤ Petro wax is used to attach the accelerometer to the test beam.
<p>A four-channel (NI -9234) data acquisition card and M+P International Smart Office Analyzer Software.</p> 	<ul style="list-style-type: none"> ➤ A four-channel (NI -9234) data acquisition card to collect the data. ➤ M+P International Smart Office Analyzer Software to analyze by M+P International Smart Office.

The M+P International Smart Office Analyzer is a software package used for dynamic signal measurements and processing. This software can analyze the time and frequency domain, Fast Fourier Transform (FFT), and modal and impact testing. A rubber impact tip is used with the impact hammer to determine the impulse shape (amplitude and duration) and the bandwidth of the excitation. The National Instrument Data Acquisition system (NI DAQ) with the Smart Office is used to collect and analyze the data where a four-channel (NI-9234) data acquisition card is connected to a computer using USB port. The measurements can be exported in *MATLAB*[®] for future analysis which can be also used to plot frequency response functions for all results obtained.

5.3 Experiment Setup and Measurement Procedure

This section describes the experimental setup for measurement of dimpled beam natural frequencies using the equipment listed in Table 5.1. The entire experimental arrangement is depicted in Fig. 5.4.

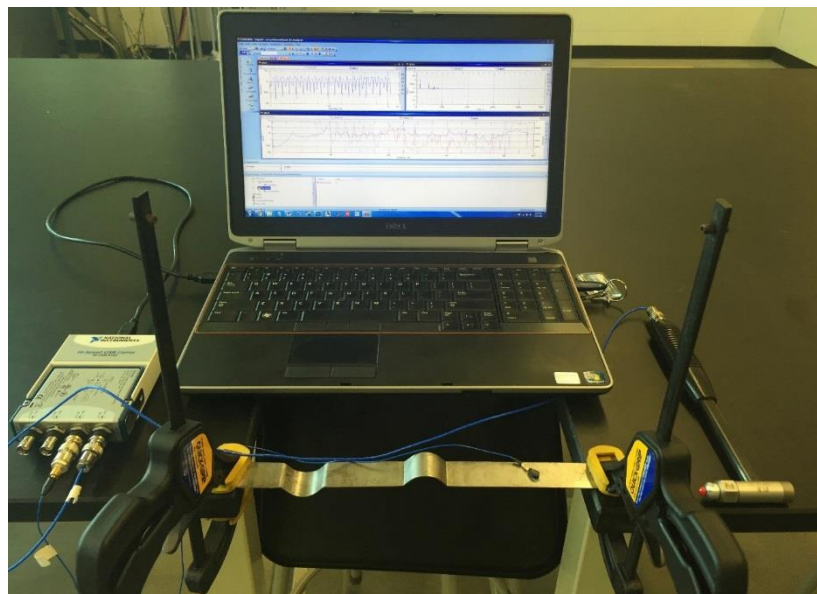
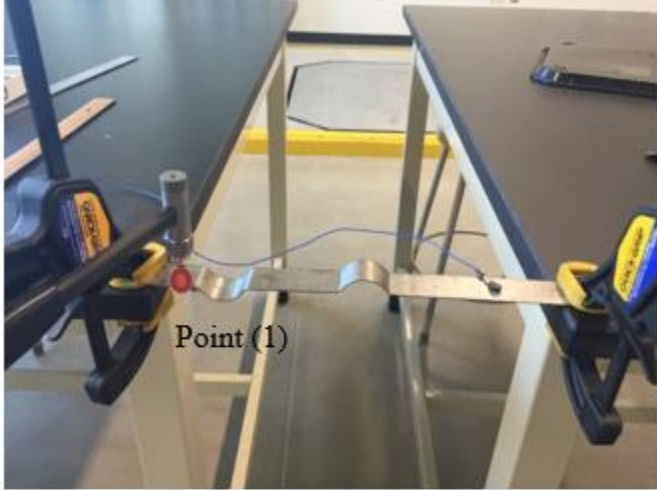


Figure 5.4: Experiment arrangement and instruments.

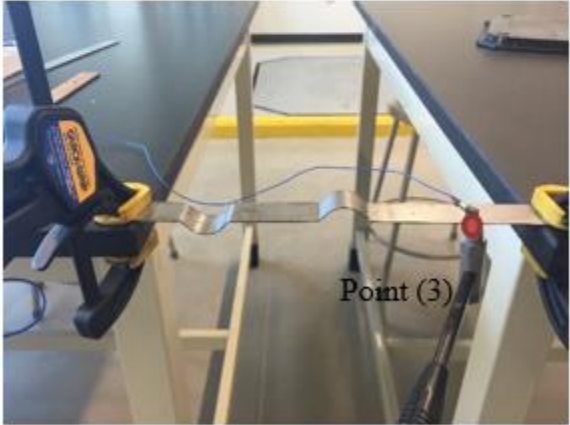
The displacement, velocity, and acceleration can be obtained through the acquisition of the Frequency Response Function (FRF) between an excitation point (hammer impact) and response (accelerometer). In this study, the input to the structure is an impulse force which is generated using an impact hammer (PCB piezotronic /model 208C02). The output response is the acceleration which is measured using a single-axis accelerometer (PCB piezotronic/ model 352C22) where this accelerometer measures the transverse vibration of the beam. It is fixed at the third segment with petro wax. The beam is impacted at 3 points (left side, middle, and right side of the beam) using the impact hammer as shown in Figs. 5.5 (a), (b), and (c).



(a)



(b)



(c)

Figure 5.5: Three possible places where the dimpled beam is excited using the impact hammer, (a) indicates point (1), (b) indicates point (2), and (c) indicates point (3).

Each location is impacted three times, and results averaged. The more time we strike at a particular position; the better results we acquire (because that will average out the extraneous noise). Since, the accelerometer is located at a third location, this point is excited from the other side (underside of the beam). To ensure transverse vibration only, the beam must be struck along its centerline. In this experiment, two channel were used, one for impact hammer and the other for a single axis accelerometer as shown in Fig.5.6.

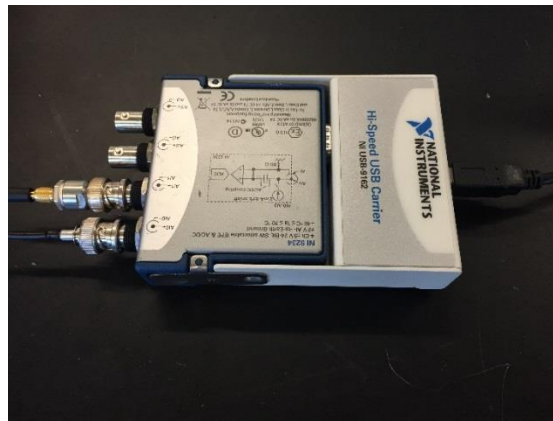


Figure 5.6: A four-channel (NI -9234) data acquisition card.

This experiment was executed in three steps: First, the experiment was carried out for a uniform beam (beam without dimples). Then, the experiment was performed once using a beam with two dimples in the same direction and then using a beam with two dimples in opposite direction as shown in Figs. 5.7 (a), (b), and (c), respectively.



(a)



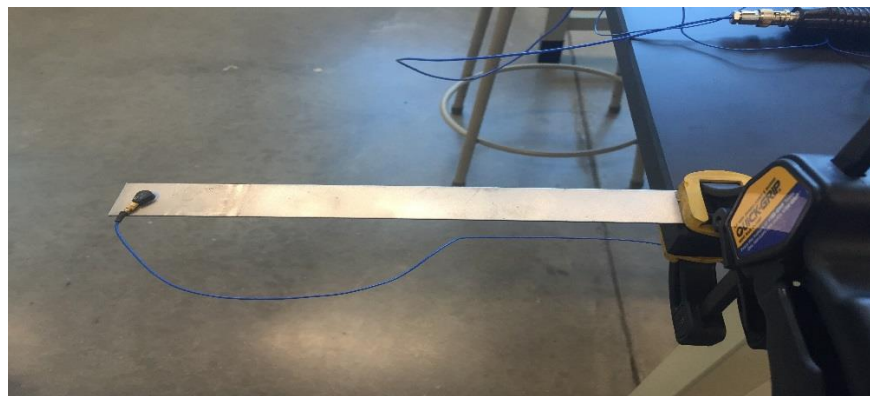
(b)



(c)

Figure 5.7: Three beam models, a beam without dimples, a beam with dimples in the same direction, and a beam with dimples in opposite direction.

Each experiment was set up for two boundary conditions. First, cantilever beam (anchored at one end and free at the other end) as shown in Fig.5.8.



(a)



(b)

Figure 5.8: Cantilever beam vibration excitation without (a) and with dimples (b).

Beam geometrical and material properties are given in Table 5.2. The overall beam length is 22.1 cm. This experiment was repeated but with a beam with two dimples in opposing direction.

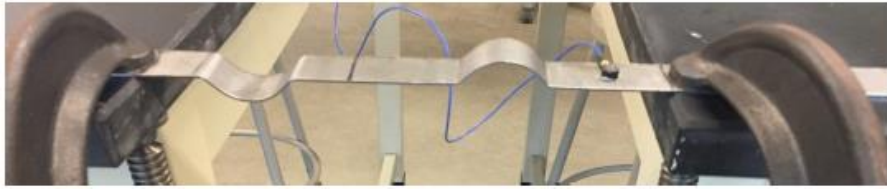
Table 5.2: Parameters for the cantilever dimpled beam ($N = 2$).

Parameter	Value
First segment length, l_1	0.055 m
Dimple cord segment length, \bar{l}_1	0.03 m
Second segment length, l_2	0.062 m
Dimple cord segment length, \bar{l}_2	0.03 m
Third segment length, l_3	0.044 m
Width, b	0.026 m
Thickness, h	0.00118 m
Dimple angle, α_1	135°
Dimple angle, α_2	135°
Elastic modulus, E	200 GPa
Density, ρ	7870 kg/m ³

Second, the fixed-fixed beam boundary condition was tested, as shown in Fig. 5.9 (a) and (b).



(a)



(b)

Figure 5.9: Fixed-fixed beam model, (a) with two dimples in the same direction (a) and (b) two dimples in the opposing direction.

The beam fixed-fixed geometrical and material properties are given in Table 5.3.

Table 5.3: Parameters for the fixed-fixed beam ($N = 2$).

Parameter	Value
First segment length, l_1	0.04 m
Dimple cord segment length, \bar{l}_1	0.03 m
Second segment length, l_2	0.062 m
Dimple cord segment length, \bar{l}_2	0.03 m
Third segment length, l_3	0.055 m
Width, b	0.026 m
Thickness, h	0.00118 m
Dimple angle, α_1	135°
Dimple angle, α_2	135°
Elastic modulus, E	200 GPa
Density, ρ	7870 kg/m ³

This experiment was repeated using the beam- with two dimples in opposite directions as shown in Figure 5.9 (b).

The results of natural frequencies of the beam with dimples in the same direction are compared to the results of the natural frequencies of the beam with dimples in the opposite direction for the two boundaries conditions in Section 5.4. These results are compared to the experimental natural frequencies of the uniform beam (beam without dimples).

5.4 Experimental Results

This section presents two different examples of beams with two boundaries: cantilever (fixed-free) and fixed-fixed beams. The results of the experimental vibration analysis (finding the natural frequencies) for both cases of dimples in the same and opposite direction are presented. Also, natural frequencies of a uniform beam are compared to these results. Then, the experimentally obtained natural frequencies are compared to the analytical (BVM) results.

5.4.1 Cantilever Beam

This section shows and explains the cantilever beam vibration analysis. The Frequency Response Function (FRF) before and after dimpling is presented, and then a comparison of natural frequency values for using two dimples on the beams in the same and opposite direction are shown. As shown from the results in Table 5.4, creating two dimples at the cantilever beam decreases all of its first five natural frequencies.

Table 5.4: Comparison between natural frequencies for a cantilever beam with $N = 2$ with and without dimples.

Frequency [Hz]	Uniform beam	Dimpled beam (dimples are in the same direction)	Dimpled beam (dimples are in the opposite direction)
f_1	18	17.3	17.1
f_2	112	105.7	103.6
f_3	316	270.1	244.2
f_4	620	444.9	534.5
f_5	1028	644.8	610.2

The beam is impacted at three measurements locations and three possible places where the response can be measured. In this experiment, the response was measured at the third place, and the beam was excited at three different locations as shown previously in Fig. 5.5. The sample rate is 2048 Hz, averaging =3, and $\Delta f = 1 \text{ Hz}$.

Figure. 5.10 illustrates the FRF curves for the cantilever beam before and after dimpling. It is obvious that from Fig. 5.10 that each curve shows five main peaks corresponding to the first five transverse natural frequencies of the uniform and the dimpled cantilever beam models for the two cases (the cantilever beam with two dimples in the same direction and the cantilever beam with two dimples in the opposite direction).

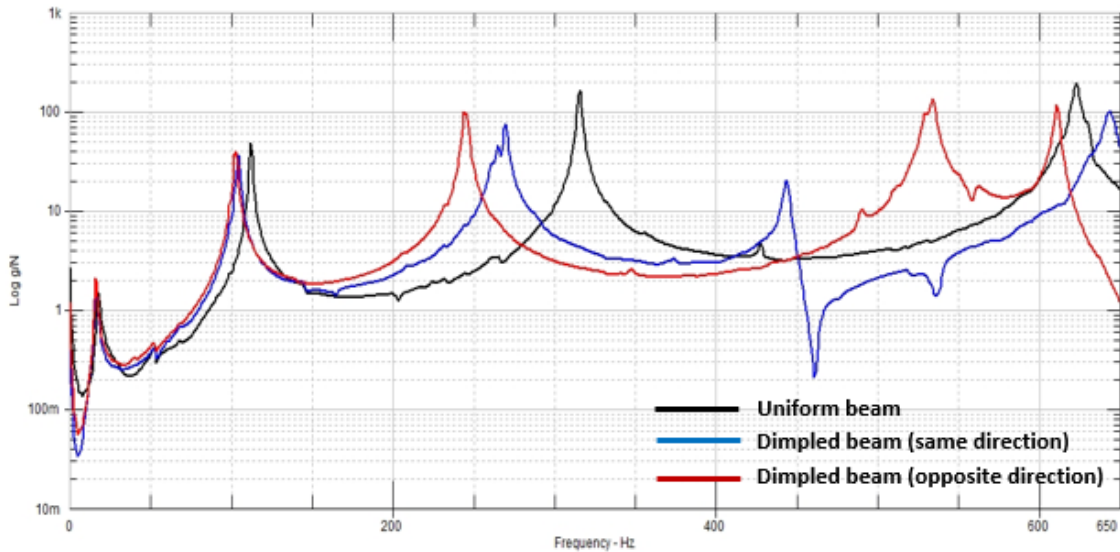


Figure 5.10: The FRF of the cantilever beam before and after dimpling for two the cases (the cantilever beam with two dimples in the same direction and the cantilever beam with two dimples in the opposite direction). The beam was excited at the first point and the acceleration response measured at the third point, (see Fig. 5.5a).

Thus, it is evident that there is a significant difference in the first five natural frequency values between the two cases (with dimples in the same and the opposite direction). The results show that the first two natural frequencies of the two cases are close (within 1.15% and 2.0% of each other, respectively). In contrast, the last three natural frequencies exhibit a “switching” behavior. The third natural frequency of the beam with two dimples in the same direction is higher

than the third natural frequency of the one with two dimples in the opposing direction (9.5%). The fourth natural frequency of the latter is much higher than the beam with two dimples in the same direction (-20.1%). Also, the changes in the fifth natural frequency of the one with two dimples in the same direction is higher than the change in the natural frequency of the beam with two dimples in the opposing direction, which is about 5.2%. Therefore, the highest change of the natural frequency between the two cases has occurred at the fourth frequency. In general, creating two dimples on the cantilever beams decrease the first five natural frequencies. There is a significant difference in using two dimples in the same direction and the opposite direction. This experiment confirms that creating two dimples in the same direction on cantilever beams shift the natural frequencies significantly different than the case of creating two dimples in opposite direction.

5.4.2 Fixed-Fixed Beam

This section presents the experimental vibration analysis of fixed-fixed beams. The Frequency Response Function (FRF) of the uniform and dimpled beams is presented and natural frequencies of these beams are extracted. The results are shown in Fig. 5.11 where the five curves indicate the first five natural frequencies for each case.

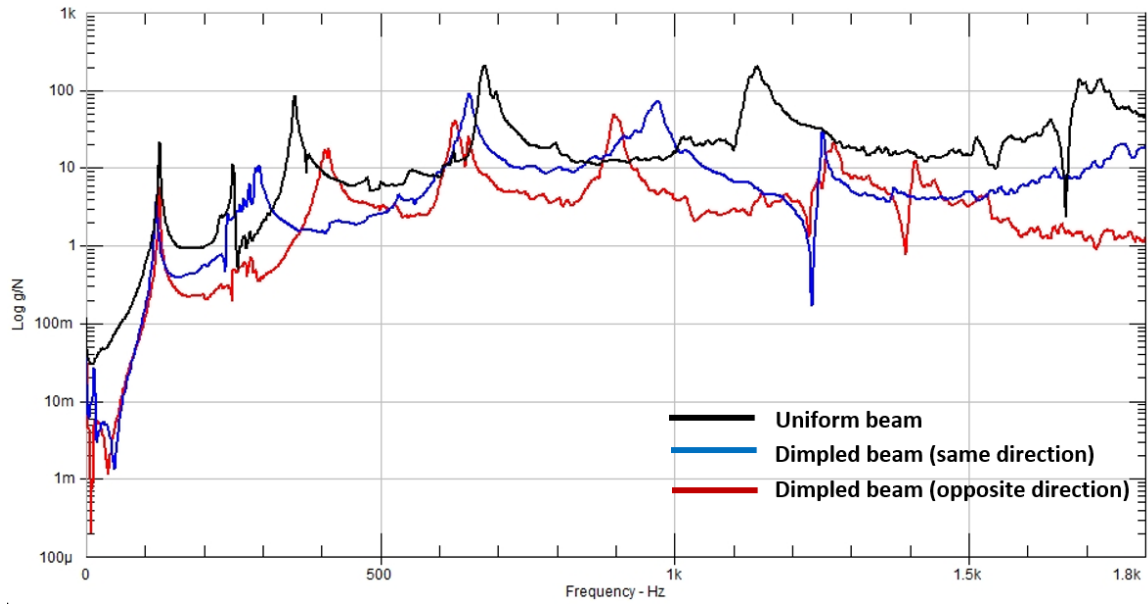


Figure 5.11: The FRF of the fixed-fixed beam before and after dimpling for two the cases (the beam with two dimples in the same direction and the beam with two dimples in the opposite direction). The beam was excited at the first point and the acceleration response measured at the third point, (see Fig. 5.5a).

Table 5.5 lists a comparison of these first five natural frequencies. In this section, we obtain the first five natural frequencies where the sample frequency is 3200 Hz, the averaging = 3, and $\Delta f = 0.78 \text{ Hz}$.

Table 5.5: Comparison between natural frequencies for fixed-fixed beam ($N = 2$) with and without dimples.

Frequency [Hz]	Uniform beam	Dimpled beam (dimples are in the same direction)	Dimpled beam (dimples are in the opposite direction)
f_1	127.50	122.7	126.2
f_2	355.0	282.7	400.6
f_3	680.0	627.3	650.6
f_4	1141.3	970.9	890.3
f_5	1727.5	1257.0	1147.5

It is obvious that there is a drastic change in the first five natural frequencies of the fixed-fixed beam between the two cases. Referring to Table 5.5, the change in the fundamental frequency for the two cases is about -2.8% (negative means the fundamental of the beam with two dimples in the same direction is lower than the fundamental in the beam with two dimples in the opposing direction), which is small difference comparing to the other frequencies. The change percentage for the second frequency of the two cases is about -41.7% which represents the highest change in frequency comparing for the first five frequencies. Also, the change in the third natural is about -3.6%. The change in the fourth natural frequency exhibits a “switching” behavior where the fourth frequency of the beam with two dimples in the same direction is increased by 8.7% comparing to the one with two dimples in the opposing direction. Also, the changes in the fifth natural frequency of the one with two dimples in the same direction is higher than the change in the natural frequency of the beam with two dimples in the opposing direction, which is about 9.5%. As a result, the first three natural frequencies of the beam with two dimples in the opposing direction is much higher than the first three frequencies in the beam with two dimples in the same direction. On the contrary, the fourth and fifth natural frequency of this beam is greater than the fourth and fifth natural frequency of the one with two dimples in the opposing direction.

5.5 Comparison of BVM, FEM, and Experimental Results

To check the accuracy of the BVM, FEM was used and the natural frequencies obtained by the BVM were compared to FEM for two examples which were given in Chapter 4. In this section, the natural frequencies of a cantilevered beam and fixed-fixed beam with two dimples for the two cases which were calculated using the BVM and those obtained from FEM will be validated experimentally.

5.5.1 Cantilever Beam

The first five natural frequencies of a cantilever beam with two dimples in the same direction are tabulated in Table 5.6 lists a comparison of these first five natural frequencies. The percentage error is calculated for the BVM with respect to experimental results.

Table 5.6: First five natural frequencies of the cantilever beam with two dimples in the same direction. Experiment vs. BVM vs. Finite Element.

Frequency [Hz]	Experimental	BVM	Finite Element	% Error
f_1	17.3	17.2	17.2	0.5%
f_2	105.7	107.4	107.4	-1.6%
f_3	270.1	254.5	254.5	5.7%
f_4	444.9	398.8	400.0	10.3%
f_5	644.8	677.3	678.2	-5.0%

The first natural frequency agrees to within 0.5% and the second natural frequency agrees to within 1.6%. The percentage error in third natural frequency is increased which is about 5.7%.

Also, the percentage error in the fourth and fifth natural frequencies are 10.3% and 5.0% respectively.

The experimental results of the cantilevered beam with two dimples in the opposite direction, agreed well with the BVM and FEM results. However, there is a small error between all methods. The first five natural frequencies for a cantilever beam with two dimples in the opposite direction are tabulated in Table 5.7.

Table 5.7: First five natural frequencies of the cantilever beam with two dimples in the opposite direction. Experiment vs. BVM vs. Finite Element.

Frequency [Hz]	Experimental	BVM	Finite Element	% Error
f_1	17.1	17.2	17.2	0.5%
f_2	103.6	107.7	107.8	-4.1%
f_3	244.2	227.6	228.1	6.8%
f_4	534.5	554.2	554.8	-3.6%
f_5	610.2	592.0	593.6	2.9%

The results show that the fundamental is agree within 0.5% where the same percentage error occurred in the beam with two dimples in the same direction. The percentage error between the experimental results and BVM and FEM results is about 4.1% and 6.8% in the second and third natural frequency. The percentage error in the fourth and fifth natural frequencies is about 3.6% and 2.9% respectively with comparing to those found from experimental.

5.5.2 Fixed-Fixed Beam

As we have seen from the results in Table 5.5, creating two dimples in the same direction on the fixed-fixed beam decreases its first fifth natural frequencies. This is different from the results obtained for creating two dimples in the opposing direction where creating two dimples (convex and concave) decreased the fundamental, third, fourth, and fifth natural frequencies. The second natural frequencies of the beam with two dimples in the opposing direction increased.

In Table 5.8, a comparison between the frequencies obtained experimentally, from BVM, and from FEM is given for a fixed-fixed beam with two dimples in the same direction. The results show that the percentage error in the fundamental frequency between the BVM results and the experimental results is about 4% where the second natural frequency agrees to within 0.03%. The percentage errors in the third and fourth natural frequencies between the experimental results and BVM results are about 3.3% and 4.1% respectively. The percentage errors in the fifth natural frequency is about 9.1%. This error is larger than the first four natural frequencies.

Table 5.8: First five natural frequencies of the fixed-fixed beam with two dimples in the same direction. Experiment vs. BVM vs. Finite Element.

Frequency [Hz]	Experimental	BVM	Finite Element	% Error
f_1	122.7	127.6	127.8	4.0%
f_2	282.7	282.8	282.9	0.03%
f_3	650.6	672.4	672.9	- 3.3%
f_4	970.9	1011.0	1011.9	- 4.1%
f_5	1255.0	1140.0	1142.8	9.1%

Furthermore, the first five natural frequencies for a fixed-fixed beam with two dimples in the opposite direction are tabulated in Table 5.9. As shown, the percentage error between the experimental and BVM results in the fundamental and second frequencies agree to within 2.1% and -2.7% where the percentage error in the third natural frequency is about 6.0%. The percentage error between the experimental results and BVM results in the fourth natural frequency is very small, which is about 0.5%. The percentage error between the BVM and the experimental results in the fifth natural frequency is large, which is about 13.2%.

Table 5.9: First five natural frequencies of the fixed-fixed beam with two dimples in the opposite direction. Experiment vs. BVM vs. Finite Element.

Frequency [Hz]	Experimental	BVM	Finite Element	% Error
f_1	126.2	123.6	123.7	2.1 %
f_2	400.6	411.4	411.3	- 2.7%
f_3	627.3	589.6	590.1	6.0%
f_4	890.3	885.5	887.1	0.5 %
f_5	1272.6	1104.4	1106.4	13.2%

Although there is a small discrepancy with the experiment results, the agreement is good between the three methods. With respect to the experimentally measured natural frequencies, the deviation between the BVM, FEM, and experimental results could be due to the following reasons:

- 1) Beam geometry, i.e. the uniform dimple thickness assumption used in the BVM and FEM models. In practical manufacturing application, the dimple thickness is not uniform (the center of the dimple is the thickest) [4].
- 2) Experimental errors, i.e. boundary conditions and experiment equipment.

CHAPTER 6

INVESTIGATION OF EFFICIENCY OF THE ANALYTICAL MODEL

The purpose of this chapter is to use an analytical model to investigate various configurations of beams and dimples. In previous sections, a comparison between adding two dimples to beams in same and opposing directions (cantilever and fixed-fixed boundary conditions) was made where the natural frequencies were shown to shift away from the values of natural frequency of the uniform beam. Adding dimples to a beam may increase or decrease its natural frequencies. Many factors that may affect the change in the natural frequencies of beams, for instance, boundary condition, dimple location, and dimple angle. All these are considered for beams with two dimples in the same and the opposite direction. The following text gives an investigation of these effects.

6.1 Boundary Condition

In this section, two boundary conditions that were not discussed previously are considered: pin-pin and pin-pin roller (axial motion allowed). Consider a beam with length of 0.2170 and $N = 2$ dimples ($E = 200$ GPa, $\rho = 7870$ kg/m³, $h = 0.00118$ m). The other beam parameters were given previously in Table 3.5 and will be used here again.

6.1.1 -Example 1: Pin-Pin Beam Model

Table 6.1 and 6.2 respectively show the results of the natural frequencies of a pin-pin beam with two dimples in the same and opposing direction.

Table 6.1: First five natural frequencies for the pin-pin beam with two dimples in the same direction.

Frequency [Hz]	Uniform Beam (BVM)	Dimpled Beam (BVM)	Dimpled Beam (FEM)
f_1	57.5	62.7	62.6
f_2	230.2	170.2	170.4
f_3	517.8	474.4	475.0
f_4	920.6	750.3	751.0
f_5	1438.5	1136.2	1140.0

Table 6.2: First five natural frequencies for the pin-pin beam with two dimples in the opposing direction.

Frequency [Hz]	Uniform Beam (BVM)	Dimpled Beam (BVM)	Dimpled Beam (FEM)
f_1	57.5	46.0	46.0
f_2	230.2	265.5	265.3
f_3	517.8	463.4	463.5
f_4	920.6	774.2	775.0
f_5	1438.5	901.6	902.9

The fundamental frequency of the beam with two dimples in the same direction increased (about 9%) with respect to the uniform beam. On the contrary, the fundamental frequency of the pin-pin beam with two dimples in the opposing direction decreased by 20% lower than the uniform pin-pin beam. The second natural frequency of the beam with two dimples in the same direction decreased (about 26%) lower than the uniform beam whereas the beam with two dimples in the opposing direction shows a different behavior where the natural frequency of dimpled beam is increased about 15.3% higher than the uniform beam. The frequencies of the higher modes (the

third, fourth, and fifth) decreased with respect to the pin-pin beam without dimples for the both cases.

6.1.2 Example 2: Pin-Pin Roller Beam Model

In this example, the change in the natural frequencies for a pin-pin roller beam is investigated. Two cases (the beam with two dimples in the same direction and opposing direction) are compared against a uniform beam.

Table 6.3: First five natural frequencies for the pin-pin roller beam with two dimples in the same direction.

Frequency [Hz]	Uniform Beam (BVM)	Dimpled Beam (BVM)	Dimpled Beam (FEM)
f_1	57.5	45.7	45.7
f_2	230.2	169.2	169.3
f_3	517.8	361.0	363.0
f_4	920.6	556.2	557.1
f_5	1438.5	755.5	756.5

Table 6.4: First five natural frequencies for the pin-pin roller beam with two dimples in the opposing direction.

Frequency [Hz]	Uniform Beam (BVM)	Dimpled Beam (BVM)	Dimpled Beam (FEM)
f_1	57.5	45.8	45.8
f_2	230.2	156.9	157.1
f_3	517.8	424.5	425.0
f_4	920.6	558.9	560.1
f_5	1438.5	779.7	780.6

The results show that the change in the natural frequency of the first five modes (Table 6.3) of dimpled pin-pin roller with two dimples in the same direction has decreased monotonically comparing to the pin-pin roller without dimples. Similarly, creating two dimples in the opposing direction in the pin-pin roller beam decreases the first five natural frequencies (Table 6.4).

6.2 Effect of Dimple Location

In Section 6.1, the location of two dimples is held constant for the two examples (pin-pin and pin-pin roller beams) to examine the percentage change of the natural frequency for each boundary condition. In this section, two examples of dimples in the same and opposite directions are considered (see Table 6.5 for beam material and geometric properties) in order to investigate the effect of dimple location on the natural frequencies. In all cases, one dimple is held fixed, and the other dimple moved along the beam.

Table 6.5: Parameters for dimpled beams.

Parameter	Value
Total beam length, L	100 cm
Width, b	5 cm
Thickness, h	1 cm
Dimple cord length, \bar{l}	10 cm
Elastic modulus, E	200 GPa
Density, ρ	7870 kg/m ³

6.2.1 Example 1: Pin-Pin Beam

In this example two cases are considered: a pin-pin beam with two dimples in the same direction and a pin-pin beam with two dimples in the opposite direction. The dimple to the far left is fixed (held at that location) while the second dimple is moved along the beam length as shown in Figs. 6.1 (a) and (b).

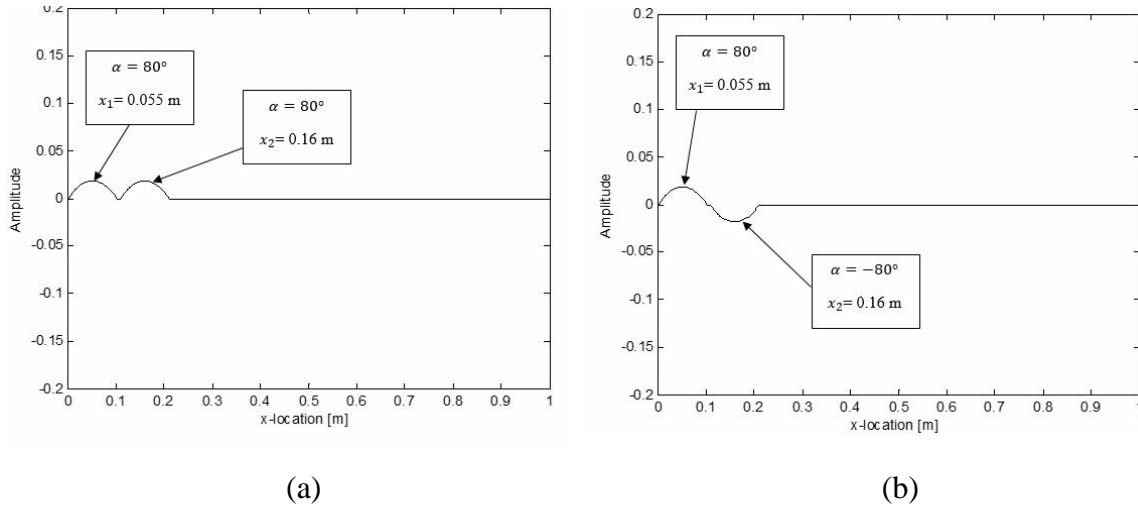


Figure 6.1: Pin-pin beam with two dimples in the same (a) and opposite (b) direction.

6.2.1.1 Pin-Pin Beam with Two Dimples in Same Direction

Table 6.6. consist of six different group set where each set represents one of six different locations for the stationary dimple while the other dimple is moved along the beam length at the location indicated. For example, the first set (set 1) correspond to the stationary dimple being placed as close to the left boundary as possible ($x_1=0.055$ m) and the roving dimple is positioned at different locations on the beam ($x_2 = 0.16, 0.2, \dots, 0.945$). The percentage change in the fundamental frequency for each location is calculated. For all cases, the dimple angle is held constant at $\alpha = 80^\circ$ for both dimples. The percentage change in dimpled beam fundamental frequency f_i with respect to the uniform beam fundamental frequency f_i^* is defined by [1]

$$\Delta f_i [\%] = ((f_i - f_i^*) / f_i^*) * 100 , \quad (6.1)$$

so that a positive change indicates that the fundamental frequency of the dimpled beam being higher than the fundamental frequency of the uniform beam.

Table 6.6: Change in the fundamental frequency of pin-pin beam with two dimples in the same direction with respect to dimple location.

Set 1	$x_1 = 0.055$ (m)							
x_2 (m)	0.16	0.2	0.3	0.4	0.5	0.7	0.8	0.945
The change (%)	0.8	0.8	1.6	2.3	2.3	1.6	0.8	0.03
Set 2	$x_1 = 0.15$ (m)							
x_2 (m)	0.26	0.3	0.4	0.5	0.7	0.8	0.945	
The change (%)	3.9	3.9	5.4	5.4	3.9	3.1	0.8	
Set 3	$x_1 = 0.25$ (m)							
x_2 (m)	0.36	0.4	0.5	0.7	0.8	0.945		
The change (%)	7.8	9.3	9.4	7.0	4.6	1.5		
Set 4	$x_1 = 0.35$ (m)							
x_2 (m)	0.46	0.5	0.7	0.8	0.945			
The change (%)	11.8	11.8	9.3	6.2	1.6			
Set 5	$x_1 = 0.45$ (m)							
x_2 (m)	0.56	0.7	0.8	0.945				
The change (%)	13.4	10.2	7.0	2.3				
Set 6	$x_1 = 0.5$ (m)							
x_2 (m)	0.66	0.8	0.945					
The change (%)	11.8	7.0	2.3					

Myers [1] and Alshabtat [4] observed that placing dimples at locations that corresponded to high modal strain energy resulted in a significant change on corresponding mode's frequency. Myers [1] investigated the effect of placing a single dimple at different locations along the length of the fixed-fixed and pin-pin beam. He observed that fundamental frequency of the pin-pin beam

is most sensitive to the placement of the dimple at the middle of the beam and insensitive when the dimple is located at boundaries. He explained this relation using the concept of modal strain energy (MSE) where the MSE of the uniform pin-pin beam is largest at beam center and zero at boundaries (fundamental mode).

The same behavior for natural frequency of the beam with two dimples in the same direction is observed here. From Table 6.6, it is apparent that The change in fundamental frequency is positive which means the fundamental frequency of the uniform beam increased after adding two dimples in the same direction to the beam ($f_1 > f_1^*$). Also, the largest variation (13.4%) in fundamental frequency occurs when the two dimples are placed close to the beam center ($x_1 = 0.45$ m and $x_2 = 0.56$ m) as shown in Fig. 6.2.

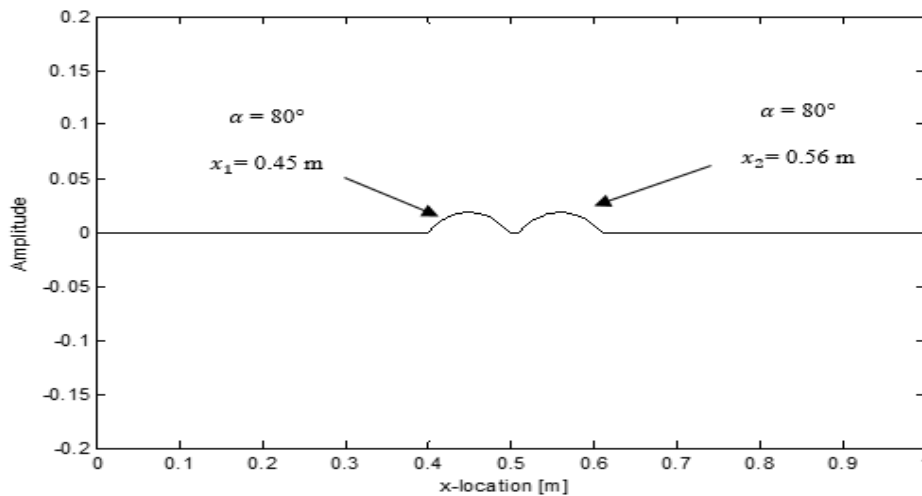


Figure 6.2: Pin-pin beam with the highest change in the fundamental frequency (two dimples in the same direction).

If each dimple is moved towards the boundaries, the change in fundamental frequency begins to decrease. For instance, if the first dimple is located at $x_1 = 0.055$ m and the second dimple is placed at $x_2 = 0.945$ m (see Fig. 6.3), the change in fundamental frequency is minimum which is about 0.03%.

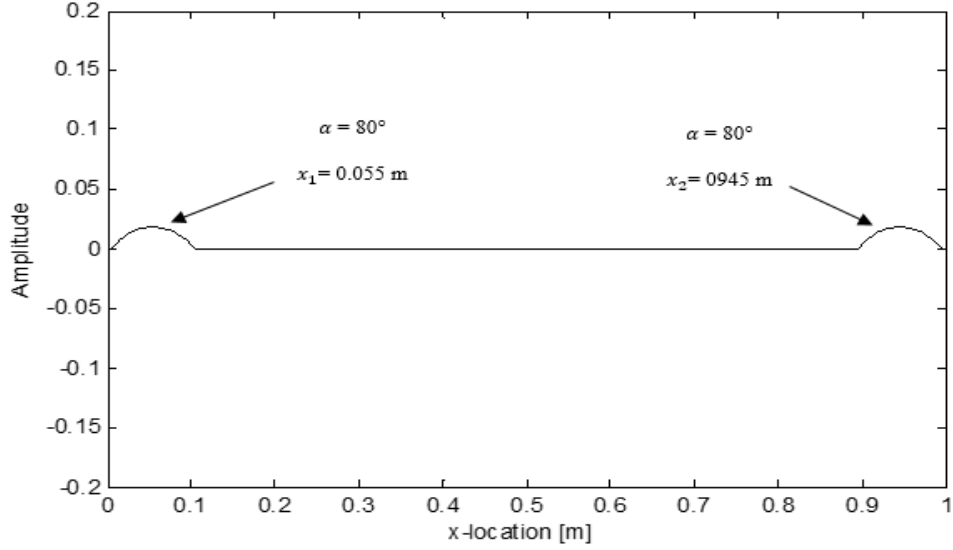


Figure 6.3: Pin-pin beam with the lowest change in the fundamental frequency (two dimples in the same direction).

This is important which indicates that adding two dimples to beams do not guarantee a change in beam natural frequency for some combination of angles and locations. Myers also found that certain combinations of dimple location and dimple angle yield no change in the beam fundamental frequency at all. This was demonstrated for fixed-fixed beam and a pin-pin beam with one dimple [1].

Myers [1] suggested that the shape of the modal strain energy curve of the uniform beam plays a crucial role in determining which dimple locations are most influential. Therefore, by examining the modal strain energy (MSE) obtained from the mode shape of the fundamental mode of the uniform beam, the trend for change in these frequencies can be described. The mode shapes of a uniform pin-pin beam [6] are given by

$$Y_i(x) = \sin(k\pi x/L), \quad (6.2)$$

and the MSE is given as

$$\Psi_k(x) = \sin^2\left(\frac{k\pi x}{L}\right). \quad (6.3)$$

Figures 6.4 and 6.5 respectively show the first three mode shapes and MSE of a uniform pin-pin beam where each plot is symmetric because of the symmetric of boundary conditions.

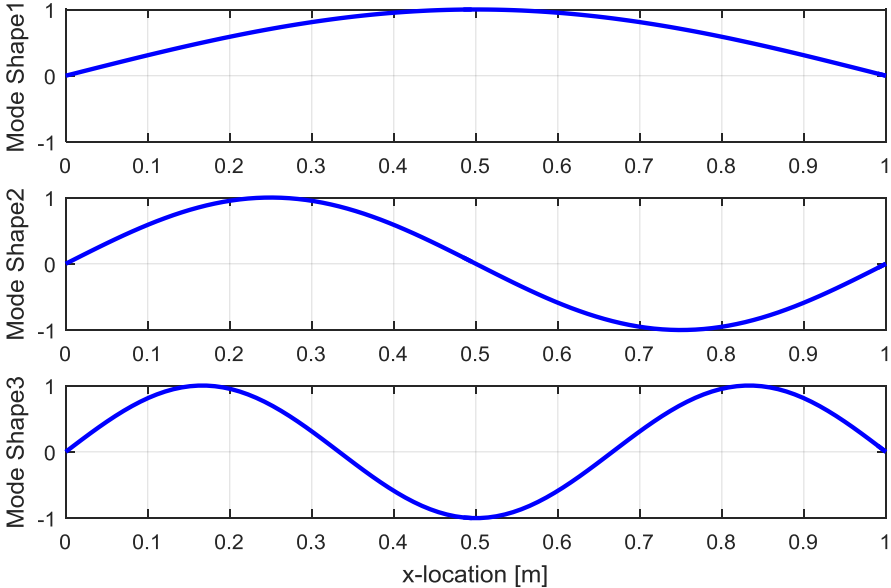


Figure 6.4: First three mode shapes of a uniform pin-pin beam.

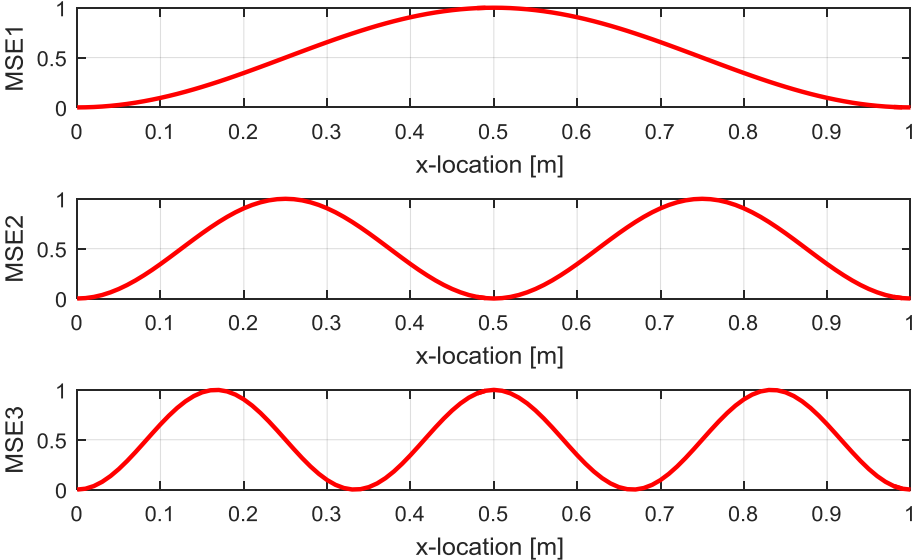


Figure 6.5: Modal strain energy, modes 1-3 (uniform pin-pin beam).

As we can see from Fig. 6.5, the MSE for the first mode (MSE 1) is largest at the beam center ($x = 0.5$ m) and zero at boundaries. Recall from results (Table 6.6) that the fundamental was most sensitive to change at the beam center (largest MSE) and least sensitive when the two dimples were located at the boundaries (zero MSE). Therefore, the fundamental exhibits maximum change if the two dimples are placed in a region of maximum MSE and minimum change if the two dimples are positioned at boundaries where the MSE is zero.

For modes 2 and 3 in Fig. 6.5, a region of high and low MSE occurs at different locations. So, this can explain why the change in frequency of the second mode and third mode are different than the first mode for the same dimple locations. Myers also noticed this when he studied the effect of the dimple location with respect to dimple angle [1, p. 91]. According to Fig. 6.5, the maximum modal strain energy of the second mode (MSE 2) is at $x = 0.25$ m and $x = 0.75$ m (the anti-nodes).

Figure 6.6 shows the change in the second frequency of the pin-pin beam with two dimples in the same direction. One dimple is held at $x_1 = 0.25$ m and the second dimple is moved along the beam length (x_1 and x_2 represents the center of the first and second dimples, respectively).

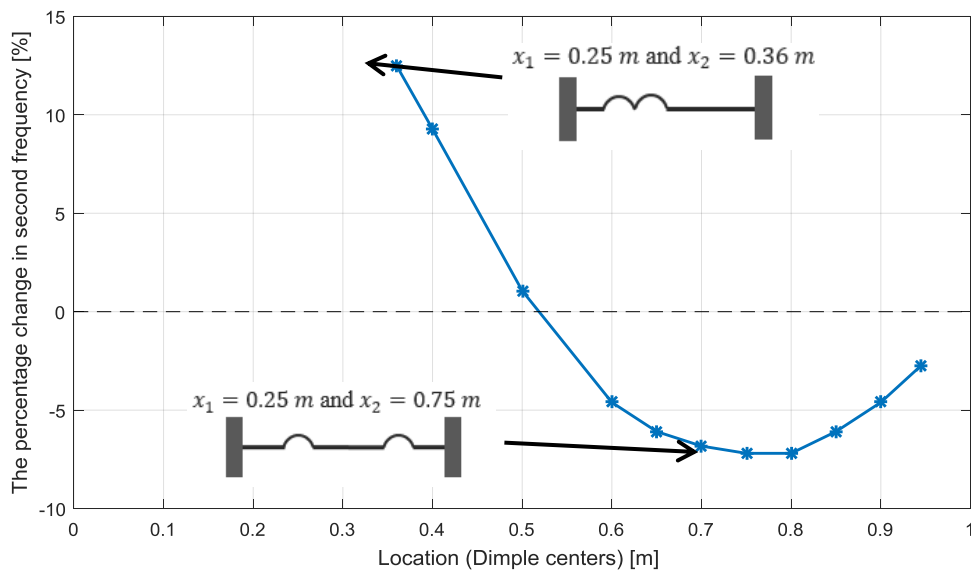


Figure 6.6: Change in the second frequency of pin-pin beam with two dimples in same direction ($x_1 = 0.25$ m and x_2 is moved along the beam length) vs. dimple location.

Therefore, if two dimples in the same direction are placed at $x_1 = 0.25 \text{ m}$ and $x_2 = 0.36 \text{ m}$ (see Fig. 6.7), so, the change in the natural frequency of the second mode at these location has the highest values (12.5%, largest increase, see Fig. 6.6) where MSE is maximum.

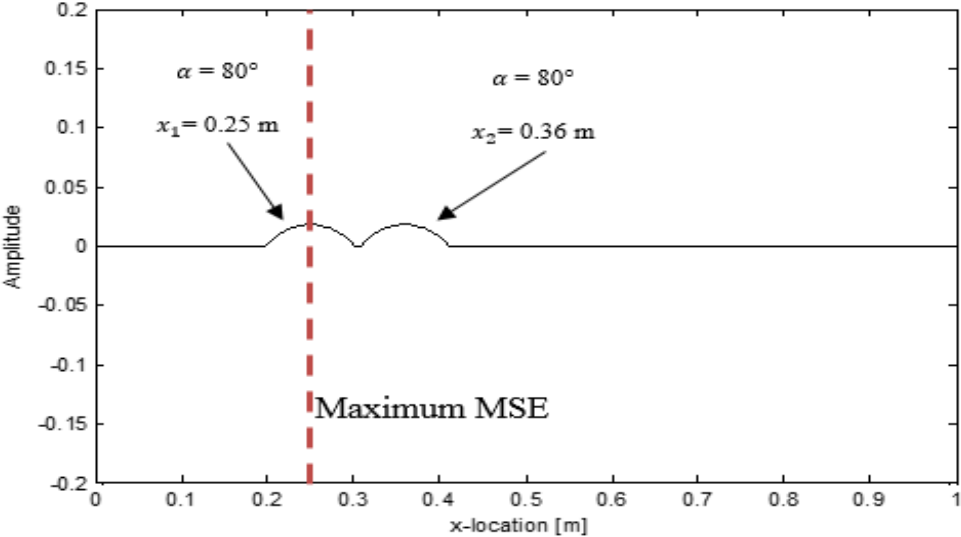


Figure 6.7: Pin-pin beam with the highest frequency for second mode, MSE 2 (red dashed line).

Similarly, if the dimples are placed at $x_1 = 0.25 \text{ m}$ and $x_2 = 0.75 \text{ m}$ as shown in Fig. 6.8 (high MSE), the change in frequency is large (about -7.2% largest decrease, see Fig. 6.6). In other words, the largest decrease in the second frequency occurs at these locations where the modal strain energy (MSE 2) is the maximum.

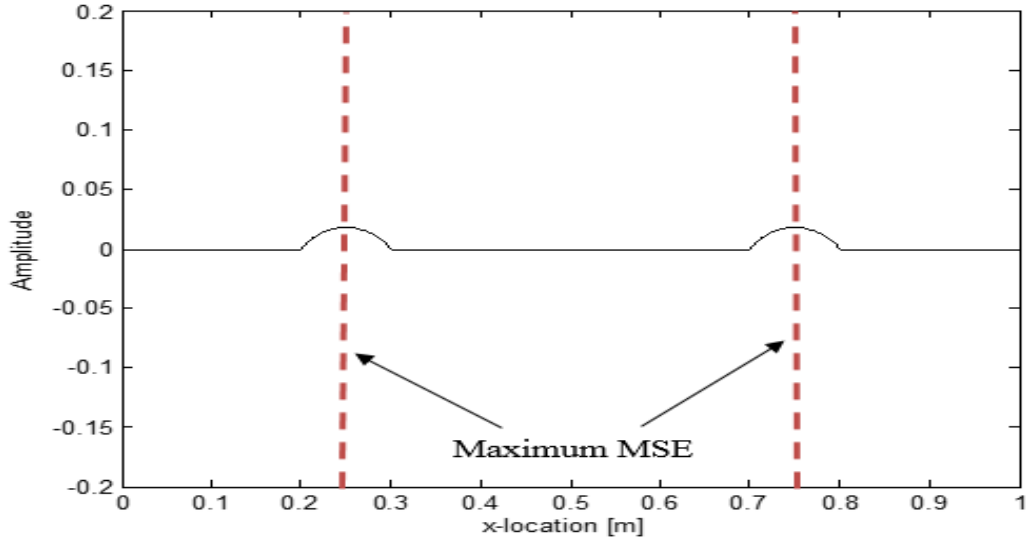


Figure 6.8: Pin-pin beam with two dimples in the same direction for the second mode (a beam with two dimples in the same direction), $x = 0.25 \text{ m}$ and $x = 0.75 \text{ m}$, the maximum MSE 2 red dashed line.

The converse is also true: the second frequency exhibits minimum sensitivity to change in the region of zero MSE at the two boundaries and $x = 0.5 \text{ m}$. For example, if the two dimples are placed at $x_1 = 0.5 \text{ m}$ and the second dimple placed at $x_2 = 0.61 \text{ m}$ (both dimples occupy the entire region of zero MSE 2 (see Fig. 6.9), then the natural frequency of the second mode exhibits a small variation of 0.08% (Table 6.7). This means that there is negligible change in second frequency ($f_2 \cong f_2^*$) when placing dimples at the location of zero modal strain energy (MSE 2 = 0).

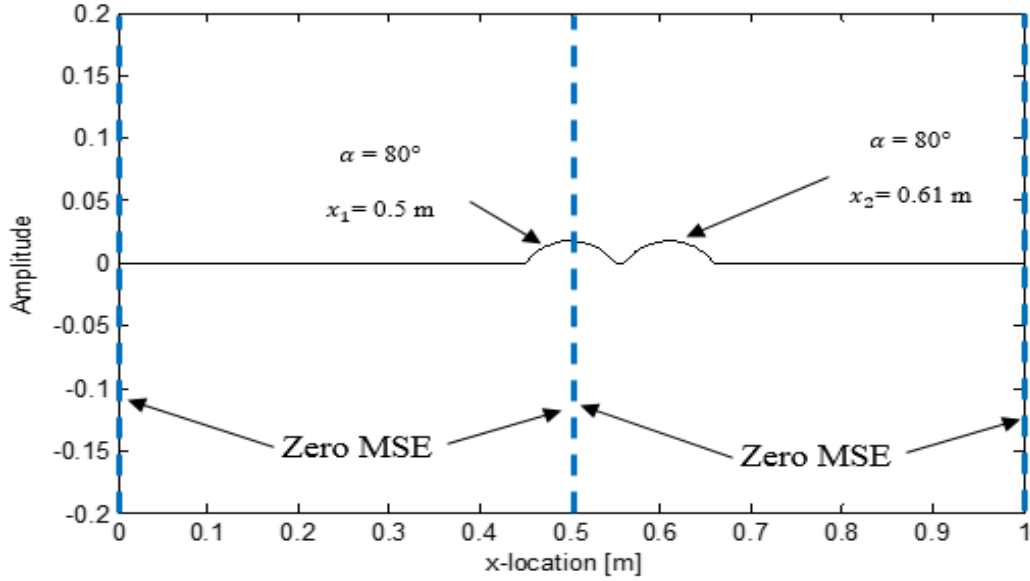


Figure 6.9: Pin-pin beam with the lowest change in frequency for the second mode. Areas of low MSE are indicated using the blue dashed lines.

Table 6.7: Change in the second frequency of pin-pin beam with two dimples in the same direction with respect to dimple location, $x_1 = 0.5 \text{ m}$, and the second dimple is moved along the beam length.

Set	$x_1 = 0.5 \text{ (m)}$							
$x_2 \text{ (m)}$	0.61	0.65	0.7	0.75	0.8	0.85	0.9	0.945
The change (%)	-0.082	0.30	1.06	1.06	0.68	0.30	-0.46	-0.8

In addition, placing one or both dimples also to the beam yields minimal change in the frequency for the second mode because of the MSE is zero at these locations. It is apparent that the dimple location has an effect on natural frequencies and the increase or decrease in these frequencies coincides with a region of high and low MSE. Myers [1] explained that region of high MSE corresponds to areas where the curvature (Y'') is large because the bending slope is rapidly changing in these areas. Therefore, in high MSE region, the internal moment is large. As a result, when dimples are placed at high bending moment areas, they have a significant effect on the beam dynamics. On the contrary, there is little effect on natural frequencies when dimples are located at areas corresponding to small internal bending moment (small MSE).

6.2.1.2 A Pin-Pin Beam with Two Dimples in Opposite Direction.

As before, a pin-pin beam with two dimples in opposing direction considered is as an example. Table 6.8 shows six sets of results in which one dimple is held constant while the location of the second dimple is moved along the beam length.

Table 6.8: Change in the fundamental frequency of pin-pin beam with two dimples in the opposing direction with respect to change in dimple location.

Set 1	$x_1 = 0.055$ (m)							
x_2 (m)	0.16	0.2	0.3	0.4	0.5	0.7	0.8	0.945
The change (%)	- 0.7	- 1.5	- 1.5	- 0.7	- 0.7	- 1.5	- 1.5	- 0.73
Set 2	$x_1 = 0.15$ (m)							
x_2 (m)	0.26	0.3	0.4	0.5	0.7	0.8	0.945	
The change (%)	- 3.0	- 3.0	- 3.8	- 3.8	- 3.00	- 2.3	- 0.7	
Set 3	$x_1 = 0.25$ (m)							
x_2 (m)	0.36	0.4	0.5	0.7	0.8	0.945		
The change (%)	- 5.2	- 5.2	- 5.2	- 4.5	- 3.7	- 1.5		
Set 4	$x_1 = 0.35$ (m)							
x_2 (m)	0.46	0.5	0.7	0.8	0.945			
The change (%)	- 6.7	- 6.7	- 6.0	- 4.5	- 1.5			
Set 5	$x_1 = 0.45$ (m)							
x_2 (m)	0.56	0.7	0.8	0.945				
The change (%)	-7.3	- 6.4	- 4.6	- 1.0				
Set 6	$x_1 = 0.5$ (m)							
x_2 (m)	0.66	0.8	0.945					
The change (%)	- 6.4	- 4.7	- 1.0					

The results indicate that the change in the fundamental for the all six location set has a negative effect on the fundamental frequency of the dimpled beam (the dimpled values are lower than the fundamental frequency of the uniform Beam). In other words, creating two dimples in the opposing direction in the pin-pin beam decrease its fundamental frequency in certain values. Several observations can be made by examination of Table 6.8. In terms of the fundamental frequency, it shows that the largest variation in fundamental frequency (about -7.3%, negative means $f_1 < f_1^*$) occurs at beam center. This is expected because the MSE for the first mode (Fig. 6.5) is large at beam center. The same observation is noted in the beam with two dimples in the same direction where the fundamental frequency is having a maximum change when the two dimples were placed at middle of the beam. Recall that the variation in fundamental frequency of the beam with two dimples in the same direction is positive while in the one with two dimples in the opposing direction the variation is negative. In the first case both dimples are in the same direction but in the second case, both dimples are in the opposing direction, that is, the slope and bending moment equations of one dimple have negative signs (Eqs. 3.38b and 3.38c) because this dimple is in the opposite side of the beam.

A comparison for the previously two cases (pin-pin beam with two dimples in the same direction and pin-pin beam with two dimples in opposing direction, is made. Figure 6.10 illustrates the comparison between the both cases, (also, see Tables 6.6 and 6.8), where one dimple is placed at $x_1 = 0.45$ m while the other dimple is positioned at different locations on the beam.

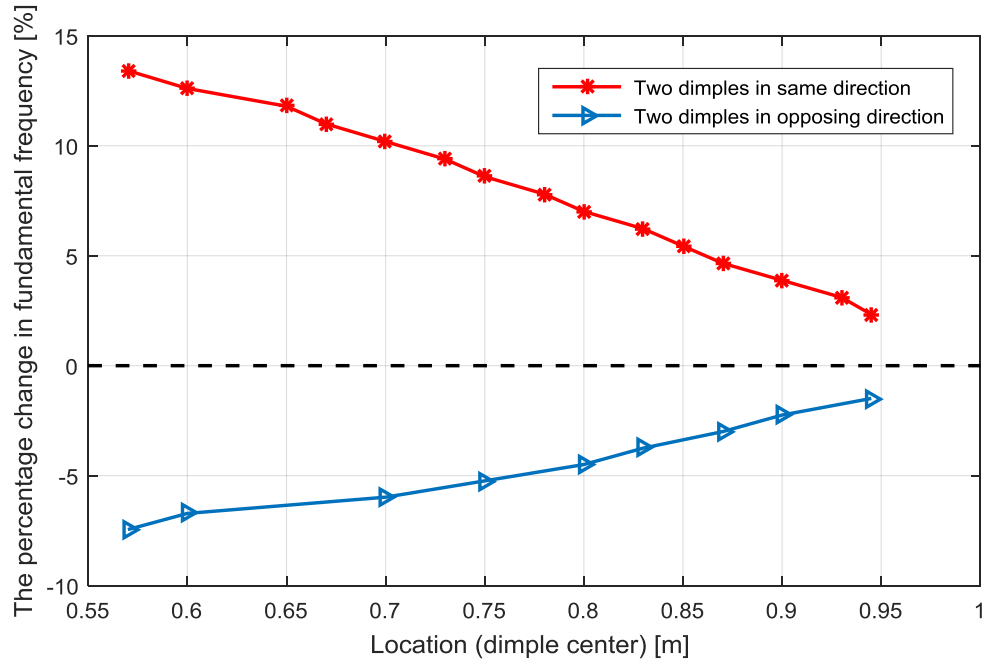


Figure 6.10: Change in the fundamental frequency vs. dimple location (pin-pin beam), $x_1 = 0.45 \text{ m}$, and x_2 is moved along the beam length, and $\alpha_1 = \alpha_2 = 80^\circ$.

Figure 6.10 shows that the largest variation in fundamental occurs when the two dimples are placed at beam center ($x_1 = 0.45 \text{ m}$ and $x_2 = 0.56 \text{ m}$). As the second dimple is moved towards the right boundary, the fundamental begins to decrease with the smallest change in fundamental frequency occurring at boundary (MSE 1= zero). It should be noted that the change in fundamental frequency of the two cases represent the same behavior where the change in the beam with two dimples in the opposing direction is negative. Recall that in the pin-pin beam with two dimples in the opposing direction, so the slope and bending moment equations are negative (Eqs. 3.38 (b) and (c)) which affect the percentage change in the fundamental frequency (negative change means fundamental is lower than that of the uniform beam ($f_1 < f_1^*$)). Because of the symmetry of pin-pin boundary condition, Fig. 6.10 is shown for only half of the beam length. So, percentage change is same at the other half boundary of the pin-pin beam where the variation is the largest at the beam center and it is minimum at the boundary.

Thus far, the analysis been limited to the fundamental frequency. Next, we will explore the question: how does the second mode behave when one dimple is fixed at a region of high MSE ($x_1 = 0.25$ m) and the second dimple is moved along the beam length? Figure 6.11 shows the behavior of the second frequency for both cases, a beam with two dimples in the same direction and opposing direction.

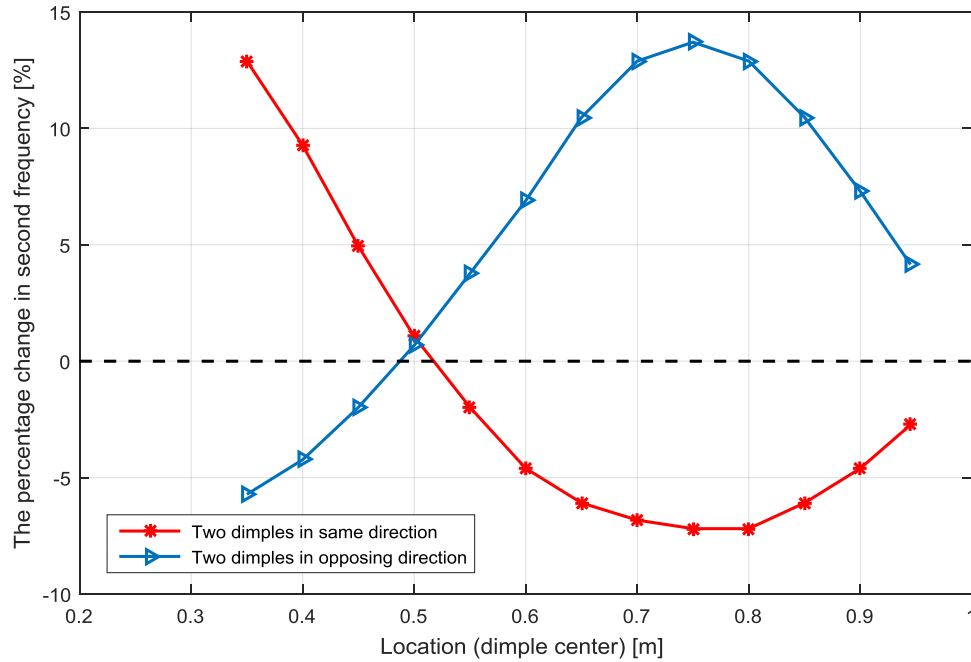


Figure 6.11: Change in the second frequency vs. dimple location (pin-pin beam), $x_1 = 0.25$ m, x_2 is moved along the beam length, and $\alpha_1 = \alpha_2 = 80^\circ$.

The modal strain energy of the second mode for uniform pin-pin beam exhibit some regions where the modal strain energy is large or equal to zero. The increase and decrease in the second frequency of the dimpled pin-pin beam correspond to these locations of high or zero modal strain energy. From Fig. 6.11, the largest variation in second frequency for case of both dimples in the same direction is about 12.5%, occurs at $x_1 = 0.25$ m and $x_2 = 0.36$ m (highest MSE 2). The largest decrease in the second frequency, which is - 7.2%, occurred when two dimples were located at $x_1 = 0.25$ m and $x_2 = 0.75$ m (highest MSE 2). Similarly, placing two dimples at $x_1 = 0.25$ m and $x_2 = 0.75$ m (anti-nodes of the second mode, largest MSE 2) will have the largest

effect on the second frequency, which is 13.7% (pin-pin beam with two dimples in the opposing direction). Also, if both dimples are placed at $x_1 = 0.25$ m, $x_2 = 0.36$ m, the largest decrease in the second mode will be about - 5.2% (pin-pin beam with two dimples in the opposing direction). As we mentioned before, modal strain energy is zero at boundary and beam center, so the change in the second frequency at these regions exhibits a small percentage change. The fundamental and second natural frequency variations will be discussed more in the Section 6.3 where different angles will be considered.

6.2.2 Example 2: Fixed- Fixed Beam Model

As before, a fixed-fixed beam is considered with properties given in Table 6.5. Combination locations of dimple centers (x_1 and x_2) are set where two cases are considered: a fixed-fixed beam with two dimples in the same direction and a fixed-fixed beam with two dimples in the opposite direction. Tables 6.9 and 6.10 respectively summarize the results of the percentage change in fundamental frequencies of both cases in which one dimple is placed at a fixed place while the other dimple is moved along the beam length.

Table 6.9: Change in the fundamental frequency of fixed-fixed beam with two dimples in the same direction with respect to dimple location.

Set 1	$x_1 = 0.055$ (m)							
x_2 (m)	0.16	0.2	0.3	0.4	0.5	0.7	0.8	0.945
The change (%)	8.5	3.8	- 3.3	- 6.3	-6.7	-2.8	2.3	18.8
Set 2	$x_1 = 0.15$ (m)							
x_2 (m)	0.26	0.3	0.4	0.5	0.7	0.8	0.945	
The change (%)	- 1.3	- 1.7	- 2.8	- 2.8	- 1.8	0.2	6.4	
Set 3	$x_1 = 0.25$ (m)							
x_2 (m)	0.36	0.4	0.5	0.7	0.8	0.945		
The change (%)	0.73	1.2	1.8	0.2	- 0.8	- 0.8		
Set 4	$x_1 = 0.35$ (m)							
x_2 (m)	0.46	0.5	0.7	0.8	0.945			
The change (%)	7.0	7.0	2.8	- 0.8	- 4.8			
Set 5	$x_1 = 0.45$ (m)							
x_2 (m)	0.56	0.7	0.8	0.945				
The change (%)	10.1	4.3	- 0.8	- 6.3				
Set 6	$x_1 = 0.5$ (m)							
x_2 (m)	0.66	0.8	0.945					
The change (%)	6.4	- 0.8	- 6.8					

Table 6.10: Change in the fundamental frequency of fixed-fixed beam with two dimples in the opposing direction with respect to dimple location.

Set 1	$x_1 = 0.055$ (m)							
x_2 (m)	0.16	0.2	0.3	0.4	0.5	0.7	0.8	0.945
The change (%)	- 2.8	- 0.8	4.8	10.1	13.3	5.9	- 0.3	- 8.2
Set 2	$x_1 = 0.15$ (m)							
x_2 (m)	0.26	0.3	0.4	0.5	0.7	0.8	0.945	
The change (%)	0.2	1.2	3.8	4.8	1.8	-1.3	- 3.3	
Set 3	$x_1 = 0.25$ (m)							
x_2 (m)	0.36	0.4	0.5	0.7	0.8	0.945		
The change (%)	- 0.8	- 0.8	- 0.8	- 0.8	- 0.3	2.8		
Set 4	$x_1 = 0.35$ (m)							
x_2 (m)	0.46	0.5	0.7	0.8	0.945			
The change (%)	-3.8	-3.8	-2.3	0.7	9.0			
Set 5	$x_1 = 0.45$ (m)							
x_2 (m)	0.56	0.7	0.8	0.945				
The change (%)	- 4.8	- 2.3	1.8	12.8				
Set 6	$x_1 = 0.5$ (m)							
x_2 (m)	0.66	0.8	0.945					
The change (%)	-3.8	1.8	12.8					

The results show that the largest increase in fundamental frequency of the beam with two dimples in the same direction occurred when each dimple was located at the boundary ($x_1 = 0.55$ m and $x_2 = 0.945$ m, see Fig. 6.12) (about 18.8%). Also, if both dimples are placed at the boundary ($x_1 = 0.055$ m and $x_2 = 0.16$ m), the fundamental frequency is large, which is about 8.8%, but not as large as when placing each dimple at $x_1 = 0.055$ m and $x_2 = 0.945$ m.

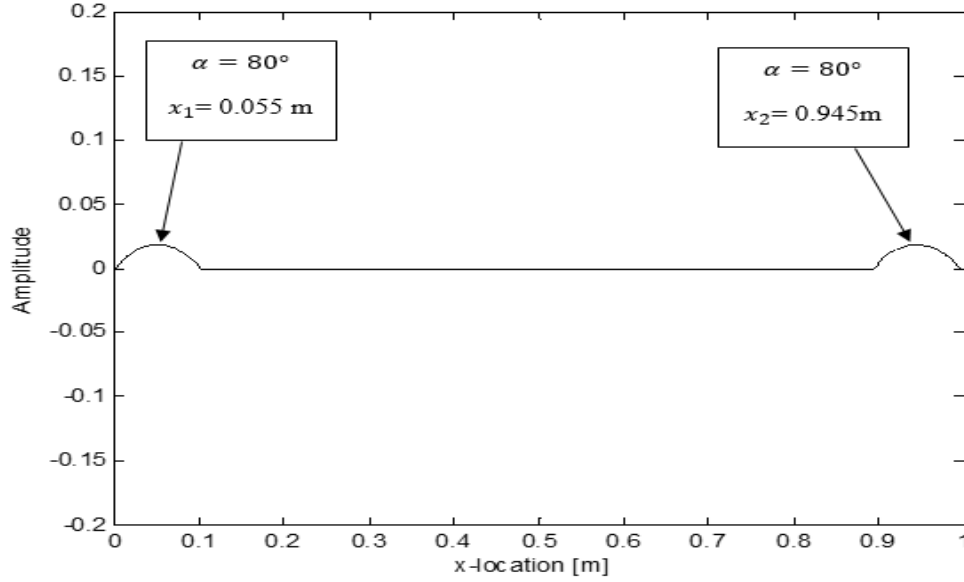


Figure 6.12: Fixed-fixed beam with the highest change in fundamental frequency (the beam with two dimples in the same direction).

In contrast, when one dimple was placed at the boundary and the second dimple was placed at the beam center, this resulted in the largest decrease in the fundamental frequency (the beam with two dimples in the same direction) (about -6.8%). Before we discuss the change in frequencies of the beam with two dimples in the opposing direction, it is important to examine the modal strain energy of the fixed-fixed beam to understand the reason why the change in frequencies is affected by the dimples location.

For the uniform fixed-fixed beam, the MSE is given by [1]

$$\Psi_k(x) = \frac{1}{4} [-\cos \beta_i x - \cosh \beta_i x + D_i(\sin \beta_i x + \sinh \beta_i x)]^2, \quad (6.4)$$

where the constant D_i is given by

$$\frac{(\cos \beta_i L - \cosh \beta_i L)}{(\cos \beta_i L + \cosh \beta_i L)}. \quad (6.5)$$

The values of $\beta_i L$ and D_i are given in Table 6.11 [21].

Table 6.11: Modal strain energy parameters (fixed-fixed beam).

Mode	$\beta_i L$	D_i
1	1.730	0.9825
2	7.853	10008
3	10.996	1.000

Figure 6.13 shows the modal strain energy curves of the first three modes of a uniform fixed-fixed beam. The modal strain energy per length for the first mode has the maximum value at the boundary, and is relatively large at the beam's center. The MSE is zero at $x = 0.22$ m and $x = 0.77$ m. The Second and third modes represent different behavior of MSE. The modal strain energy for mode 2 is large at the boundary and relatively large at $x = 0.3$ m and $x = 0.7$ m. It is zero at $x = 0.13$ m, $x = 0.5$ m and $x = 0.87$ m. Mode 3 exhibits a very different MSE curve as shown in Fig. 6.13.

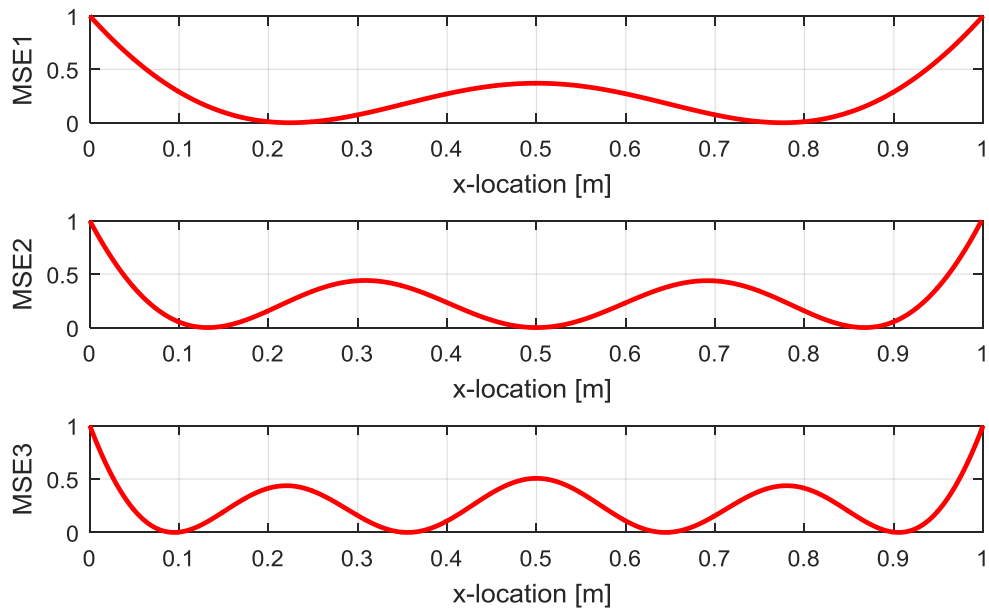


Figure 6.13: Modal strain energy, modes 1-3 (uniform fixed-fixed beam).

Thus, now it is apparent that the fundamental, second, and third frequencies each have maximum MSE at the boundary and relatively large or zero MSE at different locations along the length of the beam. More observation can be made by examination of Figure 6.14 which shows the effect of dimple locations against the percentage change of the fundamental frequency. One dimple is held at $x_1 = 0.055$ m and the second dimple is moved along the beam length. The plots represent a fixed-fixed beam with two dimples in the same direction (the beam with two dimples in the same direction) and a fixed-fixed beam with two dimples in the opposing direction (the beam with two dimples in the opposing direction).

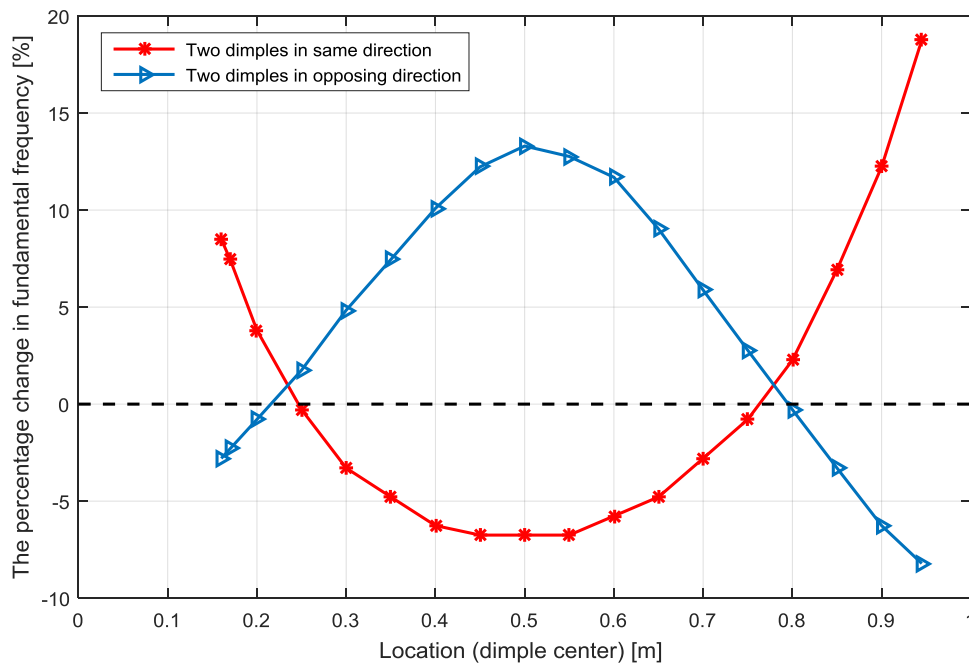


Figure 6.14: Change in the fundamental frequency vs. dimple locations (fixed-fixed beam), with $x_1 = 0.055$ m, x_2 is moved along the beam length, and $\alpha_1 = \alpha_2 = 80^\circ$.

From Fig. 6.14, it is apparent that various combinations of dimple locations can increase or decrease the fundamental frequency with respect to the uniform beam when the two dimple angles are 80 degrees. Figure 6.14 shows that the largest increase in the fundamental frequency (dimples are in the same direction), which is about 18%, occurs when each dimple is placed at each boundary $x_1 = 0.055$ m and $x_2 = 0.955$ m, high MSE. Also, the largest decrease in fundamental frequency (the beam with two dimples in the same direction) occurs when each dimple is located at $x_1 = 0.055$ m and $x_2 = 0.5$ m, relatively large MSE. In addition, locating

each dimple at $x_1 = 0.22$ m and $x_2 = 0.77$ m (zero MSE) exhibits no change in the fundamental frequency. It was observed that the fundamental frequency of the fixed-fixed beam with two dimples in the same direction begins to decrease when one dimple is fixed at the left boundary and the second dimple is moved towards the beam center. At certain location (beam center), the fundamental frequency starts to increase.

The largest decrease, which is about -8.2% , in fundamental frequency for the beam with two dimples in the opposing direction occurs when each dimple is placed at each boundary (largest MSE, Fig. 6.13). Also, the largest increase in the fundamental frequency, which is about 13.3% , occurs when one dimple is fixed at the boundary (the largest MSE), and the other dimple is placed at beam center (low MSE). The least amount of variation of fundamental frequency occurs where both dimples are placed at $x = 0.22$ m and $x = 0.77$ m (zero MSE) respectively. The examples presented here have demonstrated that both cases exhibit the same trend; the effect of creating two dimples is significant when dimples are placed at the area of high strain energy as shown in Fig. 6.13. In other words, the fundamental frequency exhibits a large variation (increasing or decreasing in frequency with respect to that of a uniform fixed-fixed beam) in regions of high MSE and small variation at regions of low or zero MSE.

6.3 Effect of Dimple Angle

In this section, the effect of dimple angle on the first three modes is studied. The two examples presented before will be investigated again by changing the dimples' angles. Fixed-fixed and pin-pin beams are known to be axially restricted boundary conditions.

6.3.1 Example 1: Pin-Pin Beam Model

In the previous section, the change in fundamental frequency with respect to the uniform beams natural frequency was shown for constant angle values. In this section, the same example given in Section 6.2.1 will be presented but now different angles are considered. The percentage change in fundamental frequency of a pin-pin is shown in Fig. 6.15.

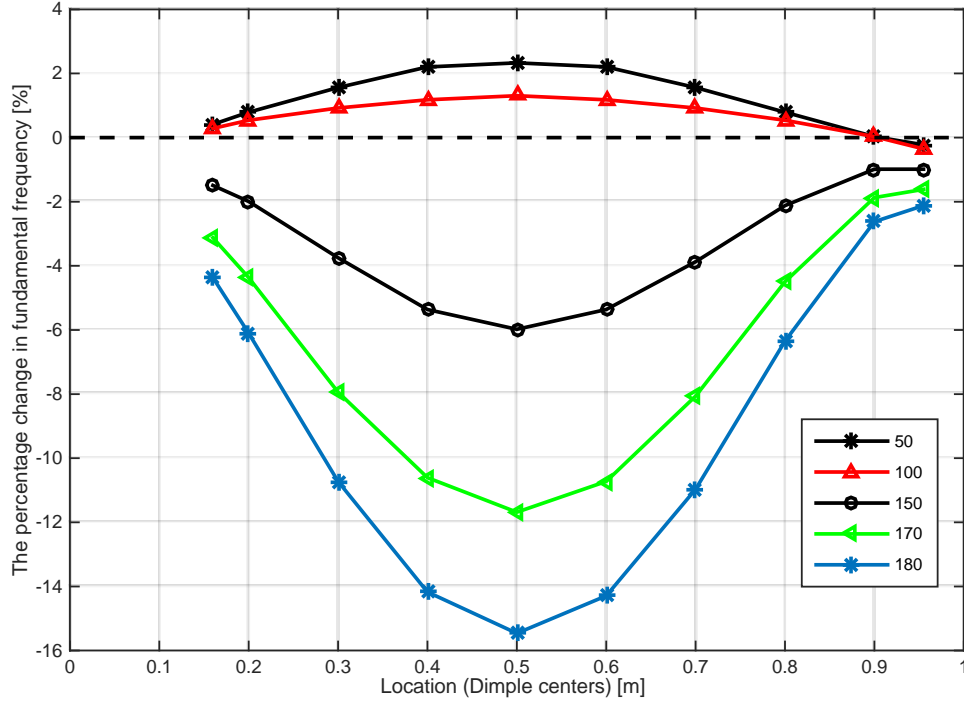


Figure 6.15: Change in fundamental frequency vs. dimple location, five different dimple angles for the pin-pin beam with two dimples in the same direction, $N = 2$ with $x_1 = 0.055$ m and the second dimple is moved along the beam length.

The percentage change in fundamental frequency is plotted against dimple locations where each curve corresponds to different dimple angles. The plots are shown for a 1 m beam length where one dimple is placed at $x_1 = 0.055$ m and the second dimple is moved along the beam length. All angles represent a variation between -15.5% when $\alpha = 180^\circ$ (largest decrease), and 2.1% when $\alpha = 50^\circ$ (largest increase). As mentioned in the previous sections, the modal strain energy for a uniform pin-pin beam is largest at the beam center and zero at boundary. Therefore, it is shown from Fig. 6.15 that the fundamental frequency is very sensitive to change in dimple angles for one dimple located at the boundary and the second dimple placed at beam center. It is also apparent that if the second dimple is moved towards the boundary, the percentage change of fundamental frequency begins to increase with certain angles or decrease for other angles. Moreover, from Fig. 6.15 it can be seen that there is a small variation between the curve of $\alpha = 50^\circ$ and $\alpha = 100^\circ$ where both of them increase the fundamental frequency of the pin-pin beam with two dimples in the same direction. The other angles (150° - 180°) decrease the fundamental frequency of the pin-pin beam with two dimples in the same direction.

Figure 6.16 shows that the change in fundamental frequency of a pin-pin beam with two dimples in the opposing direction against dimple locations for five different dimple angles.

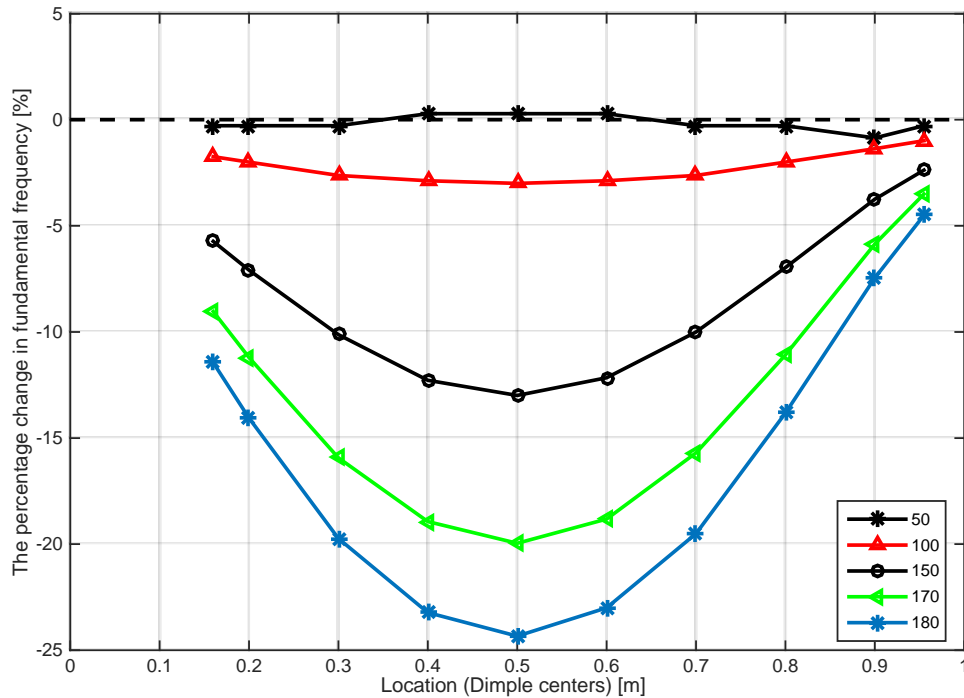


Figure 6.16: Change in fundamental frequency vs. dimple locations, five different dimple angles for the pin-pin beam with two dimples in the opposing direction, $N = 2$ with $x_1 = 0.055$ m and the second dimple is moved along the beam length.

Figure 6.16 illustrates that the percent change in fundamental frequency for all angles is negative which means the fundamental frequency of dimpled pin-pin beam is lower than the uniform pin-pin beam. For the dimple angles shown, the variation behaves in a similar trend as in the first case (pin-pin beam with two dimples in the same direction). The results demonstrated that adding two dimples in the opposing direction to the pin-pin beam with a combination of various dimple angles and locations decreased the fundamental frequency of the pin-pin beam more than creating two dimples on the pin-pin beam in the same direction.

Next, the percent change in fundamental frequency of the pin-pin beam with two dimples in the same and opposite direction with changing dimple angle is investigated. In Figs. 6.17 and 6.18, three dimples locations are considered: each dimple is located at the left and right boundary, both dimples are placed near the beam center, and one dimple is positioned at beam center, and

the other dimple is placed at the boundary. These locations are interesting due to the effect of MSE on the fundamental frequency in these regions.

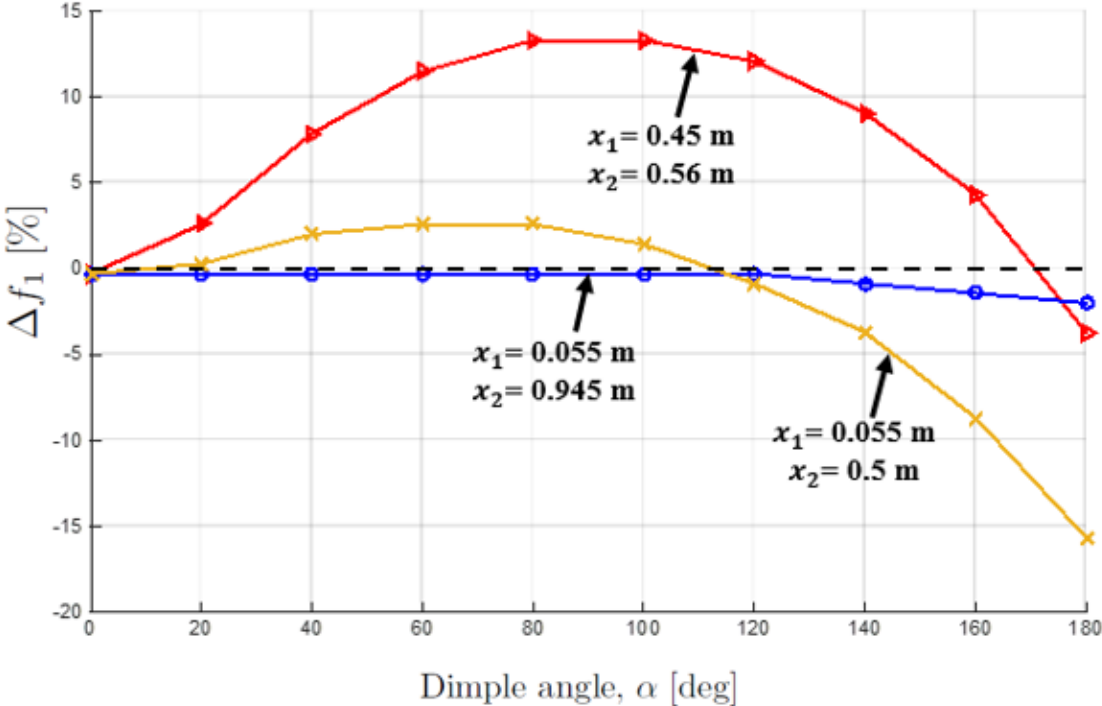


Figure 6.17: Change in fundamental frequency vs. dimple angles, three different dimple locations (pin-pin beam with two dimples in the same direction).

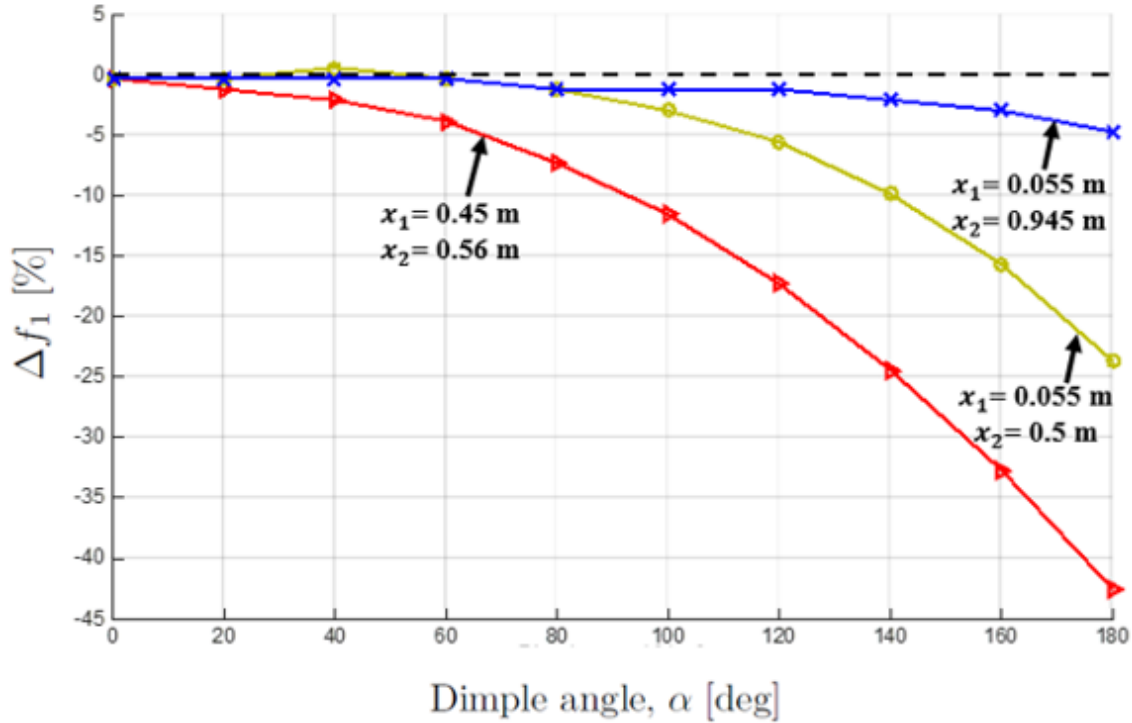


Figure 6.18: Change in fundamental frequency vs. dimple angles, three different dimple locations (pin-pin beam with two dimples in the opposing direction).

Recall from Fig. 6.5 that the fundamental frequency was most sensitive to changes in dimple angle at beam center (largest MSE) and least sensitive when dimples were located at the boundaries. As a result, comparing the sensitivity of the maximum and minimum change in fundamental frequency at these locations for both cases, the fundamental frequency is most sensitive to changes in dimple angle when both dimples are placed close to each other at beam center, $x_1 = 0.45$ m, $x_2 = 0.56$ m (largest MSE). Also, the fundamental frequency exhibits a moderate sensitivity to dimple angles occurring when one dimple is located at $x_1 = 0.055$ m (the left boundary, zero MSE) and the other dimples is placed at the beam center (largest MSE). A comparatively very small sensitivity to dimple location is observed when each dimple is located at each boundary (zero MSE). For the dimples placed at the left boundary and at the beam center ($x_1 = 0.055$ m and $x_2 = 0.5$ m, the beam with two dimples in the same direction), there is also an initial increase and decrease of the fundamental frequency, although the peak change in natural frequency is not as large compared to the dimples placed at beam center. In addition, it is observed that the variation of

the fundamental frequency of the pin-pin beam with two dimples in the opposing direction is negative which indicates that the fundamental frequency of dimpled pin-pin beam is lower than the fundamental frequency of the uniform pin-pin beam.

Thus far, in the previous section, an example of the pin-pin beam with two dimples was presented. Next, the same example will be presented with five different angles to investigate the behavior of the change in the natural frequency of the second mode (the beam with two dimples in the opposing direction). To illustrate, one dimple is fixed at $x_1 = 0.055$ m and the other dimple is moved along the beam length.

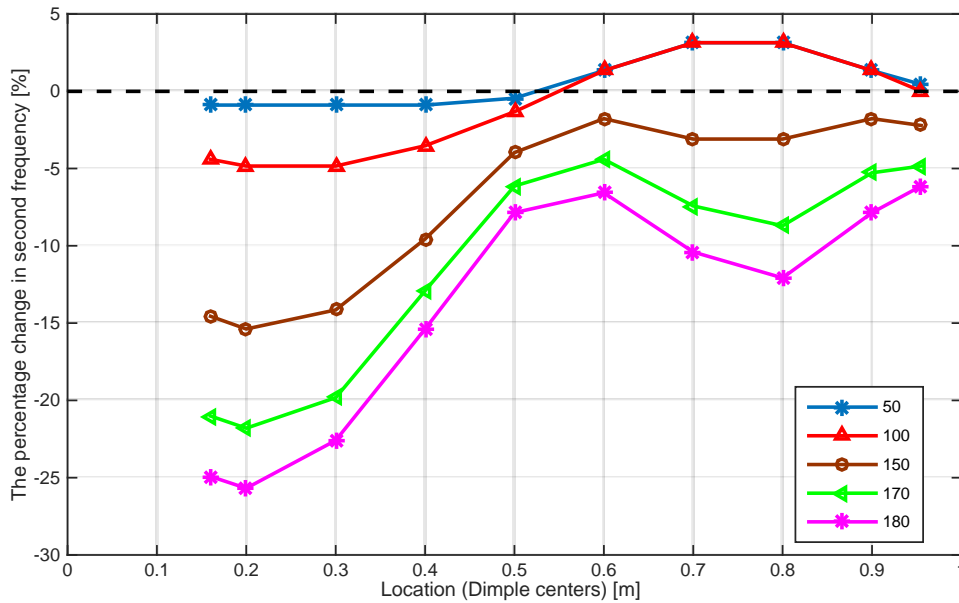


Figure 6.19: Change in second frequency vs. dimple locations, five different dimple angles for pin-pin beam with two dimples in the opposing direction, $N = 2$ with $x_1 = 0.055$ m and the second dimple is moved along the beam length.

With reference to Fig. 6.19, each curve represents the change in the second frequency against the dimples locations. The variation is between 4% (at $\alpha = 50^\circ$ and $\alpha = 100^\circ$) and -26% (at 180°) where the change in second frequency of these angles $\alpha = 50^\circ$ and $\alpha = 100^\circ$ is small. Also, the percentage change in the second frequency is small when one dimple is placed at left boundary, and the other dimple moved towards the beam center where the MSE of the second mode is zero at beam center and boundaries.

Next, the analysis of the second frequency is investigated using the same beam with two dimples in the same and opposite direction where the regions of high and low modal strain energy are selected to locate the dimple. In Figs. 6.20 and 6.21, the change in second frequency of a pin-pin beam with two dimples in the same and opposite direction is plotted against dimple angle.

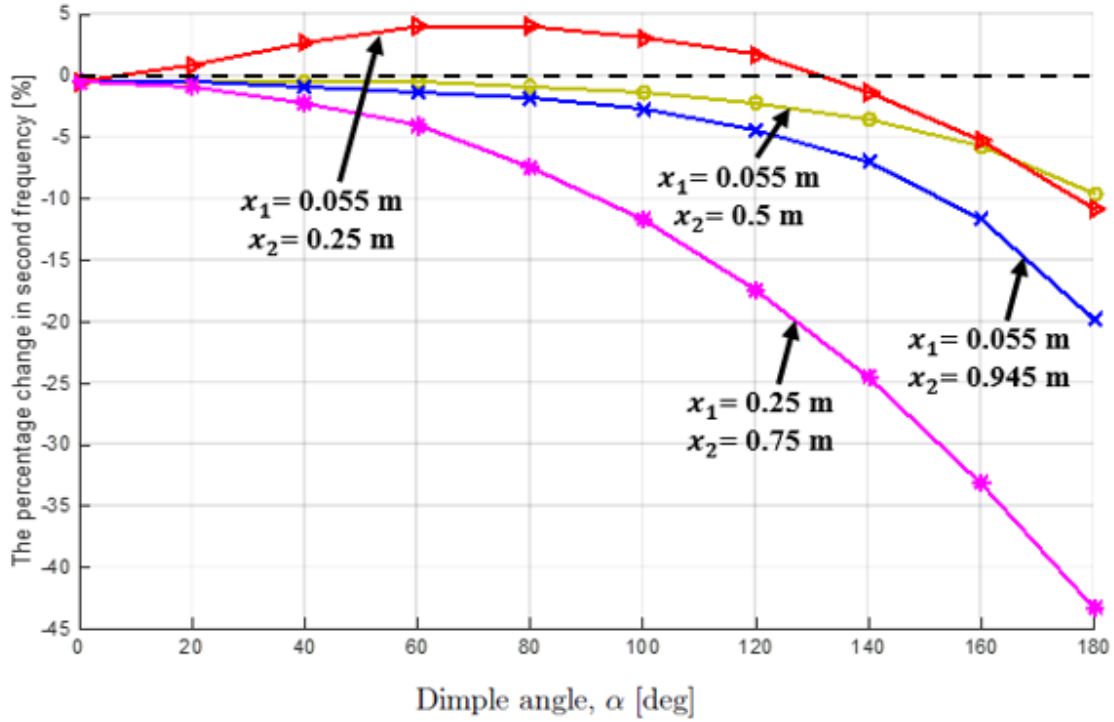


Figure 6.20: Change in second frequency vs. dimple angles, four different dimple locations (pin-pin beam with two dimples in the same direction).

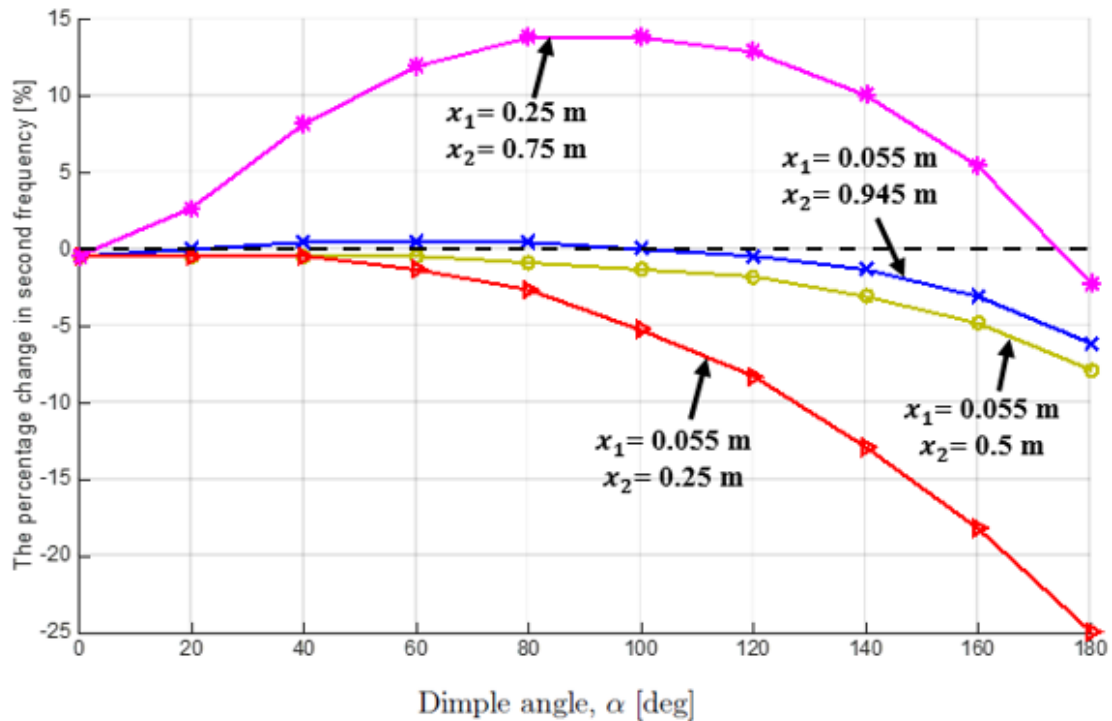


Figure 6.21: Change in second frequency vs. dimple angles, four different dimple locations (pin-pin beam with two dimples in the opposing direction).

For comparison, four different locations are chosen as shown in Figs. 6.20 and 6.21. Comparing the sensitivity of the second frequency at the four locations ($\max(\Delta f_2) - \min(\Delta f_2)$), we observed that for the dimples placed at $x_1 = 0.25$ m and $x_2 = 0.75$ m (high MSE), the second frequency is most sensitive to change in dimple angles where the beam with two dimples in the same direction exhibits a negative change for all dimple angles. Also, for the dimples placed at $x_1 = 0.25$ m and $x_2 = 0.75$ m, the beam with two dimples in the opposing direction (Fig. 6.21) illustrates that there is a rapid rise in the second frequency, followed by a rapid decrease. The least sensitivity occurs for the dimples approximately placed at zero MSE ($x = 0.055$ m, $x = 0.945$ m, and $x = 0.5$ m) for both cases.

6.3.2 Example 2: Fixed-Fixed Beam Model

For a fixed-fixed beam, two cases are studied, a fixed-fixed beam with two dimples in the same direction and a fixed-fixed beam with two dimples in the opposing direction. Both plots (Figs. 6.22 and 6.23) demonstrate the change in fundamental frequency with different dimples angles.

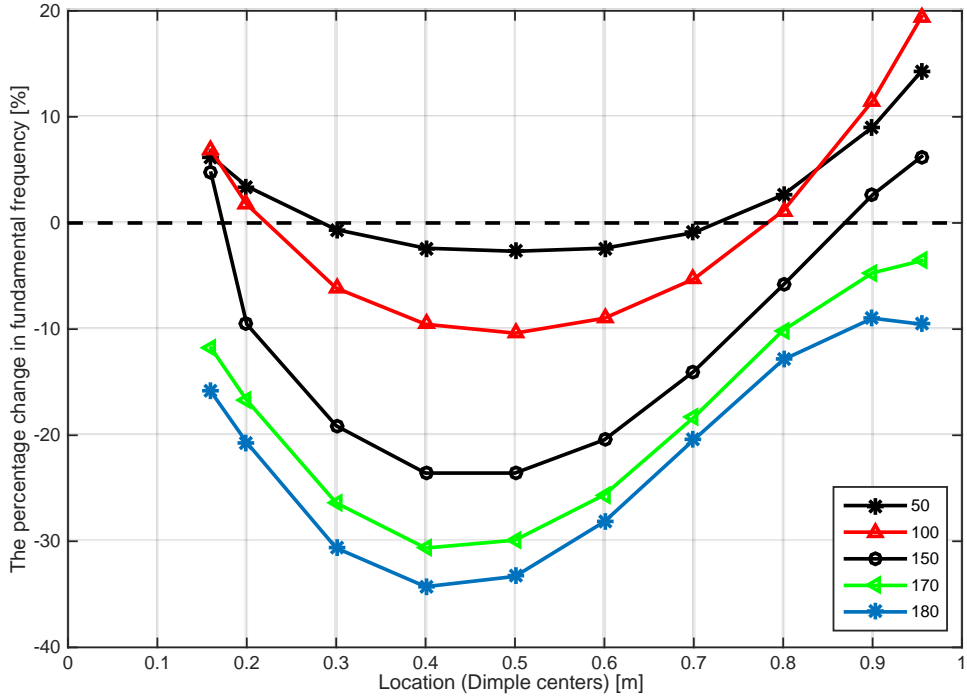


Figure 6.22: Change in fundamental frequency vs. dimple location, five different dimple angles fixed-fixed beam (the beam with two dimples in the same direction).

The variation in fundamental frequency can be understood by examining the MSE for the first mode. In both cases, one dimple is placed at the left boundary while the other dimple is moved along the beam length.

For the beam with two dimples in the same direction (Fig. 6.22), the percentage change in fundamental frequency decreases with increase in the dimples angles. The results show that the highest increase (20%) in fundamental frequency occurs when $\alpha = 100^\circ$ while the highest

decrease (-34%) occurs when $\alpha = 180^\circ$. The increasing and decreasing in fundamental frequency can correspond to a region of high and low MSE as mentioned before.

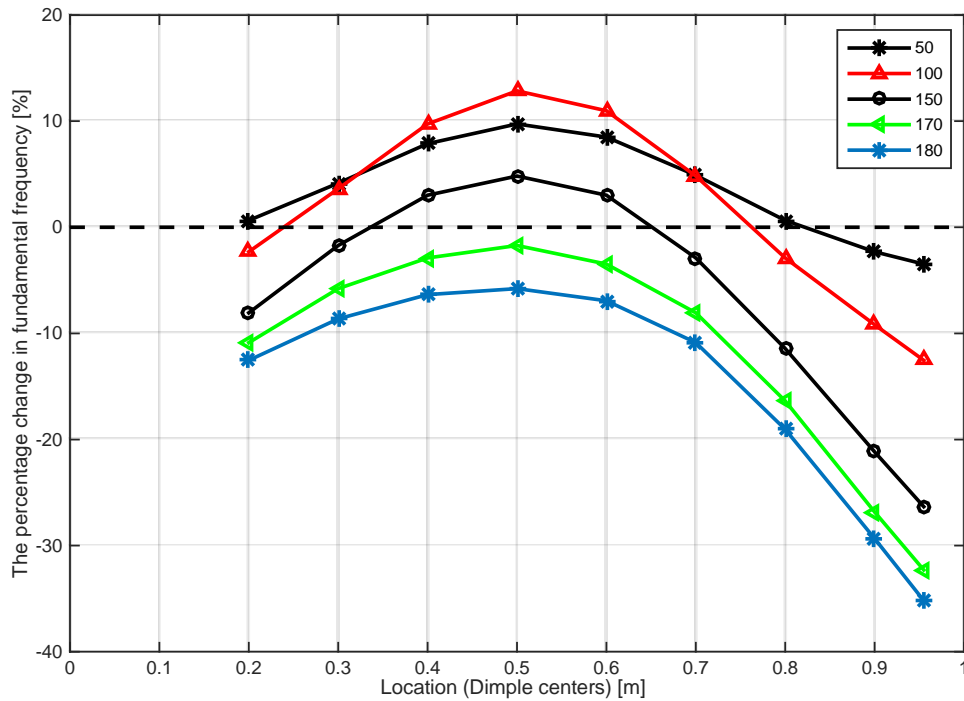


Figure 6.23: Change in fundamental frequency vs. dimple location, five different dimple angles fixed-fixed beam (the beam with two dimples in the opposing direction).

For the fundamental frequency of the beam with two dimples in the opposing direction (Fig. 6.23), the highest increase (13%) in fundamental frequency occurs when $\alpha = 100^\circ$ and the highest decrease (-37%) occurs at $\alpha_2 = 180^\circ$. With one dimple fixed at left boundary and the other dimple moved to beam center, the change in the fundamental frequency increases for certain angles ($\alpha = 50^\circ$ and $\alpha = 100^\circ$) then begins to decrease when the second dimple moves towards the right boundary. In addition, some combination of dimples locations and angles have very small effect on the fundamental frequency, i.e. at $x_1 = 0.055$ m and $x_2 = 0.22$ m when $\alpha_1 = 100^\circ$ and $\alpha_2 = 100^\circ$, therefore, there is a negligible change in the fundamental frequency of the uniform beam at these locations and angles.

Next, four different locations as shown in Figs. 6.24 and 6.25 are examined to get a better understanding of the effect of dimples locations on the change in the fundamental frequency. Two

cases are considered: a fixed-fixed beam with two dimples in the same direction and a fixed-fixed beam with two dimples in the opposing direction.

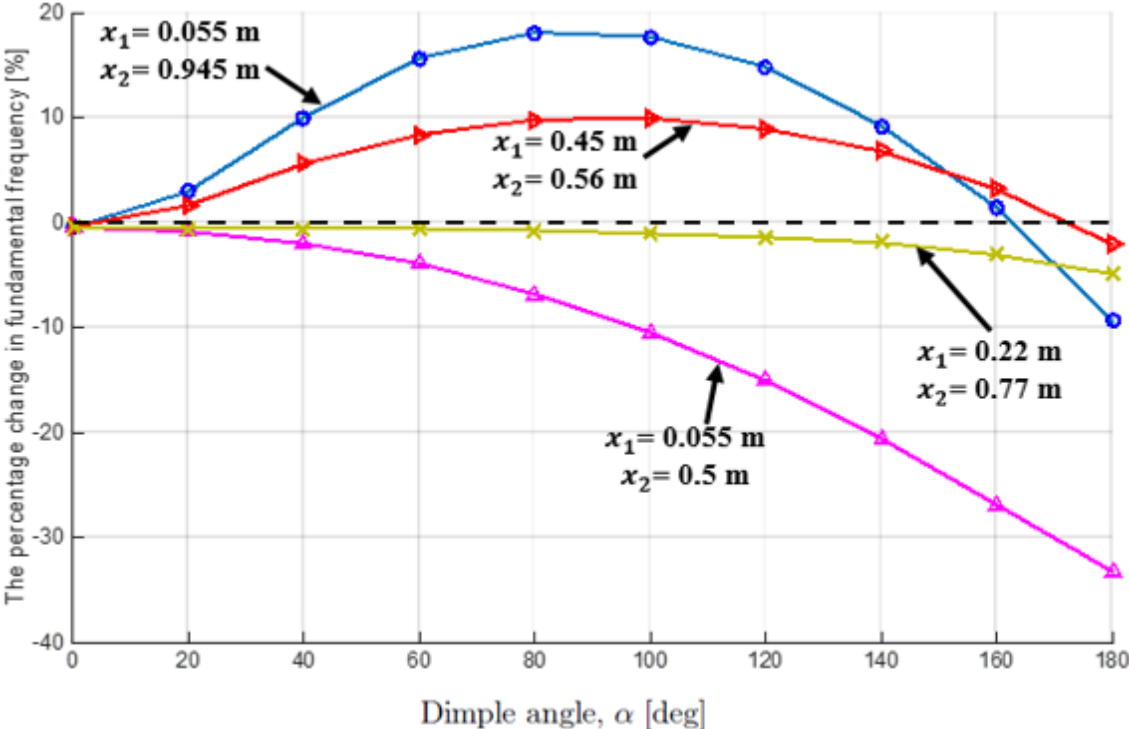


Figure 6.24: Change in fundamental frequency vs. dimple angle, four different dimple locations (fixed-fixed beam with two dimples in the same direction).

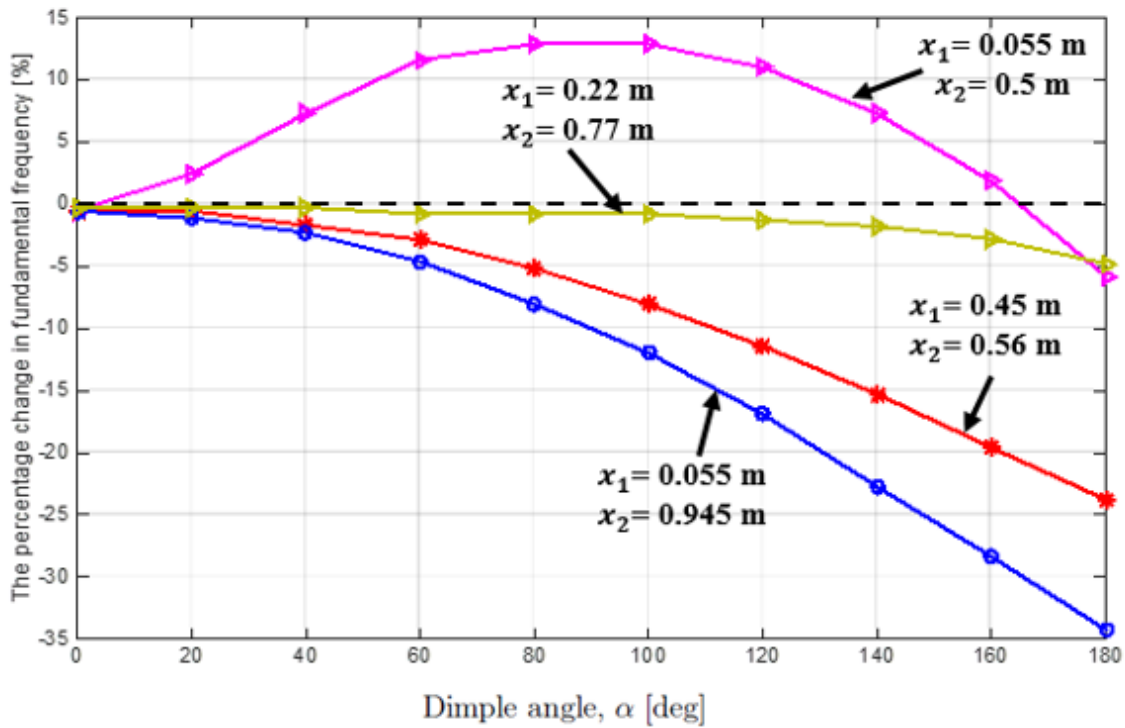


Figure 6.25: Change in fundamental frequency vs. dimple angle, four different dimple locations (fixed-fixed beam with two dimples in the opposing direction).

By observing the MSE for the first mode of a fixed-fixed uniform beam (see Fig 6.13), the highest MSE occurs at the boundaries. The MSE is relatively high at beam center, and it is zero at $x = 0.22$ m and 0.77 m, respectively. The observation of Figs. 6.24 and 6.25 show that the fundamental frequency is the most sensitive to changes in dimple angle if one dimple is placed at left boundary and the second dimple is located at beam center, for the beam with two dimples in the same direction. For the beam with two dimples in the opposing direction, the fundamental frequency is the most sensitive to changes in dimple angle when the two dimples are placed at each boundary ($x_1 = 0.055$ m and $x_2 = 0.945$ m, the largest MSE). The fundamental frequency demonstrates less sensitivity at dimples locations $x_1 = 0.45$ m and $x_2 = 0.56$ m for the beam with two dimples in the same direction. Also, at the dimples locations $x_1 = 0.055$ m and $x_2 = 0.5$ m (relatively large MSE), the fundamental frequency exhibits a moderate sensitivity to changes in dimples angles for the beam with two dimples in the opposing direction. The least sensitivity in the fundamental frequency for both cases occurs at $x_1 = 0.22$ m and $x_2 = 0.77$ m (MSE is zero at

these regions). In other words, dimples placed at $x_1 = 0.22$ m and $x_2 = 0.77$ m exhibit very small change in the fundamental frequency for all angles.

In Fig. 6.26, the second frequency with different angles illustrates a different trend since the region of high and low MSE for the second mode occurred at different locations (see Fig. 6.13) where all modes have the maximum MSE at boundaries.

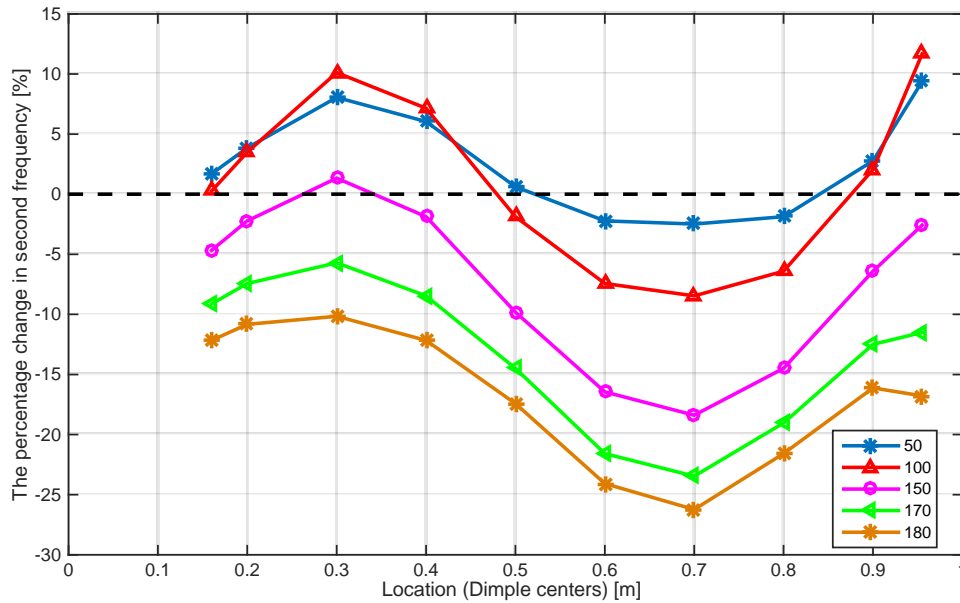


Figure 6.26: Change in second frequency vs. dimple location, five different dimple angles fixed-fixed beam (the beam with two dimples in the opposing direction).

The variation in second frequency is between 13% when $\alpha = 100^\circ$ and -26 % when $\alpha = 180^\circ$. From Fig. 6.26, it is apparent that the second natural frequency has less sensitivity to change in region of zero MSE which is occurred at $x = 0.12$ m, $x = 0.5$ m, and $x = 0.88$ m (see Fig. 6.13).

CHAPTER 7

CONCLUSION AND FUTURE WORK

7.1 Conclusion

The goal of this study was to investigate the effect of dimples on the change in beam natural frequencies. To this end, a boundary value model was developed for a beam with two dimples in the same direction and a beam with two dimples in the opposite direction and subjected to different boundary conditions. The formulation of the coefficients matrix for the fixed-fixed beam with one dimple (concave) was shown.

Hamilton's Principle is used to develop a boundary value model (BVM) of a dimpled beam. The dimpled beam consisted of two dimple segments connected to three straight segments. The differential equations of motion for each segment were derived where their solution satisfied the beam boundary conditions and continuity conditions. A coefficient matrix of 30×30 was formulated and the numerical solution of the differential equations yields the natural frequencies of the dimpled beam. The mass of the dimpled beam was assumed to be constant before and after adding dimples. The dimple thickness was less than the straight segment, the dimple thickness assumed to be uniform while in manufacturing application, the dimple center was the thickest due to the pressing process. The results showed that the efficiency of dimpling technique to decrease first five natural frequencies of the cantilevered beam. The first five natural frequencies of the fixed-fixed beam demonstrated a different behavior where in first mode, the natural frequency was decreased for the two cases, (a beam with two dimples in the same direction and a beam with two dimples in the opposite direction). In the second mode, the natural frequency of the first case, the beam with dimples in the same direction, was decreased, while in the second case, the beam with two dimples in the opposite direction, was increased. The higher modes represented a decrease in the natural frequencies for both cases.

A finite element model was developed using ANSYS Parametric Design Language (APDL) to check the accuracy of the analytical solution. The first five natural frequencies of the

beam without dimples (uniform beam) and dimpled beam were calculated using this FEM model. Comparison of these results showed FEM was in excellent agreement with the results found using BVM.

The effect of adding two dimples to a beam on its natural frequencies were investigated experimentally in order to validate the analytical results. Stamping process was used in order to create dimples in the beam model where this process was repeated different times in order to reach the approximate maximum dimple height before material failure. The experiment was carried out for two boundary conditions: a cantilever beam and fixed-fixed beam. Two cases were considered, a beam with two dimples in the same direction and a beam with two dimples in the opposite direction. A cantilever and fixed-fixed beams were excited by impact hammer and the acceleration was measured using a single axis accelerometer. A four channel (NI-9234) data acquisition card and (M+P) international Smart Office software were used to collect and analyze measured data. The Frequency Response Function (FRF) were plotted where each curve indicated a main peak corresponding to each natural frequency of the beam. The results of the natural frequencies were compared to those found using BVM and FEM and the results were found to be in agreement.

The efficiency of the analytical model was investigated by examining the boundary conditions, dimples locations, and dimples angle. In terms of the boundary condition, two examples were given: a pin-pin beam and a pin-pin roller beam with two dimples. As before, the two dimples cases were considered. The results illustrated that adding two dimples to pin-pin and pin-pin roller beams may increase or decrease the natural frequencies. Next, the location of each dimple was studied by fixing one dimple location and moving the other dimple along the beam length. Pin-pin and fixed-fixed beams were used as examples. The results showed that the fundamental frequency exhibited large sensitivity to changes in dimples angles when dimples placed at high modal strain energy (MSE) regions. In contrast, dimples placed at zero modal strain energy (MSE) exhibited the least sensitivity to changes in dimple angles.

7.2 Future Work

This study has led to greater understanding of how adding two dimples in opposite direction has a significant effect on beams natural frequencies than adding two dimples in the same direction. However, some factors were not considered in this investigations.

In this study, the dimple thickness was assumed to be uniform. In reality, the dimple is thicker at the dimple center. The research area should seek to develop an analytical model with dimples having a non-uniform thickness. Also, future research could explore MSE using many dimples in same and opposite directions.

In addition, future research would explore the possibility of tailoring beam vibrations (frequency and mode shape) to desired values. This could be accomplished using many dimples and could be used to reduce the sound radiated from vibrating beam.

REFERENCES

- [1] K. Myers, *Analysis of Vibroacoustic Properties of Dimpled Beams Using A Boundary Value Model*, A Dissertation Submitted to the Graduate College in Partial Fulfillment of the Requirements for the Degree of Doctor of Philosophy, Department of Mechani and Aerospace Engineering, Western Michigan University, 2015.
- [2] A. Leissa, *Vibration of Shells*, Acoustical Society of America, 1993.
- [3] "merriam-webster," [Online]. Available: <http://www.merriam-webster.com/>. [Accessed 04 08 2016].
- [4] N. Alshabtat, *Beading and dimpling techniques to improve the vibration and acoustic characteristics of plate structures*, Western Michigan University, PhD Thesis, 2011.
- [5] L. Meirovitch, *Analytical Methods in Vibrations*, New York: The Macmillan Company, 1967.
- [6] S. Rao, *Vibration of Continuous Systems*, Hoboken, NJ: John Wiley & Sons, 2007.
- [7] S. M. Han, H. Benaroya and T. Wei, "Dynamics Of Transversely Vibrating Beams Using Four Engineering Theories," *Journal of Sound and Vibration*, vol. 255, no. 5, pp. 935-988, 1999.
- [8] K. Myers and K. Naghshineh, "Analytical model and numerical optimization of vibrating dimpled beam," *The 22nd International Congress of Sound and Vibration*, 2015.
- [9] P. M and C.C. Fleischer, "Free vibration of a curved beam," *Journal of Sound and*, vol. 18 (1), pp. 17-30, 1971.
- [10] P. Chidamparam and A. Leissa, "Vibrations of planar curved beams, rings, and arches," *Applied Mechanics Reviews*," vol. 46, pp. 467-483, 1993.
- [11] S. Y. Lee and J. Y. Hsiao, "Free in- plane vibrations of curved non uniform," vol. 155, pp. 173-189, 2002.
- [12] J. Henrych, *The dynamics of arches and frames*, Amsterdam: Elsevier Scientific Pub. Co., 1981.

- [13] S. S. Rao, "Effect of transverse shear and rotary inertia on the coupled twist bending vibrations of circular rings," *Journal of Sound and Vibration*, vol. 16 (4), pp. 551-566, 1971.
- [14] T. E. Lang, "*Vibration of thin circular rings, part i: Solutions for modal characteristics and forced excitation*", Tech. Rep. 32-261, Jet Propulsion Laboratory, California Institute of Technology, Pasadena, CA, 1962.
- [15] W. Cheng, C. Cheng and G. Koopmann, "Dynamic beam modification using dimples," *Journal of Vibration and Acoustics*, vol. 130, 2008.
- [16] W. Cheng, C. Cheng and G. Koopmann, "A new design strategy for minimizing sound radiation of vibrating beam using dimples," *Journal of Vibration and Acoustics*, vol. 133, October 2011.
- [17] N. Alshabatat and K. Naghshineh, "A design approach for improving the vibroacoustic characteristics of plate structures," in *Proceedings of the ASME 2011 International Mechanical Engineering Congress & Exposition*, Denver, CO, Nov. 11-17, 2011.
- [18] N. Alshabatat and K. Naghshineh, "Optimization of the natural frequencies of beam via dimpling technique," *International Journal of Modelling and Simulation*, vol. 32, no. 2, pp. 134-144, 2012.
- [19] F. Nelson, "In-plane vibration of a simply supported circular ring segment," *Int.J. Mech. Sci*, vol. 4, pp. 517-527, 1962.
- [20] S. S. Rao, *Mechanical vibrations*, Addison-Wesley , 1990.
- [21] C. M. Harris and A. G. Piersol, *Harris' Shock and Vibration Handbook*, New York: McGraw-Hill, 2002.

APPENDIX A

MATLAB CODE (UNIFORM CANTILEVER BEAM)

**%MATLAB SAMPLE CODE TO CALCULATE THE NATURAL FREQUENCIES OF %THE
UNIFORM CANTILEVERED BEAM**

```
clc;clear all;
```

```
E      = 200e9;  
b      =0.026;  
h      = 1.18e-3;  
rho    =7870;  
L      =0.2210;  
beta   = [3.5160  22.0345  61.6972   120.9019  200.0]  
I      =(b*h^3)/12;
```

```
for ii= 1:length(beta)  
    w(ii)= beta(ii)*(sqrt((E*I)/(rho*b*h*L^4))); % Circular frequency  
  
    f(ii)=w(ii)/(2*pi) % The natural frequency  
end
```

APPENDIX B
PLOTTING MODE SHAPES OF DIMPLED BEAM

The following steps explain how to plot the mode shape of a dimpled beam.

- 1) A beam without vibration is considered where it discretizes into uniformly spaced points into x-direction as shown in Fig. (B1).

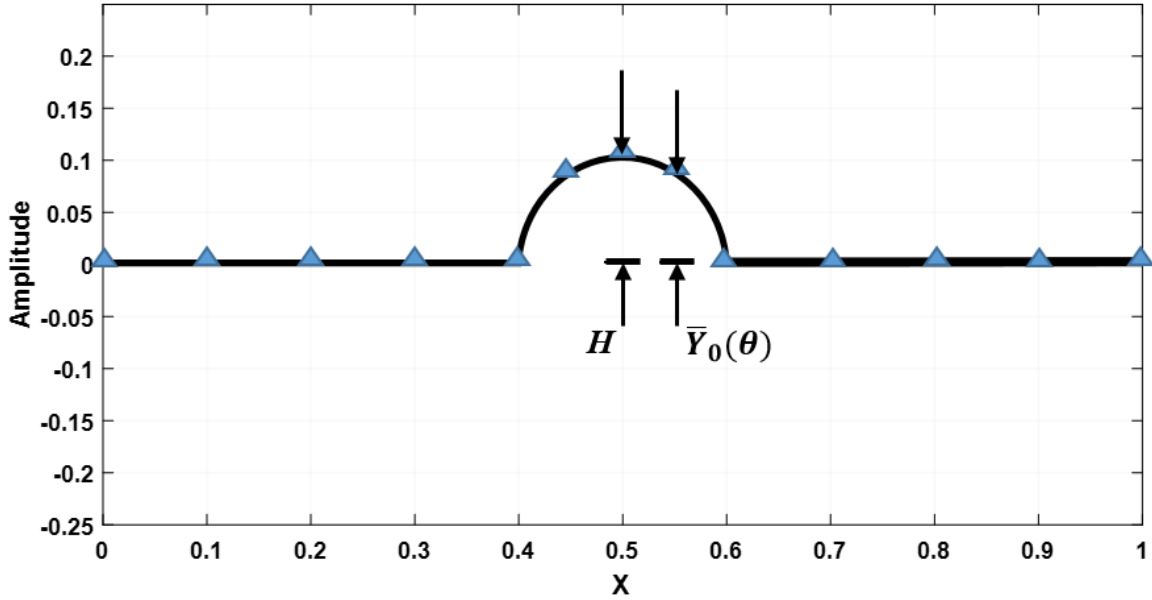


Figure B.1: A discretized beam with one dimple

H represents the maximum high of the dimple and $\bar{Y}_0(\theta)$ is the vertical height of any point on the dimple. The following equation [1] describes the relationship between the local x -coordinates of the dimple \bar{x}_0 and the angular coordinates θ ,

$$\bar{x}_0 = \frac{\bar{l}}{2} - R \sin\left(\frac{\alpha}{2} - \theta\right), \quad (\text{B.1})$$

where the radius of the dimple is given by Eqn. (4.1). Also, the following equation [1] calculate the location of any points located vertically on the dimple and is used to plot the undisplaced dimple

$$\bar{Y}_0(\theta) = \frac{1}{2} \left(H - \frac{\bar{l}}{4H} \right) + R \cos\left(\frac{\alpha}{2} - \theta\right) \quad (\text{B.2})$$

where \bar{l} is the dimple chord, α is the dimple angle, and the height of the dimple is given by Eq. (4.2).

- 2) The following relations [1] defines the transformation needed for the eigenfunctions $V_i(\theta)$, $W_i(\theta)$ of the dimple,

$$\begin{Bmatrix} \bar{U}_i(\theta) \\ \bar{Y}_i(\theta) \end{Bmatrix} = \begin{bmatrix} \cos(\frac{\alpha}{2} - \theta) & \sin(\frac{\alpha}{2} - \theta) \\ -\sin(\frac{\alpha}{2} - \theta) & \cos(\frac{\alpha}{2} - \theta) \end{bmatrix} \begin{Bmatrix} V_i(\theta) \\ W_i(\theta) \end{Bmatrix}, \quad (\text{B.3})$$

where $\bar{U}_i(\theta)$, $\bar{Y}_i(\theta)$ represents the horizontal and vertical displacements with assuming that a clockwise rotation and the downward is positive direction.

- 3) Now, we can plot the mode shape by adding the local horizontal and vertical displacements to the global coordinates of displaced beam. So, for the straight segment, global x-coordinate of the displaced beam = $X + \bar{U}_i(x)$ and for the dimple segment, x-coordinate of the displaced beam = $X + \bar{U}_i(\theta)$. Similarly, global y-coordinate of the displaced beam in the straight segment = $-Y_i(x)$ and in the dimple segment, y-coordinate = $\bar{Y}_{0i}(\theta) - \bar{Y}_i(\theta)$, (for convex dimple). The y-coordinate of the displaced beam = $\bar{Y}_{0i}(\theta) + \bar{Y}_i(\theta)$, (for the concave dimple).

APPENDIX C
FINITE ELEMENT CODE (DIMPLED CANTILEVER BEAM)


```
LSTR,3,7 ! PLOT LINE FROM 3 TO 7
LSTR,6,2 ! PLOT LINE FROM 6 TO 2
LARC,4,3,5 ! PLOT ARC FROM 4 TO 3 TO 5 FOR FIRST DIMPLE
LARC,7,6,8 ! PLOT ARC FROM 7 TO 6 TO 8 FOR SECOND DIMPLE
```

```
FLST,2,5,4,ORDE,2
```

```
FITEM,2,1
```

```
FITEM,2,-5
```

```
LGLUE,P51X
```

```
FLST,5,3,4,ORDE,2
```

```
FITEM,5,1
```

```
FITEM,5,-3
```

```
CM,_Y,LINE
```

```
LSEL, , , ,P51X
```

```
CM,_Y1,LINE
```

```
CMSEL,S,_Y
```

```
!*
```

```
!*
```

```
CMSEL,S,_Y1
```

```
LATT,1,1,1,1,,,
```

```
CMSEL,S,_Y
```

```
CMDELE,_Y
```

```
CMDELE,_Y1
```

```
!*
```

```
CM,_Y,LINE ! DEFINE COMPONENT NAMED _Y
```

```
LSEL,,,,4
```

```
CM,_Y1,LINE
```

```
CMSEL,S,_Y
```

```
!*
```

```
!*
```

```
CMSEL,S,_Y1
```



```

LATT,1,2,1,,,,
CMSEL,S,_Y
CMDELE,_Y
CMDELE,_Y1
!*
CM,_Y,LINE
LSEL,,,,5
CM,_Y1,LINE
CMSEL,S,_Y
!*
!*
CMSEL,S,_Y1
LATT,1,3,1,,,,
CMSEL,S,_Y
CMDELE,_Y
CMDELE,_Y1
!*
ESIZE,0.003,0, !USE 0.003 INCREMENTAL POINTS FOR MESH WHICH 81 ELEMENTS
PER LNIE
FLST,2,5,4,ORDE,2
FITEM,2,1
FITEM,2,-5
LMESH,P51X
!!!!!!!!!!!!!!!!!!!!!!!!!!!!!!!!!!!!!!!!!!!!!!!!!!!!!!!!!!!!!!!!!!!!!!!!!!!!!!!!!!!!!!!!!!!!!!!!!!!!!!!!!!!!!!!!!!!!!!!!
!solve the model
/SOLU
ANTYPE,2 !Modal analysis
MODOPT,LANB,5
EQLV,SPAR
MXPAND,5, , ,0
LUMPM,0

```

```
PSTRES,0
MODOPT,LANB,10,0,10000, ,OFF
```

```
!* Define boundary Conditions for the Cantilever beam
```

```
FLST,2,1,4,ORDE,1
```

```
FITEM,2,1
```

```
/GO
```

```
DK,P51X, ,0, ,0,ALL, , , , ,
```

```
SOLVE
```

```
!!!!!!!!!!!!!!!!!!!!!!!!!!!!!!!!!!!! Read the first five natural frequencies!!!!!!!!!!!!!!!!!!!!!!!!!!!!!!!!!!!!
```

```
FINISH
```

```
/POST1
```

```
SET,FIRST
```

```
SET,FIRST
```

```
SET, NEXT
```

```
SET, NEXT
```

```
SET, NEXT
```

```
SET, NEXT
```

```
SET,LIST
```

```
*GET,f1,MODE,1,FREQ
```

```
*GET,f2,MODE,2,FREQ
```

```
*GET,f3,MODE,3,FREQ
```

```
*GET,f4,MODE,4,FREQ
```

```
*GET,f5,MODE,5,FREQ
```

```
!Sample listing frequencies :
```

```
***** INDEX OF DATA SETS ON RESULTS FILE *****
```

SET	TIME/FREQ	LOAD STEP	SUBSTEP	CUMULATIVE
1)	17.195	1	1	1
2)	107.75	1	2	2
3)	228.06	1	3	3
4)	554.77	1	4	4
5)	593.59	1	5	5

APPENDIX D
FINITE ELEMENT CODE (UNIFORM CANTILEVER BEAM)

```

FINISH
/CLEAR
/TITLE, Uniform Cantilever Beam

! Define the dimensions of the beam
*SET,b,0.026
*SET,t,1.18e-3
*SET,A,t*b

/PREP7

!Plot Beam
K,1,0,0 ! Enter keypoints
K,2,0.2210,0
L,1,2 ! Create line

! Select the element type and properties
ET,1,BEAM3 ! Element type
R,1,A,(1/12)*b*(t)**3,t,,, ! Real Const: area,I,thickness

! Define the material properties
MP,EX,1,200e9 ! Young's modulus
MP,PRXY,1,0.3 ! Poisson's ratio
MP,DENS,1,7870 ! Density
LESIZE,ALL,,50 ! Element size
LMESH,1 ! Mesh line FINISH

!solve the model
/SOLU
ANTYPE,2 ! Modal analysis
MODOPT,SUBSP,5 ! Subspace, 5 modes
EQLV,FRONT ! Frontal solver
MXPAND,5 ! Expand 5 modes
DK,1,ALL ! Constrain keypoint one # Boundary conditions

SOLVE
FINISH
!!!! Natural Frequencies!!!!
/POST1 ! List solutions
SET,LIST

```